Characterization of Novel Mutations in Receptor-Tyrosine Kinases in Multiple Myeloma

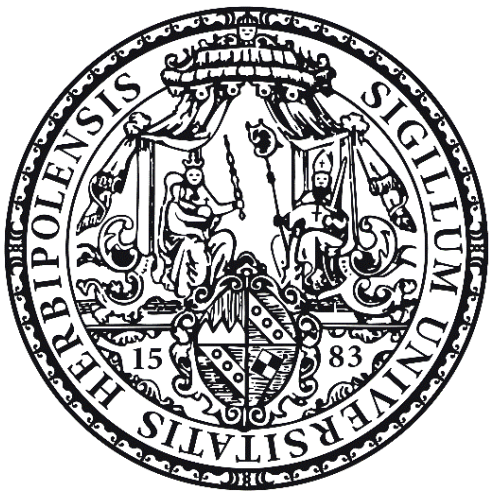

Dissertation zur Erlangung des

naturwissenschaftlichen Doktorgrades

der Julius-Maximilians-Universität Würzburg

vorgelegt von

Sarah Keppler

aus Heilbronn

Würzburg, September 2017

Eingereicht am: .....

Mitglieder der Promotionskommission:

Vorsitzender:

Gutachter: Prof. Dr. Andreas Rosenwald

Gutachter: Prof. Dr. Ricardo Benavente

Tag des Promotionskolloquiums: .....

Doktorurkunde ausgehändigt am: .....

Eidesstattliche Erklärung

Erklärungen nach §4 Abs. 3 Satz 3, 5, 8 der Promotionsordnung der Fakultät für Biologie

Affidavit

I hereby declare that my thesis entitled: „**Characterization of Novel Mutations in Receptor-Tyrosine Kinases in Multiple Myeloma**" is the result of my own work.

I did not receive any help or support from commercial consultants. All sources and / or materials applied are listed and specified in the thesis.

Furthermore I verify that the thesis has not been submitted as part of another examination process neither in identical nor in similar form.

Eidesstattliche Erklärung

Hiermit erkläre ich an Eides statt, die Dissertation: „**Characterization of Novel Mutations in Receptor-Tyrosine Kinases in Multiple Myeloma**", eigenständig, d. h. insbesondere selbständig und ohne Hilfe eines kommerziellen Promotionsberaters, angefertigt und keine anderen, als die von mir angegebenen Quellen und Hilfsmittel verwendet zu haben.

Ich erkläre außerdem, dass die Dissertation weder in gleicher noch in ähnlicher Form bereits in einem anderen Prüfungsverfahren vorgelegen hat.

Würzburg, den ----------

Sarah Keppler

Danksagung

An dieser Stelle möchte ich mich bei all jenen bedanken, die zum erfolgreichen Gelingen dieser Arbeit beigetragen haben.

Mein Dank gilt Prof. Dr. Andreas Rosenwald für die Möglichkeit meine Dissertation am Pathologischen Institut anzufertigen, sowie Prof. Dr. Ricardo Benavente für die nette Zweitbetreuung.

Besonders danken möchte ich Frau Dr. Ellen Leich-Zbat für die persönliche Betreuung in den letzten Jahren. Danke für deine vielen Rat- und Vorschläge, dein Interesse, die unzähligen fachlichen Diskussionen und für deine Hilfe in manch schwieriger Phase.

Ein großes Dankeschön geht auch an meine Kollegen der Arbeitsgruppen Rosenwald und Leich. Hierbei gilt mein Dank besonders Dr. Susann Diegmann für die gründliche Einarbeitung und Hilfestellung in der Anfangsphase, Dr. Jordan Pischimarov für die bioinformatische Auswertung der Amplicon-Daten, Dr. Hilka Rauert-Wunderlich sowie Theodora Nedeva und Tina Grieb für die Hilfe bei allen kleineren und größeren Problemen im Labor. Besonders bedanken möchte ich mich auch bei Marlene Schwarzfischer für die gute Zusammenarbeit. Vielen Dank euch allen für die schöne und lustige Zeit, sowie die vielen aufmunternden Worte in den letzten Jahren.

Ebenfalls möchte ich mich bei all unseren Kooperationspartnern bedanken. Hierbei sind besonders Dr. Thorsten Stühmer für die Hilfe und die Ratschläge bei der Durchführung der funktionellen Analysen, sowie Prof. Dr. Christian Langer und die gesamte DSMM für die Bereitstellung der Patientenproben, der zytogenetischen und klinischen Daten der DSMM XI und DSMM XII Patientenkohorten hervorzuheben.

Ein großer Dank gilt auch allen Freunden und Kommilitonen, die mich in den letzten Jahren motiviert und unterstützt haben.

Dem größten Dank bin ich jedoch meinen Eltern Iris und Roland Keppler, sowie meinen Geschwistern und Großeltern verpflichtet. Ohne eure Unterstützung und den notwendigen Rückhalt hätte es diese Doktorarbeit nie gegeben. Danke!

Table of contents

1 Summary

Multiple myeloma (MM) is a disease of terminally differentiated B-cells which accumulate in the bone marrow leading to bone lesions, hematopoietic insufficiency and hypercalcemia. Genetically, MM is characterized by a great heterogeneity. A recent next-generation sequencing approach resulted in the identification of a signaling network with an accumulation of mutations in receptor-tyrosine kinases (RTKs), adhesion molecules and downstream effectors. A deep-sequencing amplicon approach of the coding DNA sequence of the six RTKs *EPHA2*, *EGFR*, *ERBB3*, *IGF1R*, *NTRK1* and *NTRK2* was conducted in a patient cohort (75 MM samples and 68 corresponding normal samples) of the "Deutsche Studiengruppe Multiples Myelom (DSMM)" to further elucidate the role of RTKs in MM. As an initial approach the detected mutations were correlated with cytogenetic abnormalities and clinical data in the course of this thesis. RTK mutations were present in 13% of MM patients of the DSMM XI trial and accumulated in the ligand-binding and tyrosine-kinase domain. The newly identified mutations were associated with an adverse patient survival, but not with any cytogenetic abnormality common in MM. Especially rare patient-specific SNPs (single nucleotide polymorphism) had a negative impact on patient survival. For a more comprehensive understanding of the role of rare RTK SNPs in MM, a second amplicon sequencing approach was performed in a patient cohort of the DSMM XII trial that included 75 tumor and 184 normal samples. This approach identified a total of 23 different mutations in the six RTKs *EPHA2*, *EGFR*, *ERBB3*, *IGF1R*, *NTRK1* and *NTRK2* affecting 24 patients. These mutations could furthermore be divided into 20 rare SNPs and 3 SNVs (single nucleotide variant). In contrast to the first study, the rare SNPs were significantly associated with the adverse prognostic factor del17p.

IGF1R was among the most commonly mutated RTKs in the first amplicon sequencing approach and is known to play an important role in diverse cellular processes such as cell proliferation and survival. To study the role of IGF1R mutations in the hard-to-transfect MM cells, stable IGF1R-knockdown MM cell lines were established. One of the knockdown cell lines (L363-C/C9) as well as a IGF1R-WT MM cell line (AMO1) were subsequently used for the stable overexpression of WT IGF1R and mutant IGF1R (N1129S, D1146N). Overall, an impact on the MAPK and PI3K/AKT signaling pathways was observed upon the IGF1R knockdown as well as upon WT and mutant IGF1R overexpression. The resulting signaling pattern, however, differed

between different MM cell lines used in this thesis as well as in a parallel performed master thesis which further demonstrates the great heterogeneity described in MM.

Taken together, the conducted sequencing and functional studies illustrate the importance of RTKs and especially of IGF1R and its mutants in the pathogenesis of MM. Moreover, the results support the potential role of IGF1R as a therapeutic target for a subset of MM patients with mutated IGF1R and/or IGF1R overexpression.

2 Zusammenfassung

Das Multiple Myelom (MM) ist eine maligne Erkrankung ausdifferenzierter B-Zellen, den sogenannten Plasmazellen, welche sich im Knochenmark anhäufen. Symptome des MM sind, unter anderem, Knochenläsionen, Hyperkalzämie und hämatopoetische Insuffizienz. Zusätzlich ist das MM durch eine große genetische Heterogenität geprägt. In einer kürzlich durchgeführten *Next-Generation Sequencing* Studie wurde eine Akkumulation von Mutationen in Rezeptortyrosinkinasen (RTK), Adhesionmolekülen und den zugehörigen Effektoren identifiziert. Dies erlaubte die Definition eines inter- und intrazellulären Signalnetzwerkes. Um die Rolle der RTKs im MM genauer zu definieren, wurde die kodierende DNA Sequenz der sechs RTKs *EPHA2*, *EGFR*, *ERBB3*, *IGF1R*, *NTRK1* und *NTRK2* in einer einheitlich therapierten Patientenkohorte (75 Patienten) der „Deutschen Studiengruppe Multiples Myelom“ (DSMM) mittels eines Amplikonansatzes sequenziert. Die identifizierten Mutationen wurden im Rahmen dieser Arbeit validiert und anschließend mit zytogenetischen Anomalitäten und klinischen Daten korreliert. RTK Mutationen waren in 13 % der MM Patienten vorhanden und akkumulierten besonders in den Ligandenbindungs- und der Tyrosinkinase- Domänen. Die neu identifizierten RTK Mutationen hatten einen signifikant negativen Einfluss auf das Überleben, jedoch konnte kein Zusammenhang zwischen den Mutationen und zytogenetischen Alterationen festgestellt werden. Besonders seltene, Patienten-spezifische SNPs hatten einen negativen Einfluss auf die Gesamtüberlebenszeit, das ereignisfreie und das progressionsfreie Überleben. Um die Rolle dieser seltenen *SNPs* im MM besser zu verstehen, wurde ein zweiter Amplikonansatz in einer neuen Patientenkohorte der DSMM XII Studie durchgeführt. Hierbei wurden die sechs RTKs *EPHA2*, *EGFR*, *ERBB3*, *IGF1R*, *NTRK1* und *NTRK2* in 75 Tumor und 184 Normalproben sequenziert. Bei diesem Ansatz wurden 23 unterschiedliche Mutationen in 24 Patienten identifiziert. Diese Mutation konnten in 20 seltene *SNPs* und 3 *SNVs* (*single nuleotide variant)* unterteilt werden und waren, im Gegensatz zu Mutationen der ersten Studie, signifikant mit dem negativ prognostischen Faktor del17p assoziiert.

IGF1R war bei der initialen Amplikon-Sequenzierstudie unter den am häufigsten mutierten RTKs und spielt eine wichtige Rolle in verschiedenen zellulären Prozessen, z. B. der Zellproliferation und dem Überleben. Um eine funktionelle Untersuchung der IGF1R Mutation in den schwer-zu-transfizierenden MM-Zellen zu ermöglichen, wurden stabile IGF1R-*knockdown* MM-Zelllinien etabliert. Eine dieser *knockdown* Zelllinien (L363-C/C9) sowie eine

IGF1R WT MM-Zelllinie (AMO1) wurden anschließend für die stabile Überexpression von IGF1R WT, IGF1R D1146N und IGF1R N1129S verwendet. Funktionelle Analysen zeigten, dass sowohl IGF1R-*knockdown* als auch die Überexpression von IGF1R WT, IGF1R D1146N und IGF1R N1129S einen Einfluss auf den MAPK und den PI3K/AKT Signalweg haben. Der Einfluss des IGF1R WT, als auch der zwei Mutanten IGF1R D1146N und IGF1R N1129S unterschied sich jedoch in den in dieser Arbeit und in einer parallel durchgeführten Masterarbeit verwendeten Zelllinien. Diese Unterschiede verdeutlichen zusätzlich die große Heterogenität für die das MM bekannt ist.

Zusammengenommen verdeutlichen die durchgeführten Sequenzier- und funktionellen Studien die wichtige Rolle der RTKs, besonders von IGF1R, im MM. Darüber hinaus unterstützen die erhaltenen Ergebnisse die potenzielle Rolle von IGF1R als therapeutisches Ziel für MM-Patienten mit mutiertem IGF1R und / oder IGF1R-Überexpression.

3 Introduction

3.1 Multiple Myeloma

3.1.1 Definition

Multiple myeloma (MM), also known as plasma cell myeloma or Kahler's disease, is a malignant disease of long-lived, terminally differentiated plasma cells [1-3]. It accounts for approximately 1 % of all cancers, 10-15 % of hematological neoplasms and is, after Non-Hodgkin's lymphoma, the second most common type of hematological malignancy [1, 2, 4]. Each year there are approximately 154000 newly diagnosed cases and 100000 deaths recorded worldwide [5]. The median age at diagnosis is 66 years, men are more frequently affected than women and the incidence rate in African-Americans is two times higher than in Caucasians [1-3, 6, 7]. Clinical features of MM include anemia, bone pain and lesions, hypercalcemia, elevated creatinine levels and secretion of monoclonal proteins (M-proteins) [3]. These M-proteins can be detected in the serum or urine in up to 97 % of MM patients and contain different classes of immunoglobulins (Ig): IgG (60 % of cases), IgA (24 % of cases), IgD (3 % of cases), IgE or IgM (<2 % of cases). Additionally, there are cases with expression of only the light chain (11% of cases) or with biclonal expression (<2 % of cases). [3, 8, 9]

Although clinical outcome for MM patients has improved over the last decade, median survival is still ranging between 6 and 7 years with a low percentage of patients surviving longer than 10 years [10, 11]. Clinical outcome is dependent on several factors: disease stage, patient condition (age, performance and comorbidities), response to therapy and cytogenetic abnormalities [11, 12]. Depending on the detected cytogenetic abnormalities e.g. chromosomal translocations, gains, losses or trisomies, patients can be divided into three groups: high risk, intermediate risk and standard risk (Table 1)[11].

Table 1: Risk stratification

Standard risk	Intermediate risk	High risk
Trisomies	t(4;14)	t(14;16)
t(11;14)	gain 1q	t(14;20)
t(6;14)		del17p

Furthermore the occurrence of elevated serum lactate dehydrogenase and the occurrence of circulating plasma cells indicates an aggressive and high-risk disease [11]. The described risk level and the eligibility for autologous stem cell transplantation (ACST) determine the

treatment strategy for newly diagnosed MM patients. A combination therapy containing either bortezomib, thalidomide and dexamethasone or bortezomib, lenalidomide and dexamethasone is currently the preferred therapy in patients eligible for ACST [11]. The development and approval of new drugs e.g. carfilzomib, ixazomib, pomalidomide or panobinostat will hopefully further improve the survival of MM patients [11].

3.1.2 B-cell differentiation and development of MM

As mentioned previously, MM is a malignant disease of plasma cells [1-3]. Plasma cells are terminally differentiated B-cells which are, together with memory B-cells, the final product of B-cell development (Figure 1) [13]. B-cell development starts in the bone marrow (BM) with hematopoietic precursor cells (HSC) which differentiate into pro B-cells. At the stage of pro B-cells the genes of the Ig heavy chain (Ig-H) are recombined. In a first step the D (diversity) and J (joining) gene segments of the Ig-H are rearranged followed by the joining of an upstream V (variable) gene segment to the DJ complex [13, 14]. The successful rearrangement of the Ig-H, known as VDJ recombination, enables the expression of a pre B-cell receptor (pre-BCR) and the progression of the pro B-cell into the pre B-cell stage [15]. The pre-BCR expression furthermore induces the rearrangement of the Ig λ and Ig κ light chains. After successful rearrangement of the Ig light chains (Ig-L) and Ig-H the cell expresses IgM on the cell surface and is now an immature B-cell [13-15]. The expression of IgM, however, can lead to autoreactivity by binding of self-antigens. Therefore, immature B-cells are checked and highly autoreactive immature B-cells either undergo apoptosis or secondary light chain rearrangement preventing the circulation of highly autoreactive B-cells in the blood [14, 15]. Immature B-cells with low or no autoreactivity can leave the BM and migrate towards the spleen and other secondary lymphoid organs. After homing to the spleen B-cells complete their maturation process by developing into either marginal zone (MZ) or follicular zone B-cells. Follicular zone B-cells are activated upon antigen recognition and differentiate into proliferating centroblasts forming the dark zone of the germinal center (GC) [15]. Moreover, proliferating B-cells activate the process of somatic hypermutation (SHM) thereby introducing mutations into the Ig V gene segment and improving the antigen affinity of the BCR [15, 16]. B-cells with a higher antigen affinity will be positively selected in the light zone with help of follicular dendritic cells (FDC) and $CD4^+$ T-cells. B-cells come into close contact to the $CD4^+$ T-cells which provide pro-survival signals. B-cells with a low affinity BCR are not able to form this close contact to the T-cells and therefore do not receive pro-survival signals and undergo

apoptosis. A part of the positively selected B-cells are furthermore subjected to class switch recombination (CSR). During this process the IgM constant region of the Ig heavy chain is replaced by the IgE, IgA or IgG constant region. At the end of the B-cell development the cells leave the germinal center as either long-lived memory B or plasma cells [13-16]. (Figure 1)

During B-cell development several steps can lead to the generation of an abnormal plasma cell. Chromosomal translocations, which are a genetic hallmark of MM, can occur as byproducts of VDJ recombination, SHM and CSR. During these processes DNA double strand breaks are induced and can lead to these aberrant chromosomal translocations and somatic mutations. These aberrant translocations and mutations can furthermore result in the deregulation of oncogenes or tumor suppressor genes leading to MM development. [9, 14, 16]

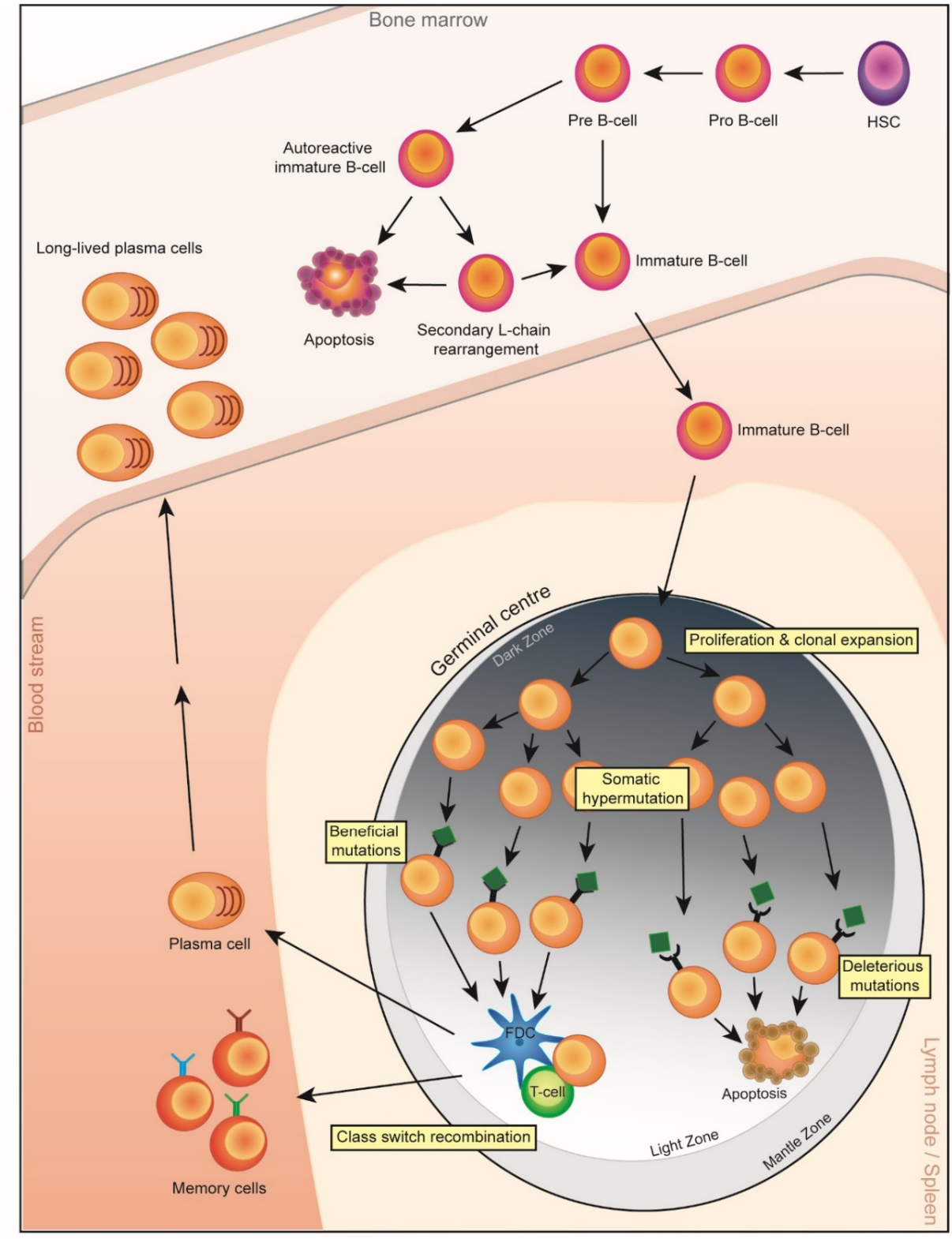

Figure 1: B-cell development
B-cell development starts in the bone marrow (BM) with a hematopoietic precursor cell (HSC) which differentiates into pro B-cell. The pro B-cell develops into a pre B-cell. Pre B-cells are tested for autoreactivity. A pre B-cell with a low autoreactivity develops into an immature B-cell and leaves the BM, a pre-B-cell with high autoreactivity either undergo apoptosis or secondary light chain (L-chain) rearrangement. Antigen activated immature B-cells migrate to the germinal center (GC) where they proliferate, undergo somatic hypermutation and class switch recombination before leaving the GC as either a memory B-cell or a plasma cell. FDC: follicular dendritic cell (Figure according to [14-16])

3.1.3 Genetic background of MM

MM is a genetically very heterogeneous disease with different distinct premalignant stages [17, 18]. The disease progresses from the indolent, asymptotic stages of monoclonal gammopathy of undetermined significance (MGUS) with a clonal plasma cell population in the BM of less than 10% and smouldering myeloma (SMM) with a plasma cell population greater than 10% to myeloma with organ damage triggered by anemia, bone, calcium and renal abnormalities. The final stage of the disease is plasma cell leukemia (PCL) characterized by extramedullary clones which are no longer BM dependent. (Figure 2) [17-21] In most patients a pre-malignant clone is detectable which will follow the disease pattern and acquires mutations along the way. Most likely mutations and genetic aberrations already present at the MGUS stage are primary genetic events and play a role in the immortalization of plasma cells and the development of MM. Acquired genetic aberrations not present in the pre-malignant stages of MM are defined as secondary genetic events and probably have an influence on disease progression and treatment failure. (Figure 2) [17, 18, 22] Primary events in MM can be classified into two subgroups: hyperdiploid and non-hyperdiploid [17, 22]. Approximately 50 % of MM tumors are hyperdiploid and affected by multiple chromosomal gains, especially trisomy of chromosomes 3, 5, 7, 9, 11, 15, 19 or 21 [22-24]. Non-hyperdiploid MM tumors are affected by chromosomal translocations. Most chromosomal translocations (>90 %) affect the *IGH* locus at 14q32.33 leading to the deregulation of genes by putting them under the control of the *IGH* enhancer [9]. The most common translocations are t(4;14), t(6;14), t(11;14), t(14;16) and t(14;20) leading to the upregulation of the oncogenes *MMSET*/*FGFR3*, *CCND3*, *CCND1*, *MAF* and *MAFB*, respectively [17, 18, 22]. In addition to translocations affecting the *IGH* locus, MM tumors are also display translocations involving *MYC* [25]. These translocations are, in contrast to translocations involving *IGH*, only secondary genetic events and lead to an overexpression of *MYC* [26, 27]. Other secondary genetic events common in MM are copy number variations, loss of heterozygosity, acquisition of mutations and epigenetic modifications. Common copy number variations in MM include the gain of 1q affecting the oncogenes *CKS1B* and *ANP32E* (40 % of MM tumors) [28, 29], the loss of 1p affecting *FAM46C, FAF1* and *CDKN2C* (30 % of MM tumors) [28, 30], the loss of chromosome 13 affecting *DIS3* and the tumor-suppressor gene *RB1* (approximately 50 % of MM tumors) [18, 28, 31] and loss of chromosome 17p affecting the tumor-suppressor gene *TP53* (10 % of MM tumors, incidence increasing in late stage disease) [32-34]. Whole-genome and whole-

exome sequencing approaches lead to the identification of acquired recurrent and rare mutations in MM. *KRAS*, *NRAS* and *BRAF*, all belonging to the mitogen-activated protein kinase (MAPK) signaling pathway, are among the most frequently mutated genes in MM and detected in approximately 40 % of all MM patients. These mutations are, however, usually observed in subclonal tumor cell populations, emphasizing their role as secondary genetic events. [35-39] The enrichment of mutations in specific pathways is also seen in NF-κB signaling and DNA repair pathway associated genes such as *TRAF3*, *CYLD* and *LTB2* or *TP53*, *ATM* and *ATR*, respectively [35-38]. Other frequently mutated genes in MM are the potential tumor suppressor genes *DIS3* and *FAM46C* whose roles in MM pathogenesis, however, still remain unclear [35-40]. Further secondary genetic events include global DNA hypomethylation during progression from MGUS to MM and gene-specific hypermethylation during progression from MM to PCL [41]. Further adding to the genetic complexity of MM is the occurrence of intraclonal heterogeneous subclones in the tumor cell population. These subclones occur due to a branched accumulation of mutations during the development and progression of MM and have an influence on clinical outcome and answer to therapy. [17, 18, 22]

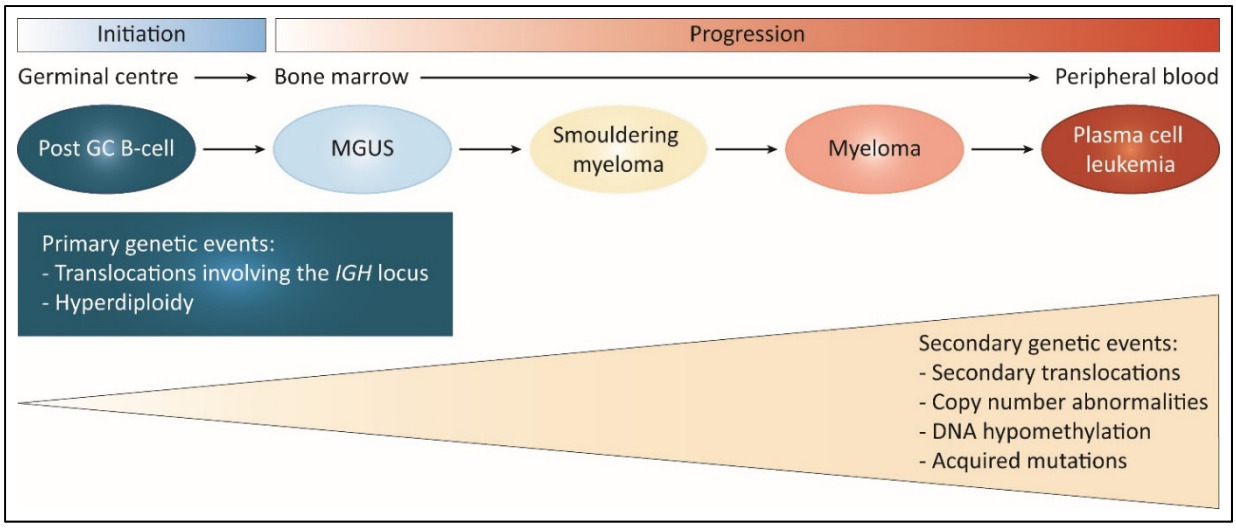

Figure 2: Initiation and progression of MM
MM progresses from the indolent phases of MGUS and smouldering myeloma to myeloma with clinical features. In late disease stages, the cells are no longer dependent on the bone marrow and can be found at extramedullary sites. Primary genetic events are thought to play a role in the immortalization of plasma cells and subsequent development of MM. Secondary genetic events are acquired over time and thought to play a role in disease progression and treatment failure. (Figure adapted by permission from Macmillan Publishers Ltd: [Nature Reviews Cancer] from [17], copyright 2012)

3.2 Receptor-tyrosine kinases

3.2.1 Structure and function

Receptor-tyrosine kinases (RTKs) play important roles in a wide range of physiological cellular processes such as cell survival, proliferation, differentiation, cell cycle control and cell death [42-45]. Sequencing of the human genome has identified 90 tyrosine kinases containing 32 nonreceptor- and 58 RTKs. These 58 RTKs can be divided into 20 subfamilies which include, among others, the ErbB receptor family, the insulin receptor (InsR) family, the tropomyosine receptor kinase (Trk) family and the erythropoietin-producing human hepatocellular receptor (Eph) family (Figure 3). [42, 46] In general, RTKs are monomeric transmembrane proteins, containing an extra- and an intracellular domain. Upon ligand binding RTKs dimerize and transfer extracellular signal to the cytoplasm by phosphorylation of tyrosine residues [47, 48]. One exception hereof is the InsR family whose members exist as di-sulfide linked dimers on the extracellular membrane even without activation (Figure 3) [46, 49]. The extracellular domain of RTKs differs between RTK families and contains different structural domains for example (e.g.) Ig-like domains, leucine-rich domains, fibronectin type III-like domains, cysteine-rich domains, ligand-binding domains or ephrin-binding domains (Figure 3) [46, 48]. The intracellular domains of RTKs usually contain a juxtamembrane, a tyrosine-kinase catalytic and a carboxy-terminal domain [48].

Activation of RTKs is a tightly regulated process. Without ligands present, RTKs exist in an unphosphorylated, monomeric state with an inactive kinase domain. In some RTKs the kinase activity is further inhibited by the interaction of the juxtamembrane with the kinase domain [50]. Ligand binding to the extracellular domain leads to the oligomerization of monomeric or to structural changes of dimeric RTKs and to the separation of the juxtamembrane and kinase domains. These changes lead to autophosphorylation of tyrosine residues in the activation loop of the kinase domain and stimulation of kinase activity. Following this process, additional tyrosine residues are phosphorylated providing docking sites for downstream signaling molecules containing phosphotyrosine binding (PTB) or Src homology 2 (SH2) domains and subsequent activation of downstream signaling pathways, e.g. MAPK and the phosphatidylinositol 3-kinase (PI3K) pathways. [45, 46, 48, 51-53]

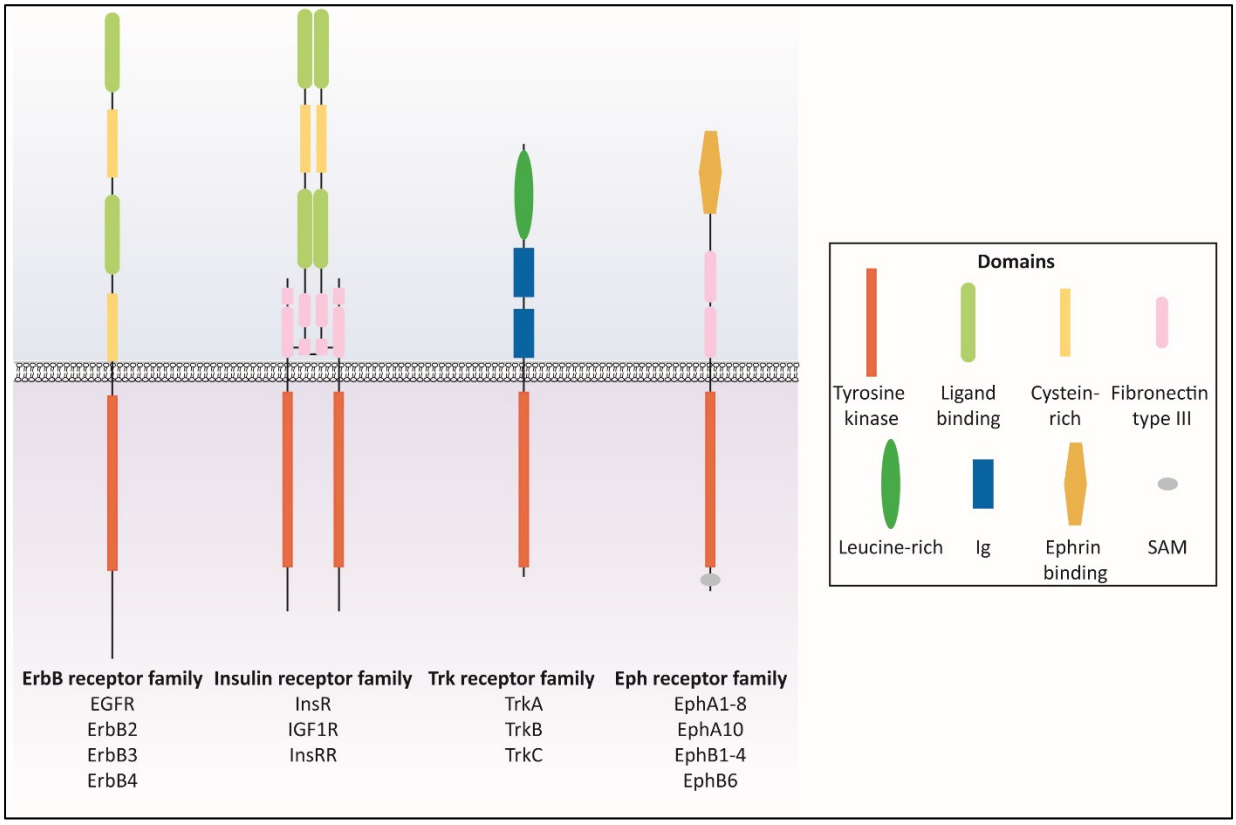

Figure 3: The ErbB, Insulin, Trk and Eph receptor tyrosine kinase families
Schematic view of the ErbB, insulin, Trk and Eph receptor families with mention of their family members. Extracellular structural domains which were identified by sequence and structure analysis, are according to the domain key. (Figure adapted from [46] with permission from Elsevier, copyright 2010)

3.2.2 The role of receptor-tyrosine kinases in cancer

Characteristic features of cancer cells include their ability to sustain chronic cell proliferation, to avoid cell death, to metastasize and invade normal tissue [44, 54]. It is therefore not surprising that the aberrant activation and deregulation of RTKs is found in a wide range of cancer entities and over 30 RTKs have been implicated in the disease so far [44, 52]. This abnormal activation and the deregulation can be the result of diverse changes in the receptors including mutations, overexpression, genomic translocations or disturbed receptor downregulation [44, 55, 56].

Mutations within the tyrosine kinase core domain, for example, can stabilize the active confirmation of the domain and thereby result in a constitutively active kinase [57]. Moreover, mutations in the kinase domain can result in an increased sensitivity of the RTK to its ligands and subsequent increased kinase activity [58]. Deletions altering the ligand-binding domains have been reported to result in truncated but constitutive active kinases [59]. Furthermore, genomic translocations of RTKs can result in the fusion of the tyrosine kinase domain to a

partner protein [60]. These fusion proteins can lead to a constitutive dimerization and activation of kinase activity independent of ligand binding. Additionally, the absence of the juxtamembrane domain in the fusion protein can further contribute to kinase activity. [61] Other ways cancer cells increase the RTK activity is by either overexpression of RTK ligands or RTKs themselves, by inhibition of tyrosine phosphatases or downregulation of RTK inhibitor proteins [53, 62]. This increased or permanent RTK activity leads to a higher and/or constant activation of downstream signaling pathways, e.g. PI3K/AKT and MAPK pathway and thereby to deregulated cell proliferation, apoptosis and migration leading to cancer development and progression [44].

3.2.3 Receptor-tyrosine kinases in MM

In recent years research has been starting to focus more on the role of RTKs in MM. As mentioned previously, activated RTKs play important roles in the oncogenesis of different cancer entities and are desirable targets for therapy [52, 53]. The common genetic translocation t(4;14) e.g. leads to an overexpression of functional fibroblast growth factor receptor 3 (FGFR3) in MM [63-65]. Additionally, activating *FGFR3* mutations have been reported in MM leading to malignant transformation of cells and to the activation of the MAPK pathway [65]. Another example is the RTK MET which is expressed by the majority of HMCL and by approximately half of primary tumors and has been shown to be necessary for hepatocyte growth factor (HGF) activated MAPK signaling in MM [66]. Other RTKs implicated in MM pathogenesis are the vascular endothelial growth factor receptor (VEGFR) [67] and the insulin-like growth factor 1 receptor (IGF1R) [68] (3.3.3). Moreover, a recent next-generation sequencing approach (NGS) found an accumulation of single nucleotide variants (SNV) in 15 out of 91 RTKs including *EGFR*, *ERBB3*, *NTRK1*, *NTRK2*, *IGF1R* and *EPHA2* [39].

3.3 The Insulin-like growth factor 1 receptor

3.3.1 Structure and function of IGF1R

The IGF1R is a RTK, one of the three members of the InsR family (Figure 3) and plays an important role in human and animal development [42, 46, 69]. The IGF1R gene is located on chromosome 15, is larger than 100 kilobases and contains a total of 21 exons coding for 1367 amino acids (aa) [70, 71]. In contrast to other RTKs, IGF1R exists as a disulfide-bound homodimer, consisting of two α and β chains, even in the absence of ligand binding [72]. The N-terminal part of the extracellular domain contains two homologous ligand-binding domains, separated by a cysteine-rich domain, whereas the C-terminal part contains three fibronectin type III domains. The intracellular domain of IGF1R contains a regulatory juxtamembrane region, followed by the tyrosine kinase domain and C-tail. [46, 73] Ligand binding to the extracellular subunits of the IGF1R leads to the autophosphorylation of tyrosine residues Y1131, Y1135 and Y1136 in the autophosphorylation loop of the intracellular tyrosine kinase domain. This autophosphorylation induces the phosphorylation of further tyrosine residues in the juxtamembrane domain and serine residues in the C-tail of IGF1R leading to the subsequent formation of binding sites for docking proteins. These docking proteins include the Src homology and collagen domain protein (SHC) and the Insulin receptor substrates 1 to 4 (IRS-1 to IRS-4). [74, 75] Binding of SHC to the phosphorylated IGF1R leads to the establishment of an SHC/Grb2/SOS complex and the subsequent activation of Ras. Activated Ras can now recruit Raf to the cell membrane where Raf is activated by phosphorylation. The activation of Raf leads to further downstream signaling by phosphorylation and activation of MEK which in turn phosphorylates ERK. Following its phosphorylation ERK can now activate diverse cytoplasmic and nuclear proteins resulting in enhanced cell proliferation (Figure 4). [76, 77] Activation of the PI3K/AKT pathway can be established by two mechanisms: the p85 subunit of PI3K either binds directly to the phosphorylated IGF1R or to the IRS docking proteins. The binding of the p85 subunits results in the activation of the p110 catalytic subunit and leads to the recruitment of the PI3K heterodimer to the plasma membrane. PI3K can now phosphorylate its substrate phosphatidylinositol 4,5-bisphosphate (PIP_2), converting it to phosphatidylinositol (3,4,5)-trisphosphate (PIP_3). PIP_3 recruits and activates PDK1 which can hereupon phosphorylate and thereby activate AKT. Activation of AKT leads, among others, to the phosphorylation of MTOR and BAD resulting in enhanced protein synthesis and inhibition of apoptosis, respectively (Figure 4). [76, 78]

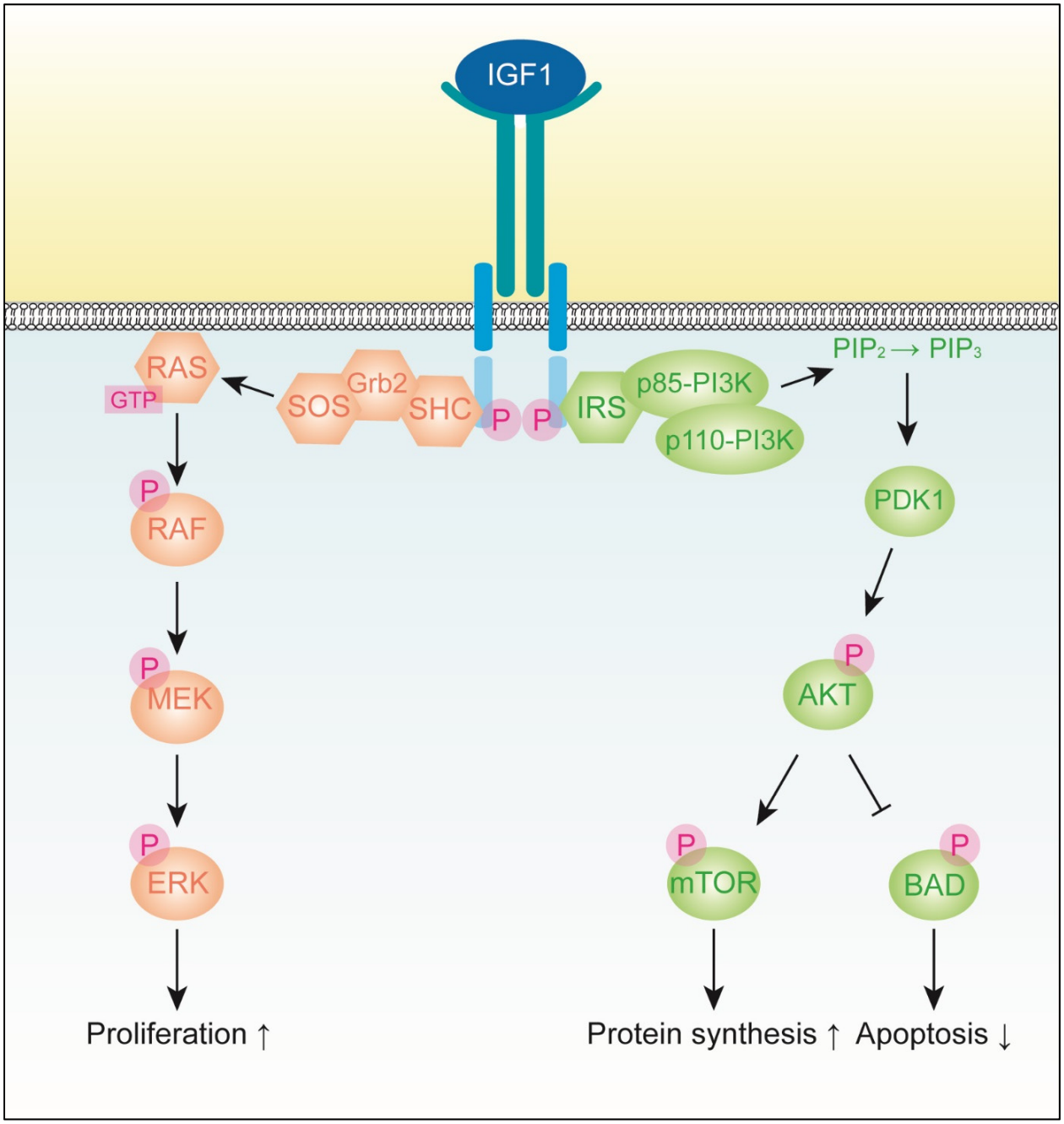

Figure 4: IGF1R mediated downstream signaling
Ligand binding leads to the phosphorylation and activation of IGF1R. Binding of the SHC/Grb2/SOS complex results in the activation of Ras and the subsequent phosphorylation and activation of the MAPK signaling effectors Raf, MEK and ERK. ERK can translocate to the nucleus and activate proteins important for proliferation. Binding of the adaptor protein IRS results in the activation of PIK3 and the conversion of PIP_2 to PIP_3 which in turn leads to PDK1 and AKT activation. Activated AKT can phosphorylate MTOR and BAD resulting in increased protein synthesis and decreased apoptosis. (Figure according to [74, 76, 78])

3.3.2 The role of IGF1R and its ligand IGF1 in cancer

IGF1R plays not only an important role in pre- and postnatal development but has, together with its ligand Insulin-like growth factor 1 (IGF1), also been implicated in a wide range of cancer entities, e.g. lung, colorectal, breast and prostate cancer [76, 79]. The expression of IGF1R is observed in up to 80 % of non-small cell lung cancer (NSCLC) cases, in up to 100 % of colorectal cancer cases and in about 26 % of breast cancer tumors [80]. In advanced NSCLC the expression of IGF1R has been postulated as an adverse prognostic event, leading to a shorter overall survival (OS) and progression-free survival (PFS) [81]. The co-expression of the receptor together with EGFR furthermore leads to a poor prognosis, a worse OS and a worse response to EGFR tyrosine kinase inhibitors [80-82]. In triple-negative breast cancer the expression of IGF1 and IGF1R significantly correlates with a poor response to therapy and increase in metastasis with IGF1 being an independent prognostic factor according to multivariate logistic regression analysis [80, 83]. Moreover, overexpression of IGF1R has been reported in approximately 40 % of breast cancer cases [84, 85] and has been shown to results in the malignant transformation of breast epithelial cells [86]. IGF1R overexpression studies in cell culture models of lung and prostate cancer have furthermore shown to result in increased cell survival, decreased apoptosis, enhanced tumor growth and enhanced cell migration [87, 88]. Overexpression of IGF1R is also observed in invasive urinary bladder cancer and is leading to higher motility of cancer cells [89]. A further demonstration of the importance of the IGF1-IGF1R axis is the fact that colorectal cancer cell lines show increased proliferation and growth upon IGF1 stimulation [90]. High levels of IGF1 have also been associated with an increased risk of developing prostate, pre-menopausal breast and colorectal cancer [79, 91]. The high levels of IGF1R and IGF1 in different cancer entities may also lead to the establishment of autocrine and paracrine signaling loops leading to the constitutive activation of downstream signaling pathways and the subsequent increase in proliferation, cell cycle progression and inhibition of apoptosis [76, 79, 80].

Genomic studies of *IGF1R* and *IGF1* identified *IGF1* polymorphism and single nucleotide polymorphisms (SNPs) that are associated with an increased breast cancer risk as well as an *IGF1R* SNP associated with an adverse prognosis [92-94]. Genetic variations of *IGF1* and *IGF1R* may also increase the risk of developing esophageal and lung cancer [95].

Taken together these results, as well as a high amount of other studies, highlight the important role of the IGF1-IGF1R axis in the development and progression of different cancer entities.

3.3.3 The role of the IGF1R system in MM

The IGF1R system has been demonstrated to play an important part in nearly all MM-specific cancer hallmarks such as homing to the BM, increased proliferation, cell survival, induction of bone disease and drug resistance (Figure 5) [96]. The importance of the IGF1R system for homing to the BM, e.g., is shown by the fact that MM cells display higher IGF1R levels after interaction with the BM microenvironment. Moreover, it was shown that MM cells display increased adhesion after IGF1 treatment by activating β1-integrin and the PI3K signaling pathway [97-99]. IGF1 is also an important growth factor in MM and induces the proliferation of MM cell lines [100, 101] and by upregulation of anti-apoptotic proteins, e.g. the Fas apoptosis inhibitory molecule, leads to an increase in cell survival [102, 103]. It was furthermore demonstrated that IGF1 facilitates vascular endothelial growth factor (VEGF) production of MM cells resulting in accelerated BM angiogenesis which is associated with poor prognosis [104, 105]. Preclinical studies have also shown that IGF1 can protect MM cells against anti-MM drugs such as dexamethasone or bortezomib [106, 107]. It is therefore not surprising that the increased expression of the IGF1-binding receptor IGF1R is associated with an adverse disease outcome in MM patients [68, 108].

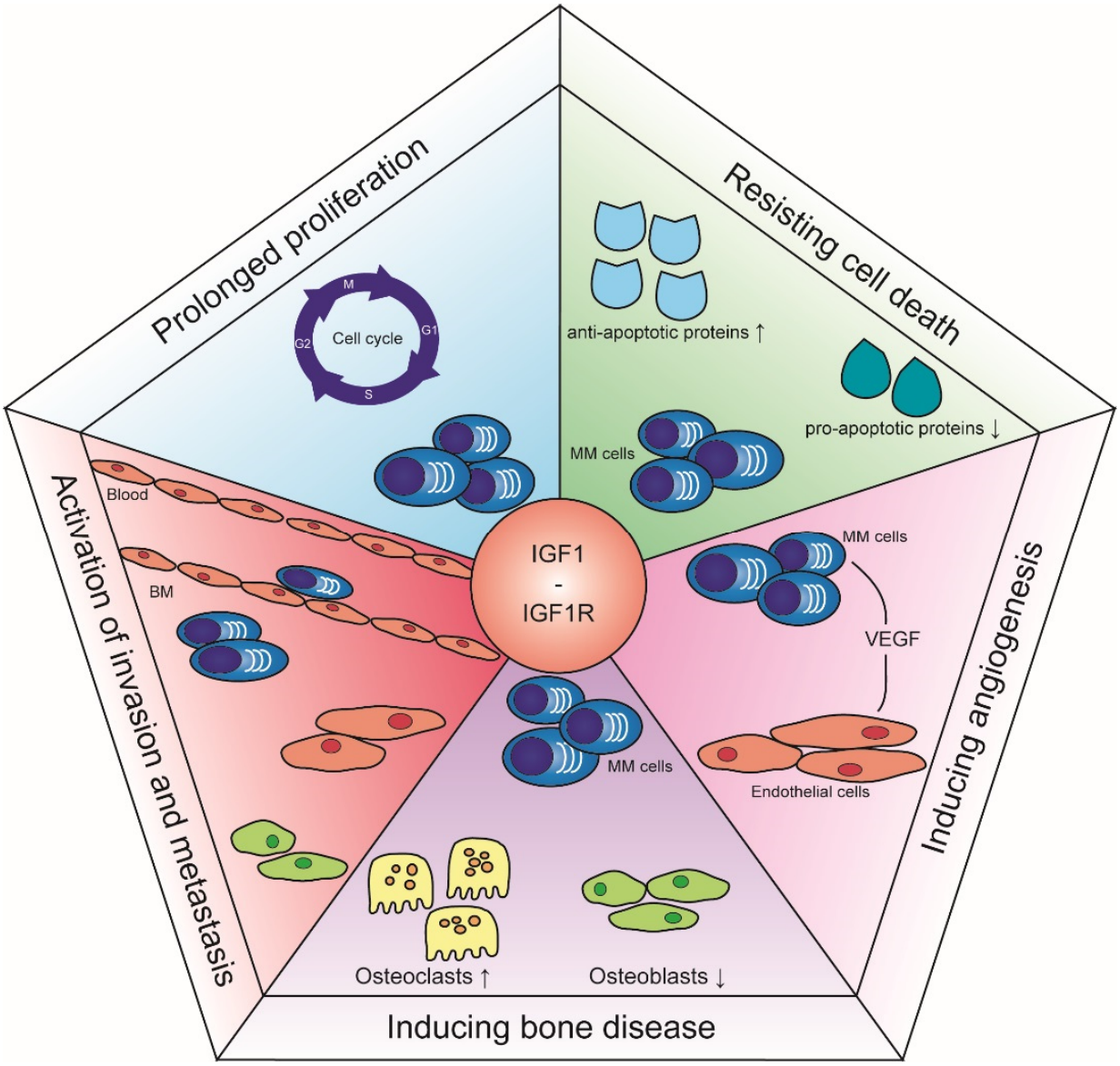

Figure 5: The role of the IGF1 system in hallmarks of MM
IGF1 and IGF1R are involved in the homing of MM cells to the BM by attracting the cells from the peripheral blood to the BM microenvironment. IGF1 has a high abundancy in the BM leading to increased cell proliferation of MM cells. IGF1 expression furthermore leads to an upregulation of anti-apoptotic proteins resulting in decreased cell death and resistance to anti-MM drugs. After IGF1 stimulation MM cells produce higher VEGF levels leading to increased angiogenesis. IGF1 also plays a direct role in MM bone disease by up- and downregulation of osteoclasts and osteoblasts, respectively. (Figure adapted from [96], no permission required under Creative Commons Attribution 3.0 License terms)

3.4 CRISPR/Cas9

The Clustered Regularly Interspaced Short Palindromic Repeats (CRISPR)/CRISPR-associated protein 9 (Cas9) technology is a novel genome engineering method enabling the precise modification of human genes [109]. The CRISPR/Cas system was first discovered as an RNA-mediated adaptive immune system in bacteria protecting the cells against foreign DNA [110]. Cas9 which belongs to the type II CRISPR system, was shown to be the only enzyme of the *cas* gene cluster capable of introducing DNA double strand breaks (DSB) [111]. CRISPR RNA (crRNA) containing the sequence of the desired genomic location, together with a transactivating CRISPR RNA (tracrRNA) which is essential for the maturation of the crRNA, are responsible for guiding the Cas9 nuclease towards the specific genomic location at which a DSB is generated [112-114]. For the successful targeting a protospacer-adjacent motif (PAM) adjacent to the RNA-binding site in the desired genomic target location is additionally required [115, 116]. Moreover, a single guide RNA (sgRNA) build of fused crRNA and tracrRNA can also facilitate Cas9-mediated DSB in mammalian cells [109, 117]. DSBs induced by the CRISPR/Cas9 system subsequently stimulate DSB repair mechanisms, either non-homologous end joining (NHEJ) or, in the presence of suitable donor DNA, homology directed repair (HDR) [116] (Figure 6). Due to the availability of a donor DNA, HDR can facilitate the precise repair of the generated DSB and has already been used to correct disease-associated genetic mutations [118, 119]. NHEJ on the other hand can introduce indel mutations at the repair site that frequently lead to subsequent frame shifts and gene disruption [120]. The NHEJ mechanism can be used for large gene function screens and has already been facilitated for the identification of genes necessary for cancer cell viability [121].

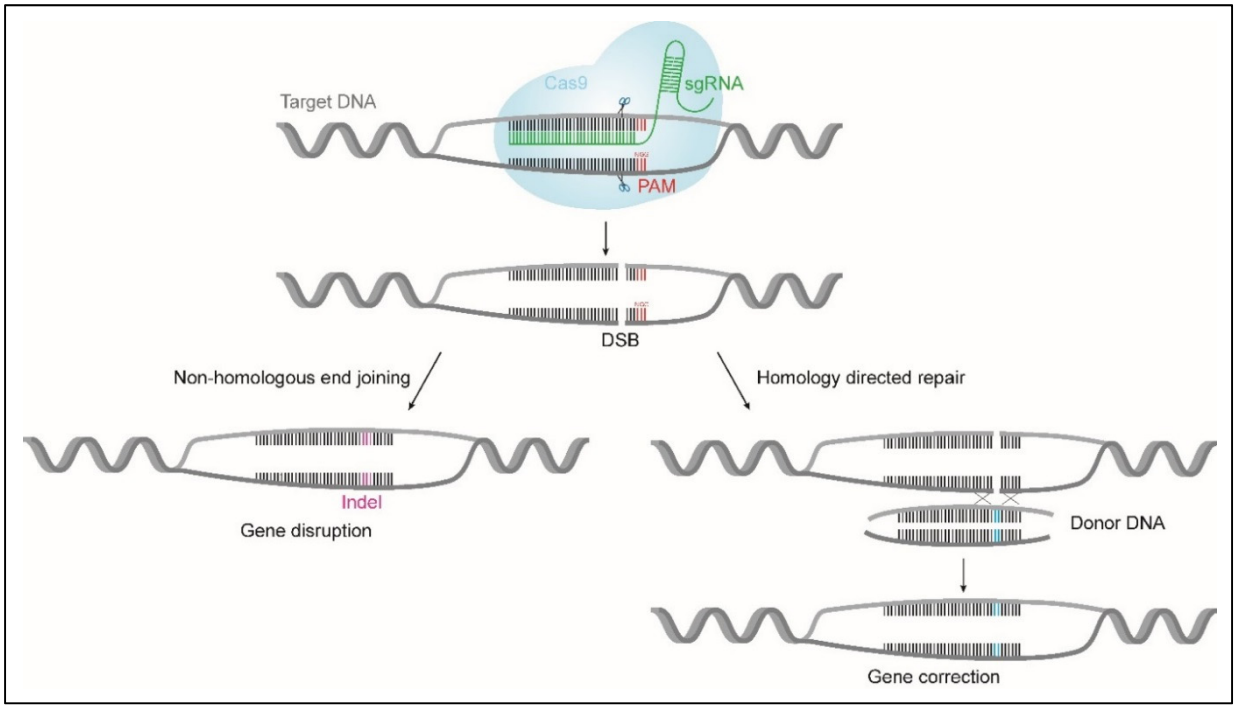

Figure 6: Targeted genome editing using CRISPR/Cas9
The Cas9 endonuclease is guided to a specific DNA sequence by the sgRNA containing the sequence of the desired genomic location which must be adjacent to a PAM site. Cas9 generates a DNA double-strand break (DSB) at the desired location which can be repaired by either non-homologous end joining (NHEJ) or homology directed repair (HDR). NHEJ can lead to indel mutations and subsequent gene disruption. HDR requires a donor DNA leading to the precise repair of the DSB and can be used for gene correction or insertion. (Figure according to [116, 122])

4 Aim of the thesis

MM is a largely incurable hematological malignancy characterized by the accumulation of monoclonal plasma cells in the bone marrow, hematopoietic insufficiency, bone lesions, hypercalcemia and a broad spectrum of heterogeneity. Recent next generation sequencing (NGS) approaches identified an accumulation of mutations in RTKs, adhesion molecules and associated signaling pathway molecules [39]. To further elucidate the role of RTKs in the development and progression of MM, the six RTKs *EPHA2*, *EGFR*, *ERBB3*, *IGF1R*, *NTRK1* and *NTRK2*, which were previously identified to be mutated in MM patients, were deep-sequenced in a uniformly treated patient cohort of the DSMM XI. One of the aims of this thesis was the validation of the identified mutations and their correlation with cytogenetic events and clinical data as well as the validation of these findings in another clinical cohort of the DSMM.

Even though NGS approaches identified numerous mutations in MM [35, 36, 38] only a small amount of studies dealt with the effect of these mutations on MM cells. Therefore, another aim of this thesis was the functional investigation of selected mutations (IGF1R D1146N and IGF1R N1129S) by overexpression and knockdown studies. For this purpose novel technologies such as the transposon-based Sleeping Beauty system as well as the genome editing tool CRISPR/Cas9 should be established and modified for the construction of stable human myeloma cell lines. These genetically engineered cell lines should subsequently be used to study the mutations' effect on receptor activity, downstream signaling and cell proliferation.

5 Material

5.1 MM patient samples

5.1.1 DSMM XI

The “Deutsche Studiengruppe Multiples Myelom” (DSMM) XI study cohort consisted of 75 primary MM samples taken from newly diagnosed patients at initial diagnosis. Corresponding normal samples, if available, were collected from peripheral blood, bone marrow aspirates or paraffin embedded tissue. Patients were treated with a combination therapy of bortezomib, dexamethasone and cyclophosphamide, followed by stem cell mobilization, high-dose chemotherapy and autologous stem cell therapy.[123] Clinical and fluorescence *in situ* hybridization (FISH) data were available for most patients (OS: n=70, EFS: n=69, PFS: n=64, response after bortezomib and HDC: n=67 and n=66). The study was approved by the Ethics Committee of the Medical Faculty, University of Würzburg (reference number: 18/09, approval renewed: 09.03.2009, reference number AZ 76/13, date of approval: 18.04.2013) and University of Ulm (application number: 307/08, date of approval: 21.01.2009). [40, 123, 124]

5.1.2 DSMM XII

The DSMM XII study cohort consisted of 75 MM and 185 normal samples from newly diagnosed MM patients taken at initial diagnosis. Patients were treated with four cycles of a lenalidomide, adriamycin, and dexamethasone (RAD) induction therapy followed by a risk-adapted stem cell transplantation and lenalidomide maintenance. Clinical and FISH data was provided. The trial is registered at ClinicalTrials.gov NCT00925821 and EudraCT Number: 2008–000007–28. All patients gave written informed consent. [125, 126]

5.2 Cells

5.2.1 Human cell lines

The human multiple myeloma cell lines (HMCL) AMO1, JJN3, KMS11, KMS12BM, L363, MOLP8, NCIH929, OPM2, RPMI8226 and U266 were purchased from the Leibniz Institute DSMZ (German Collection of Microorganisms and Cell Cultures) (Braunschweig, Germany). The HMCL MM1.S was purchased from LGC Biolabs (Wesel, Germany) and the HMCL INA6 was a

gift from Prof. Martin Gramatzki (Kiel, Germany). The human embryonal kidney cell line HEK293FT was purchased from Thermo Fisher Scientific (Darmstadt, Germany).

5.2.2 Prokaryotic cells

Chemical competent *E. coli* NEB10β were purchased from New England Biolabs (Frankfurt, Germany), chemical competent *E. coli* α-Select Silver competent cells were purchased from Bioline (Luckenwald, Germany).

NEB10β: Δ*(ara-leu) 7697 araD139 fhuA* Δ*lacX74 galK16 galE15 e14-* φ*80*d*lacZ*Δ*M15 recA1 relA1 endA1 nupG rpsL* (Str^R) *rph spoT1* Δ*(mrr-hsdRMS-mcrBC)*

α-Select Silver Competent Cells: F- *deo*R *end*A1 *rec*A1 *rel*A1 *gyr*A96 *hsd*R17(rk-, mk+) *sup*E44 *thi*-1 *pho*A Δ(*lac*ZYA-argF)U169 Φ80*lac*ZΔM15 λ-

5.3 Media for bacteria and cell culture

5.3.1 Cell culture media

Table 2: Media for human cell culture

Name	Manufacturer
RPMI 1640, no glutamine	Thermo Fisher, Darmstadt, Germany
DMEM, high glucose	Thermo Fisher, Darmstadt, Germany
Opti-MEM I Reduced Serum Medium	Thermo Fisher, Darmstadt, Germany
Sodium Pyruvate (100 mM)	Thermo Fisher, Darmstadt, Germany
MEM Non-Essential Amino Acids Solution (100X)	Thermo Fisher, Darmstadt, Germany
FBS, EU Professional	PAN-Biotech GmbH, Aidenbach Germany
L-Glutamine 200mM	PAN-Biotech GmbH, Aidenbach Germany

Complete medium consisted of RPMI 1640 medium supplemented with 10 % filtered bovine serum (FBS) and 2 mM L-glutamine. Electroporation medium was supplemented with 15 % FBS, 2 mM L-glutamine and 1x Penicillin/Streptomycin (P/S). DMEM was supplemented with 10 % FBS, 0.5 mg/ml Geneticin, 6 mM L-glutamine, 1 mM Sodium Pyruvate und 1x MEM Non-Essential Amino Acids containing 0.1 mM glycine, 0.1 mM L-alanine, 0.1 mM L-asparagine, 0.1 mM L-aspartic acid, 0.1 mM L-glutamic acid, 0.1 mM L-proline and 0.1 mM L-serine.

Starvation medium for MM cells consisted of RPMI 1640 medium supplemented with 0.5 % FBS and 2 mM L-glutamine, starvation medium for HEK293FT cells consisted of DMEM supplemented with 0.5 % FBS and 6 mM L-glutamine.

Freezing medium for MM cells consisted of 70 % RPMI 1640, 20 % FBS and 10 % DMSO.

5.3.2 *E. coli* media

Table 3: Media for bacterial cell culture

Name	Manufacturer
LB Broth	Carl Roth, Karlsruhe, Germany
LB Agar	Carl Roth, Karlsruhe, Germany
SOC Outgrowth Medium	New England Biolabs, Frankfurt, Germany

25 g LB broth dry powder was dissolved in 1 L H_2O, autoclaved for 20 min at 121°C and 103 kPA and stored at 4°C. LB plates consisted of 40 g LB Agar dry powder dissolved in 1 L H_2O, autoclaved for 20 min at 121°C and 103 kPA and supplemented with either Kanamycin with a final concentration of 50 mg/L, Ampicillin with a final concentration of 100 mg/L or Chloramphenicol with a final concentration of 25 mg/L. Dry LB plates were stored at 4°C.

5.3.3 Antibiotics

Table 4: Antibiotics for human and bacterial cell culture

Name	Final concentration	Manufacturer
Ampicillin	100 mg/L	Carl Roth, Karlsruhe, Germany
Kanamycin	50 mg/L	Carl Roth, Karlsruhe, Germany
Geneticin	0.5 mg/ml	Thermo Fisher, Darmstadt, Germany
Penicillin/Streptomycin	100 U/ml/0.1 mg/ml	PAN-Biotech GmbH, Aidenbach Germany
Puromycin	Cell line dependent	Carl Roth, Karlsruhe, Germany
Chloramphenicol	25 mg/L	Carl Roth, Karlsruhe, Germany

5.4 Oligonucleotides

5.4.1 Primer

For the amplicon library preparation multiplex primers were designed and manufactured by Fluidigm (Munich, Germany). LNA primers were manufactured by GATC (Konstanz, Germany). All other primers were purchased from either Integrated DNA Technologies (Leuven, Belgium) or Eurofins Genomics (Ebersberg, Germany).

Table 5: Primers for amplicon library preparation

Primer		Sequence	°C T_M	% GC	Product Length
EGFR_Exon 1_1	F	CCCTGACTCCGTCCAGTATTGAT	62	52	171 bp
	R	GGGAGCCGGCGAGACA	61	75	
EGFR_Exon 2_1	F	CCTGGACCTTGAGGGATTGTTTT	61	48	180 bp
	R	CCAAGGACCACCTCACAGTTATT	60	48	
EGFR_Exon 2_2	F	GAGTAACAAGCTCACGCAGTTG	60	50	196 bp
	R	TTTCTCCACTTAGATTTTCTCCAATTTT	58	29	
EGFR_Exon 3_1	F	CCCTGGACCCATTTTAGACCTTG	61	52	198 bp
	R	ACTGCTAAGGCATAGGAATTTTCG	59	42	
EGFR_Exon 3_2	F	ACACAGTGGAGCGAATTCCTTTG	62	48	189 bp
	R	TGTCTGCATTTATGAACCCCCAG	61	48	
EGFR_Exon 4_1	F	GCTCACCGCAGTTCCATTCT	61	55	199 bp
	R	GAGCTGGAGGCAGAGATAGTG	60	57	
EGFR_Exon 5_1	F	AAGGGCGTCATCAGTTTCTCATC	61	48	192 bp
	R	TAAGCAAGTGAAGGAAGAGAGGG	60	48	
EGFR_Exon 6_1	F	TGGGAAATGATCCTACCCTCACT	61	48	183 bp
	R	ATCTTACCAGGCAGTCGCTCTC	62	55	
EGFR_Exon 6_2	F	TCAGTGACCAAAATCATCTGTGC	60	43	200 bp
	R	AAGTCTTCTGTCCTGGTGTGGG	62	55	
EGFR_Exon 7_1	F	GCTTTCTGACGGGAGTCAACA	61	52	192 bp
	R	GGGTTCACATCCATCTGGTACG	61	55	
EGFR_Exon 7_2	F	CTCCATAGGTCTGCCGCAAATTC	62	52	195 bp
	R	ACAAGGATGCCTGACCAGTTAGA	61	48	
EGFR_Exon 8_1	F	ACCTTCCTTTCATGCTCTCTTCC	60	48	193 bp
	R	CCTCAGCAGCCGAGAACAA	60	58	
EGFR_Exon 9_1	F	GAATTCCTTCCTGCTTCCCTCTG	61	52	185 bp
	R	CACTGATGGAGGTGCAGTTTTTG	61	48	
EGFR_Exon 9_2	F	CTGCAGTGTGTAACGGAATAGGT	61	48	192 bp
	R	ACCAGTTAAAAAGGCAGATTTTGTTT	59	31	
EGFR_Exon 10_1	F	TGCCTTTTTAACTGGTAGAGATTGGT	61	39	186 bp
	R	TCTCTCTCTAAAACACTGATTTCCCA	60	39	
EGFR_Exon 11_1	F	ACAAAAAAGAAACTCCTACGTGGT	59	38	179 bp
	R	TAATCTACCAGGCTTTGGCTGTG	61	48	
EGFR_Exon 12_1	F	TCACCACATGATTTTTCTTCTCTCCA	61	39	187 bp
	R	CGGAGGTCCCAAACAGTTTTTTC	60	48	
EGFR_Exon 12_2	F	TACGCTCCCTCAAGGAGATAAGT	60	48	200 bp
	R	AGGACCCATTAGAACCAACTCCA	61	48	
EGFR_Exon 13_1	F	CCTCGGGTCCCTGCTCT	60	71	181 bp
	R	CCAGAAGGTTGCACTTGTCCAC	62	55	
EGFR_Exon 13_2	F	AGGTCTGCCATGCCTTGTG	59	58	188 bp
	R	AGCTATAACAACAACCTGGAGCC	61	48	
EGFR_Exon 14_1	F	CCTGCAATAATGTCTCAGGGGTG	62	52	184 bp
	R	TCCCATGAAATGGACGTGGATAG	61	48	
EGFR_Exon 15_1	F	CCATTTTGAAAGAGAAAAGAAAGAGACAT	60	31	164 bp
	R	CTTCCAGACCAGGGTGTTGTTTT	61	48	
EGFR_Exon 15_2	F	GCAGGGACCAGACAACTGTATC	62	55	191 bp
	R	TGTTCTGTTCTCCTTCACTTTCCA	59	42	
EGFR_Exon 16_1	F	TGGGTTTTGGCATTTTCAATACACTT	58	35	174 bp
	R	AGTGGGAGACTAAAGTCAGACAG	61	48	
EGFR_Exon 17_1	F	TTATAGTGTTACACCAGGGCTCC	61	48	173 bp
	R	GCTGGGCTCCCGCTCT	59	75	
EGFR_Exon 17_2	F	AGTCTCAAAGCCATGTTATTCTGC	59	42	165 bp
	R	GCATCCACCCCAACCCAG	61	67	

EGFR_Exon 17_3	F	CTGCTCAGGAGTCATGCTTAGG	62	55	186 bp
	R	AGGGGTGGCAGAAAGGAAAAG	60	52	
EGFR_Exon 18_1	F	AAATCTCCAAAATATATGCCAAAGAAGT	58	29	188 bp
	R	AAATGCAGGAAAGCATCTTCACC	59	43	
EGFR_Exon 19_1	F	ATGCAGGGGCGTGTTGAG	58	61	174 bp
	R	GGCGCCTTCGCATGAAGAG	61	63	
EGFR_Exon 19_2	F	ACCTCATTCCAGGCCTAAGATCC	62	52	185 bp
	R	GCTCCTGAGCCCACCCA	60	71	
EGFR_Exon 20_1	F	CATGGTGAGGGCTGAGGTG	60	63	188 bp
	R	TGCCAGGGACCTTACCTTATACA	61	48	
EGFR_Exon 20_2	F	CTCTTACACCCAGTGGAGAAGC	60	55	175 bp
	R	CTCCCCACCAGACCATGAGA	61	60	
EGFR_Exon 21_1	F	GCATGTGGCACCATCTCACAAT	62	50	182 bp
	R	CCCCACACAGCAAAGCAGAAA	62	52	
EGFR_Exon 22_1	F	GTCTTCACCTGGAAGGGGTC	60	60	191 bp
	R	GGCAGCCGAAGGGCAT	60	69	
EGFR_Exon 22_2	F	TCCAGGAAGCCTACGTGATG	60	55	196 bp
	R	ATTACCTTTGCGATCTGCACACA	61	43	
EGFR_Exon 22_3	F	GCAGCTCATGCCCTTCG	59	65	174 bp
	R	TCCCAGGAGCGCAGAC	58	69	
EGFR_Exon 23_1	F	CTGGCATGAACATGACCCTGAA	61	50	186 bp
	R	CCAAAATCTGTGATCTTGACATGCTG	61	42	
EGFR_Exon 23_2	F	GCCAGGAACGTACTGGTG	58	61	192 bp
	R	TGTGTTAAACAATACAGCTAGTGGG	59	40	
EGFR_Exon 24_1	F	ACTTTTTCCAACAGAGGGAAACTAA	59	36	178 bp
	R	GGCCTCAGTACAAACTCATTAGCA	61	46	
EGFR_Exon 25_1	F	TGATGACTAAAGCAAGGGATTGTGA	61	40	176 bp
	R	GAGGGAGGCGTTCTCCTTTC	60	60	
EGFR_Exon 25_2	F	TTTGGGAGTTGATGACCTTTGGA	60	43	175 bp
	R	CAGCTAGGCAGTGTGGACAG	60	60	
EGFR_Exon 26_1	F	AGCAATGCCATCTTTATCATTTCTT	58	32	199 bp
	R	TCTTCCCAATGGAAGCACAGAC	61	50	
EGFR_Exon 27_1	F	CTGCTCCTATAGCCAAGAAGTGG	60	52	190 bp
	R	CCTGCTGTGGGATGAGGTACT	61	57	
EGFR_Exon 27_2	F	TTGCCAAGTCCTACAGACTCCAA	62	48	196 bp
	R	TGAGTAGACACAGCTTGAGAGAGA	61	46	
EGFR_Exon 28_1	F	AGTGGATGAGATGTGGTACAAGC	61	48	168 bp
	R	TCCATGTAAAATAGAGCCATAGTGGA	60	38	
EGFR_Exon 29_1	F	CGGAGTAACCTTCCCTCATTTCC	62	52	171 bp
	R	GAGCAGGACTGTTTCCAGACAAG	62	52	
EGFR_Exon 30_1	F	TTGAGGACATTCACAGGGTTC	58	48	200 bp
	R	TCCTGGTAGTGTGGGTCTC	59	58	
EGFR_Exon 30_2	F	GCTCTGTGCAGAATCCTGTCTAT	61	48	190 bp
	R	CTAATTTGGTGGCTGCCTTTCTG	61	48	
EGFR_Exon 30_3	F	GCAACCCCGAGTATCTCAACAC	62	55	183 bp
	R	CATTTTCAGCTGTGGAGCCCTTA	61	48	
EGFR_Exon 30_4	F	CTGGACAACCCTGACTACCAG	62	57	192 bp
	R	CTTGGTCCTGGGTATCGAAAGAG	62	52	
EPHA2_Exon 1_1	F	TATTCTTGGCCGATGGGGCTC	62	57	187 bp
	R	CTGCTCCAGCCCCTAACTCT	61	60	
EPHA2_Exon 2_1	F	GCAGCCTCTGGAGTGGGA	61	67	163 bp
	R	GCACGGTGTCCGAGTGG	60	71	
EPHA2_Exon 2_2	F	CATCTGCACCACCTTCTCGATG	62	54	174 bp
	R	CTCACCTGCAGTGCTTCCT	59	58	
EPHA2_Exon 3_1	F	AATTGAGGTCATCATGGGCAGAG	61	48	181 bp

	R	CCCCTCCGCCATCTACCAG	63	68	
EPHA2_Exon 3_2	F	TTGTCCAGGATGCTGACGATG	60	52	198 bp
	R	CAGAGGGTTTCAGTGGCTTTCTG	62	52	
EPHA2_Exon 4_1	F	CCCCTGCAGTTTGAGATGAGTAA	61	48	186 bp
	R	CCATTTCCTACCGGAAGTTCACC	62	52	
EPHA2_Exon 4_2	F	CGTGGTTGGACAACTCCCAG	61	60	188 bp
	R	CCAGAGGGCACAGTGGTGA	61	63	
EPHA2_Exon 5_1	F	ACCATGCAGGGCGAAGG	58	65	192 bp
	R	ACCTGGCCAACATGAACTATGTG	61	48	
EPHA2_Exon 5_2	F	CAGGCCAAAGTCAGACACCTT	60	52	189 bp
	R	AGCTGAGCGCCTGTGC	57	69	
EPHA2_Exon 6_1	F	GGCCAGCCCTGAACCC	59	75	176 bp
	R	GCCCACTTACCTCTCACCTG	61	60	
EPHA2_Exon 7_1	F	GACAGAGCCCCTGCTAAGTG	61	60	186 bp
	R	GTGGCCATCAAGACGCTGAAAG	62	55	
EPHA2_Exon 7_2	F	GGATGATGTTGTGGTGGCTGAA	60	50	192 bp
	R	CACTCCCCTGACCCTGTCT	61	63	
EPHA2_Exon 8_1	F	CCCACACTGTGTCACCACC	61	63	182 bp
	R	AACTGAAGCCCCTGAAGACATAC	61	48	
EPHA2_Exon 8_2	F	ACCTGCTCCGATCACCTTCT	59	55	164 bp
	R	CTGAGCTGCCTGTGACCC	61	67	
EPHA2_Exon 9_1	F	CAGTGCCCTGGGAACACC	61	67	191 bp
	R	CTGACCTCCCTGCATTTGGTTC	62	55	
EPHA2_Exon 10_1	F	GCCCCATTTTCCCACCCAAG	61	60	191 bp
	R	GGGAACTCCCTTGTCATCAGC	62	57	
EPHA2_Exon 11_1	F	CCAAGATGTCTCAATTGCTTGGT	59	43	183 bp
	R	GTTTCTCCGTGACCCTGGAC	61	60	
EPHA2_Exon 11_2	F	GGAATTCGTGCACCTTGCT	57	53	192 bp
	R	CTGCCCTGCCCTCACT	57	69	
EPHA2_Exon 12_1	F	CAGAAGGGTGCTTCTTCAGATGG	62	52	191 bp
	R	CACCTCGCTTAGCGTCTCC	61	63	
EPHA2_Exon 12_2	F	TTCTTGCGGTAAGTGACCTCGTA	61	48	159 bp
	R	TAGGCAGCTTCTTACCCACTTCC	62	52	
EPHA2_Exon 13_1	F	TCCTCCTTAAGCCCCACCTG	61	60	164 bp
	R	CCCCACATGAACTACACCTTCAC	62	52	
EPHA2_Exon 13_2	F	CTGTCTGGTTGATGCTGACACT	60	50	162 bp
	R	GCTACTCGGAGCCTCCTCAC	63	65	
EPHA2_Exon 13_3	F	TCCACGGTGAAGGTGTAGTTC	60	52	192 bp
	R	GCCCCCTCAGGACAGC	59	75	
EPHA2_Exon 13_4	F	GCACTGTTCGCAGGTGACG	61	63	160 bp
	R	CAGCACAGCACTGACTCCTC	61	60	
EPHA2_Exon 14_1	F	CGGACACGTCACCCTCAGT	61	63	175 bp
	R	CATCTGAGAGCCCCTGCTTG	61	60	
EPHA2_Exon 14_2	F	CTGAGGTGCCCGGAAGAAG	61	63	173 bp
	R	TGAACTGATGTCCTTGTGCTCTG	61	48	
EPHA2_Exon 15_1	F	CCTGGGAATGCAGAACCC	58	61	192 bp
	R	CCGGCACCTGTGTGGA	57	69	
EPHA2_Exon 15_2	F	GCACAGGCACTGCCCAAT	58	61	168 bp
	R	GGCCTGGCCCACTTCC	59	75	
EPHA2_Exon 15_3	F	CACAGTGGCCAGGGAAGG	61	67	162 bp
	R	CTCACCCGCAAAGGCTTCTA	59	55	
EPHA2_Exon 15_4	F	TTGTAGTAGACACGGACGGAGAG	62	52	186 bp
	R	CCTGTTCACCAAGATTGACACCA	61	48	
EPHA2_Exon 15_5	F	CGTGGCGTGCCTCGAA	57	69	189 bp
	R	TCAAGTTTACTGTACGTGACTGC	59	43	

EPHA2_Exon 15_6	F	CGACTCGGCATAGTAGAGGTTGA	62	52	174 bp
	R	GTGTGCAACGTGATGTCTGG	59	55	
EPHA2_Exon 15_7	F	GAGCTCAATGAAGATACGCTCA	58	45	177 bp
	R	CACCTGCCCACACTAACCTG	61	60	
EPHA2_Exon 16_1	F	GACCAGCAGCCCCATTCTC	63	58	173 bp
	R	GGTCTGACTCCTGAAGACACC	62	57	
EPHA2_Exon 17_1	F	TGCGCGCGTCAAGGAG	57	69	190 bp
	R	GATCGGACCGAGAGCGAGAAG	64	62	
IGF1R_Exon1_1	F	TGAGAAAGGGGAATTTCATCCCAAA	61	40	182 bp
	R	AGCCCCTCGGAGGAAAAGT	59	58	
IGF1R_Exon2_1	F	TGAAAACCAACTGTATTATTGTTTGGAA	58	29	198 bp
	R	TCCTCGGCCTTGGAGATGAG	61	60	
IGF1R_Exon2_2	F	ATCCGCAACGACTATCAGCAG	60	52	192 bp
	R	GTTGGGGAAGAGGTCTCCG	61	63	
IGF1R_Exon2_3	F	CTTCCCCAAGCTCACGGTCATTA	62	52	183 bp
	R	TTCCTCAGGTTGTAAAGCCCAAT	59	43	
IGF1R_Exon2_4	F	CGGCTGGAAACTCTTCTACAACT	61	48	186 bp
	R	ATGTAGTTATTGGACACCGCATC	59	43	
IGF1R_Exon2_5	F	TTGGGCTTTACAACCTGAGGAAC	61	48	190 bp
	R	ATCGGCTTCTCCTCCATGGTC	62	57	
IGF1R_Exon2_6	F	AACTACATTGTGGGGAATAAGCC	59	43	191 bp
	R	AGAGGAGAGAGAGAGGCAGA	59	55	
IGF1R_Exon3_1	F	CCAGGCCCAGAGAAGGC	60	71	188 bp
	R	GTAGTGGCGGCAAGCTACAC	61	60	
IGF1R_Exon3_2	F	CGTGCACCGAGAACAATGAGT	60	52	178 bp
	R	CAGAAGTCACGGTCCACACAG	62	57	
IGF1R_Exon3_4	F	CCGCCCAACACCTACAG	58	65	200 bp
	R	GTGGGGCGGGTAGTGA	57	69	
IGF1R_Exon4_1	F	AATGCAAGAAGACAGACTCAATTATG	58	35	189 bp
	R	GAGCAAATTGCCCTTGAAGATGG	61	48	
IGF1R_Exon4_2	F	GTACTGCATCCCTTGTGAAGGTC	62	52	184 bp
	R	GAGATCTAGCCGTTTTTCCAGGG	62	52	
IGF1R_Exon5_1	F	TCCAAGTATGTCACCCTTACACC	61	48	188 bp
	R	CCTAGGATGAGGCGAAGGTTTTT	61	48	
IGF1R_Exon5_2	F	CAGAGCTGGAGAACTTCATGG	60	52	164 bp
	R	AACGTCAGCTCATGAAATTTGGG	59	43	
IGF1R_Exon6_1	F	GCAAAGAGGACCTGTGTTACGTG	62	52	182 bp
	R	GTACATTTTCCCTGCTTTGATGGT	59	42	
IGF1R_Exon6_2	F	TACTCCTTCTACGTCCTCGACAA	61	48	192 bp
	R	GTTCCTGGTGTTTATGTCCCCTT	61	48	
IGF1R_Exon6_3	F	AAAATGTACTTTGCTTTCAATCCCA	56	32	192 bp
	R	GGAGGAGGGTCTGCTGTTATC	62	57	
IGF1R_Exon7_2	F	CTGTCACTCACGGATGTACTCTT	61	48	186 bp
	R	AATGGCATCACCCAAAGCAGAAA	59	43	
IGF1R_Exon8_1	F	TTTTTGAGGGTTTTGATGTCAGAG	58	38	184 bp
	R	TTCAGCCCATGTAGTAAGATGCC	61	48	
IGF1R_Exon8_2	F	ATGCCTGCGGCTCCAA	54	63	192 bp
	R	TGCGAATGTACAAGATCTCACTC	59	43	
IGF1R_Exon8_3	F	GGCATCTTACTACATGGGCTGAA	61	48	200 bp
	R	ACAAGCAAGGCCAGTGAG	56	56	
IGF1R_Exon9_1	F	AGAGTATCTGATAGCCTGACTCTT	59	42	178 bp
	R	CACAATGTAGTAACTCAGGTTGCC	61	46	
IGF1R_Exon9_2	F	TCTTTCAGCATCGAACTCCTCTT	59	43	192 bp
	R	GAATGAACGGTCACACCCTC	59	55	
IGF1R_Exon10_1	F	GCATGTATAACGGCTTTCATTCCC	61	46	189 bp

	R	CTGCTTCTCGGCTTCAGTTTTGG	62	52	
IGF1R_Exon10_2	F	GAGGTCACAGAGAACCCCAAG	62	57	199 bp
	R	CAGTGGGTTTTGCCAACTGAAAT	59	43	
IGF1R_Exon11_1	F	TCAAGTCATAGAAAAGACAAAAGAGGTAA	60	31	191 bp
	R	GGGTACTCTGTCTCCAGCTCTTC	64	57	
IGF1R_Exon11_2	F	CAAGTGGCCAACACCACCAT	59	55	185 bp
	R	CTGTGGATATCGATGCGGTACA	60	50	
IGF1R_Exon11_3	F	AGAGTGGATAACAAGGAGAGAACTG	61	44	192 bp
	R	TAGGTTGTGAGGAAGGTGGCAAT	61	48	
IGF1R_Exon12_1	F	TTATTCTCAGGTCAGCCCAGT	72	48	178 bp
	R	TCAATCCATTGGGATTCTCAGGTT	59	42	
IGF1R_Exon12_2	F	GGAGCAGATGACATTCCTGGG	62	57	192 bp
	R	CATATGCTGTCAATGGATGGAAGT	59	42	
IGF1R_Exon13_1	F	CAGTGTGGTGAGTTTAGTTGGC	60	50	192 bp
	R	CAGAGAGAGATGTGGCCTGAAT	60	50	
IGF1R_Exon13_2	F	AGGAAGTATGGAGGGGCCAAG	62	57	180 bp
	R	GGACCACCCTGCTTTCAGTTTT	60	50	
IGF1R_Exon14_1	F	ACCTGGTGATATTTTATCATTTCCTCCT	61	36	160 bp
	R	ACTTTGCACATCACTGACCTCTT	59	43	
IGF1R_Exon14_2	F	TTCATCCATCTGATCATCGCTCT	59	43	161 bp
	R	TCACCTTCACTCACATTCAAATCA	58	38	
IGF1R_Exon15_1	F	ACCGTGTGAGAGAGGATAAATGA	59	43	188 bp
	R	CCGGACTCTTACCATCAGCAG	62	57	
IGF1R_Exon15_2	F	GAGTGCTGTATGCCTCTGTGAAC	62	52	177 bp
	R	GACAGATCCAAGGCCAAAGGTAG	62	52	
IGF1R_Exon16_1	F	ACGTTCTGTCTAAGGGCTTGTTT	59	43	180 bp
	R	TCAGGTTCATCTTTCACCACACC	61	48	
IGF1R_Exon16_2	F	CGGTTTCTTCTCCAGTGTACGTT	61	48	174 bp
	R	CGGCCTCGTTCACTGTTTTAATG	61	48	
IGF1R_Exon16_3	F	GGTGTGGTGAAAGATGAACCTGA	61	48	185 bp
	R	TTGTGTGATACCCTCTCCCTGTG	62	52	
IGF1R_Exon17_1	F	CAGAGACAGTTCCAGACAACACA	61	48	178 bp
	R	CCTCAGAGACCGGAGATAACTTT	61	48	
IGF1R_Exon17_2	F	CTGGGTGTGGTGTCCCAA	58	61	192 bp
	R	TTAAAGACACAGCATTTCCTTGC	57	39	
IGF1R_Exon18_1	F	TGCAAACCTCGAAAGAAATTGGC	59	43	183 bp
	R	TCTCTGTGGACGAACTTATTGGC	61	48	
IGF1R_Exon18_2	F	AAGATGATTCAGATGGCCGGAG	60	50	192 bp
	R	GCCAACAAAGTCCTCAAAACACC	61	48	
IGF1R_Exon19_1	F	AATGAGTGTAGGGTCCTCTGCTG	62	52	178 bp
	R	CCTTGAGGGACTCAGGAGACAT	62	55	
IGF1R_Exon19_2	F	GCCCTCTCTTCCCTTACAGATTT	61	48	177 bp
	R	GCTGGCAATGCAGTAAAGGTTC	60	50	
IGF1R_Exon20_1	F	TGTAAGAAGTGCTGGAAAGGAGG	61	48	174 bp
	R	CCATGACGAAGCGAAGGACTTG	62	55	
IGF1R_Exon20_2	F	CCTGTAGGTCCTTCGGGGTC	63	65	188 bp
	R	TGAGAAGAGAACTCAGAAGAGCA	59	43	
IGF1R_Exon21_1	F	CGTACGCTTGTATGCGGGAAA	60	52	186 bp
	R	CTCCTCTTTGATGCTGCTGATGA	61	48	
IGF1R_Exon21_2	F	TGTCTTGGCTGCAGGTTTGA	57	50	192 bp
	R	CATGTTCTCTGGCTCCAGGTC	62	57	
IGF1R_Exon21_4	F	CGGGAGGTCTCCTTCTACTACAG	64	57	190 bp
	R	CGCGGAGGACCAGCAC	59	75	
IGF1R_Exon21_5	F	GACAGACACTCAGGACACAAGG	62	55	191 bp
	R	GCACACGTTACTGTTTGCAC	57	50	

ERBB3_Exon1_1	F	GTGGCTCTTGCCTCGATGT	59	58	200 bp
	R	TCCCAGGTGCCGAGCC	59	75	
ERBB3_Exon2_1	F	GTGATCTTTGGGGATGGCAGAT	60	50	191 bp
	R	CACAATCTCAAGGTTCCCCATCA	61	48	
ERBB3_Exon2_2	F	GGACTCTGAATGGCCTGAGTGT	62	55	191 bp
	R	GGGAGAATAAAGAGGAGCAGGT	60	50	
ERBB3_Exon3_1	F	TAATGCCTGAAGGAGGAGAGGAG	62	52	192 bp
	R	GCAAACTTCCCATCGTAGACCT	60	50	
ERBB3_Exon3_2	F	TGTCACAGTGGATTCGAGAAGTG	61	48	161 bp
	R	GTGGCTGGAGTTGGTGTTATAGT	61	48	
ERBB3_Exon3_3	F	CCAGGTCTACGATGGGAAGTTTG	62	52	191 bp
	R	CACTTAGAGTGAGCAGTCTTGGG	62	52	
ERBB3_Exon3_4	F	GTCAGTTCCCGATGGTTCCTTCT	62	52	163 bp
	R	GGGCCCTCTATTGCTTAGGGA	62	57	
ERBB3_Exon4_1	F	CTTTTGGATGGGTGGAGAGGTAA	61	48	192 bp
	R	TTGTCCTTCACCACTATCTCAGC	61	48	
ERBB3_Exon4_2	F	GGGGTGTTTATATTGAGAAGAACGA	60	40	174 bp
	R	AAGAAGGGAGTCACTCTGGTTTG	61	48	
ERBB3_Exon5_1	F	AACAAGCCTTTCTTAGCCCTGAT	59	43	159 bp
	R	GCGTATGAGTGAAGTTTTTGGAGG	61	46	
ERBB3_Exon6_1	F	AGTGGCCTCAGAATTCAGTCCTA	61	48	184 bp
	R	ACATACAAAGCAGTCTGTGTCCT	59	43	
ERBB3_Exon6_2	F	ATAGTGACCAAGACCATCTGTGC	61	48	173 bp
	R	CAAAGGCCACATCCCAATTTCAG	61	48	
ERBB3_Exon7_1	F	CTGAAATTGGGATGTGGCCTTTG	61	48	192 bp
	R	ACTGATACTTGGTGTGGGGATTG	61	48	
ERBB3_Exon7_2	F	TCAATGACAGTGGAGCCTGTGTA	61	48	158 bp
	R	ATCATTGTTCCTTCCCCTCAGAC	61	48	
ERBB3_Exon8_1	F	TAATGGTGTCCTCCTCCTCTTCC	62	52	161 bp
	R	TCTTACCATCTCCTACCCACCTT	61	48	
ERBB3_Exon8_2	F	TGGTGGATCAAACATCCTGTGTC	61	48	160 bp
	R	CGCAGGCTCAGAGGAAAGG	61	63	
ERBB3_Exon9_2	F	CCCCACTGAACCTCTCTTACATT	61	48	176 bp
	R	CTAAGGAGGGAAGGCAGGATCTC	64	57	
ERBB3_Exon10_1	F	TCATTGCCATTGAGTTATACCTTTACC	60	37	183 bp
	R	ATGCCAGTGGTTCACCTATTCTT	59	43	
ERBB3_Exon11_1	F	GCCAGGAGAACCCAAGAAAGAAG	62	52	184 bp
	R	AAGATGCCATTTCCTCCATACCC	61	48	
ERBB3_Exon12_1	F	TCCTTTGAATAGTTAATGTTCCCTTAGT	59	32	192 bp
	R	CAAAGAGTGGTGGTAGCAGAGC	62	55	
ERBB3_Exon12_2	F	GCTTCCGATCCCTGAAGGAAAT	60	50	192 bp
	R	CCCTATTCTCACCACCTAGCAGA	62	52	
ERBB3_Exon13_1	F	CTGGAAGCAGTAACGAGGAAGAA	61	48	188 bp
	R	ACCTCCTCGGCTATAATTTCGAC	61	48	
ERBB3_Exon13_2	F	CTCCTAACCCACCCCTTCCTTTC	64	57	186 bp
	R	ATCCTTGACTGGCTCCCCTTA	60	52	
ERBB3_Exon14_1	F	GTTGTGAGATCGGAGCATGAAGG	62	52	189 bp
	R	CCTTGGAGATCCTGGTGCTACT	62	55	
ERBB3_Exon15_1	F	TTGCTGGGAGGTATGGAATTGAC	61	48	170 bp
	R	GGTACTTGTAGATTGGGCCCTTG	62	52	
ERBB3_Exon15_2	F	CAGGGCTCTGATACTTGTGCT	60	52	190 bp
	R	TGACCCCCTCTCCTTATTATCCC	62	52	
ERBB3_Exon16_1	F	CTGTTGAAATTGAGCCTCTGCTG	61	48	172 bp
	R	ACCTCTCTCCCAACTCCCAAATA	61	48	
ERBB3_Exon17_1	F	TTGTAAGGAAGATGCAAACCCAG	59	43	183 bp

	R	CAAGTATCGCCTCATAGCCCTTT	61	48	
ERBB3_Exon17_2	F	TTGACAGTGATAGCAGGATTGGT	59	43	180 bp
	R	AGAGACTTCCAGGACATGCAAAA	59	43	
ERBB3_Exon18_2	F	GCCTTTCCTGAGTAACTCCTTCC	62	52	187 bp
	R	ACCTCTCCAGAATTCCTATGGGT	61	48	
ERBB3_Exon19_1	F	GGATTGACCTAGGGAGAATGACC	62	52	180 bp
	R	AGCGGCATACAGAATTTCCTTCA	59	43	
ERBB3_Exon20_1	F	ATGCTGAGTGTATGTGAACCTGT	59	43	186 bp
	R	TTGTCTCACATGATCCAGCAGAG	61	48	
ERBB3_Exon20_2	F	ACATTGTAAGGCTGCTGGGAC	60	52	190 bp
	R	GCAGTTCTTATCACAGAATTCCTCC	61	44	
ERBB3_Exon21_1	F	CAGTGACTGATTCCCCCAACC	62	57	157 bp
	R	CACACCAAAATCTGCCACCTGAA	61	48	
ERBB3_Exon21_2	F	ACATGGTATGGTGCATAGAAACCT	59	42	192 bp
	R	TCCCTATCCCCATGCTTCACTC	62	55	
ERBB3_Exon22_1	F	TGGGACTTGGAAATCCTAAGAAAA	58	38	174 bp
	R	GATGGTAGAGAGGGCATCCAGA	62	55	
ERBB3_Exon23_1	F	CCTTCACTTCATGCCCATGTCTA	61	48	175 bp
	R	GATCTGGGGCTGTGCCAAC	61	63	
ERBB3_Exon23_2	F	AGTTTGGGAGTTGATGACCTTCG	61	48	172 bp
	R	GAGAAAATGGTTGGGCTCAGCAG	71	52	
ERBB3_Exon24_1	F	CGGCCATGGAATGTATTCTCTTT	59	43	180 bp
	R	TCCTTAGCACCTCCTACTCCCTA	62	52	
ERBB3_Exon25_1	F	TGCTAAGGAAATTTAGAAAAAGGAGGA	59	33	191 bp
	R	CCTCTGCTTCCAAGTCTAGGTC	62	55	
ERBB3_Exon25_2	F	CTGACAAACAAGAAGCTAGAGGA	59	43	192 bp
	R	GAGGGCTCAGGGTGCAAAG	61	63	
ERBB3_Exon26_1	F	ATTAACTACTCAAAGGCCCCCAT	59	43	182 bp
	R	CTAAAACCCAGCCTCTCAGCAAC	62	52	
ERBB3_Exon27_1	F	GGCAGTGAACAACCCAATATCCT	61	48	191 bp
	R	CCCTCTGATGACTCTGATGCC	62	57	
ERBB3_Exon27_2	F	CGTCCAGTCTCTCTACACCCAAT	62	52	168 bp
	R	CTGGGAATGGTAGGCGCTAT	59	55	
ERBB3_Exon27_3	F	AGGAGCCGGAGCCCAC	59	75	186 bp
	R	TCGAGGAAAAATTGAGGAAAGCC	59	43	
ERBB3_Exon28_1	F	TTTTTCAAACTTTCCCCTACCCT	57	39	189 bp
	R	GTGGACTGTGCCTTCTCCTC	61	60	
ERBB3_Exon28_2	F	CCTTTCTTCAGTGGGTCTCAGTT	61	48	188 bp
	R	GTGTGCTGCCCAGAGAGG	61	67	
ERBB3_Exon28_3	F	CTAGGCCAAGTTCCCTTGAGGAG	64	57	174 bp
	R	CTCCATCTCGTTGCCGATTCATA	61	48	
ERBB3_Exon28_4	F	CTGGGCAGCACACAGAGTT	59	58	179 bp
	R	GCTCTCATCTCTTCATACCCTTGC	63	50	
ERBB3_Exon28_5	F	GGCACAACTCCAGATGAAGACTA	61	48	178 bp
	R	TTTTTAGGCGGGCATAATGGACA	59	43	
ERBB3_Exon28_6	F	TGAAGAGATGAGAGCTTTTCAGGG	61	46	184 bp
	R	GAGTGCCACAGGGAGCAG	61	67	
NTRK1_Exon1_1	F	CAGAGTGCAGATGCCTGCTT	59	55	159 bp
	R	GGCACAGAGAGAGAGAACGAAAA	61	48	
NTRK1_Exon2_1	F	TCTGCCCTTGGACAAGAGACTAA	61	48	189 bp
	R	ATGGTGTCCCAGGACTTCACC	62	57	
NTRK1_Exon2_2	F	AGGGAGTCTCTCTACTTTTCAGG	61	48	178 bp
	R	AATGATCCAAATGGCTGGTGAGA	59	43	
NTRK1_Exon3_1	F	CTGGGAGCGCACAGACG	60	71	176 bp
	R	GGGCAGCAGGCATCGG	59	75	

NTRK1_Exon3_2	F	CCTGCTGGCTTGGCTGATAC	61	60	157 bp
	R	CACTCACAGCTCAGTCAGGTTCT	62	52	
NTRK1_Exon3_3	F	CTCCTCGGGACTGCGATG	61	67	176 bp
	R	CTGCCTGACCAGCAAACAAG	59	55	
NTRK1_Exon4_1	F	GCATGTGTATTGTGAGGGAGTAAGT	71	44	188 bp
	R	CACCCACAGTCCCCGTTTC	61	63	
NTRK1_Exon5_1	F	GCCAGGGGCCCAGAGTA	60	71	170 bp
	R	GTCCTCCCCAACTCCCACT	61	63	
NTRK1_Exon6_1	F	CTCCCCTCCCTCATTCTGGTC	64	62	191 bp
	R	CACACACACACTTGGTGCTCTTG	62	52	
NTRK1_Exon7_1	F	CTGCCTAACTGCTCCCTCTTATC	62	52	184 bp
	R	GACACTGCAGCTTCTGTTCAGG	62	55	
NTRK1_Exon7_2	F	GAACCCTCTGCACTGTTCTTGTG	62	52	191 bp
	R	AGGCAGGTAGGTCTCTTCCC	61	60	
NTRK1_Exon8_1	F	GCCACTCCCAGCTCTAACAC	61	60	185 bp
	R	GGCTGACTGCTCCAGCTCT	61	63	
NTRK1_Exon8_2	F	CCAATGCCTCGGTGGATGT	59	58	188 bp
	R	CTCTCTTTCCCCATCTTTGTCCC	62	52	
NTRK1_Exon9_1	F	CAGCCCCAAGCTGGCTAAAG	61	60	189 bp
	R	CAGGAGACGTTGACCTGAACAGA	62	52	
NTRK1_Exon9_2	F	CCATCCCTGGGGCTGAC	60	71	190 bp
	R	CACCCTACATCCTCTTTTGAGGG	62	52	
NTRK1_Exon10_1	F	CGTGGACTTGTCGGGTGTG	61	63	192 bp
	R	AGCACGGAGCCATTGAAGAG	59	55	
NTRK1_Exon10_2	F	CTTTCTGGCCCACAGTCCC	61	63	182 bp
	R	CTCATTGGCTGCCGGCTC	61	67	
NTRK1_Exon10_3	F	CTCAATGAGACCAGCTTCATCTT	59	43	192 bp
	R	GAACTCGAAAGGGTTGTCCATGA	61	48	
NTRK1_Exon10_4	F	TGTCTGCGCCTCAACCAG	58	61	172 bp
	R	GGGCAGGGTTCAGGATGG	61	67	
NTRK1_Exon11_1	F	CCATGAAGGAATGAGTCCCAGAG	62	52	170 bp
	R	CCAGAGACCAGGCAGAACCT	61	60	
NTRK1_Exon12_1	F	GGAGGCTACAGTGTGTGTCAAG	62	55	191 bp
	R	TCTGACCAGAAATGACATGCAGA	59	43	
NTRK1_Exon13_1	F	CTGGATCTAACTACCCCTGTCCC	64	57	186 bp
	R	AAACAAAGCCAGGAGAACAGACA	59	43	
NTRK1_Exon14_1	F	GGCCAAGGTGTGGGCAAA	58	61	190 bp
	R	TCACTGAAGTATTGTGGGTTCTCG	61	46	
NTRK1_Exon14_2	F	CTGGCTCCAGAGGATGGG	61	67	164 bp
	R	CTGCCCTTGACCCAGCATAG	61	60	
NTRK1_Exon15_1	F	CAAGACAGTCCCCGCTACAAC	62	57	163 bp
	R	TTGTGGCACTCAGCAAGGAA	57	50	
NTRK1_Exon15_2	F	AAGCGCCGGGACATCG	57	69	192 bp
	R	CCACTCTGTCCTGATGTGATGGA	62	52	
NTRK1_Exon16_1	F	CAGCAGTGAGGGCTCGG	60	71	169 bp
	R	GGCCCTCGGTGCAGAC	59	75	
NTRK1_Exon16_2	F	CTGCAGCACCAGCACATC	58	61	186 bp
	R	AGCAGGGATGTCTATAGGGAAGG	62	52	
NTRK1_Exon17_1	F	TCAGGCTCCTGGGAGTTCTATC	62	55	161 bp
	R	CGCAGCGACCTGGCTA	57	69	
NTRK1_Exon17_2	F	TGGGGAGGATGTGGCTCC	61	67	180 bp
	R	CTGCTCATGCCAAAATCACCAAT	59	43	
NTRK1_Exon17_3	F	GGCGGGTCTGCATTTTGTG	59	58	184 bp
	R	GGATCCAGGGTGTCTACAGTTTG	62	52	
NTRK1_Exon18_1	F	GGTAGGCTGTGCCTTGACG	61	63	190 bp

	R	GTAGGTGAAGATCTCCCAGAGCA	62	52	
NTRK1_Exon18_2	F	GCTGCCCATTCGCTGGAT	58	61	174 bp
	R	CCAGCAAGGGGTGACCAT	58	61	
NTRK1_Exon19_1	F	GGACTGGCCTCACTCTCTTG	61	60	189 bp
	R	ATCCTTGATGCTGTGGCGTTG	60	52	
NTRK1_Exon19_2	F	CCTGCCCACCAGAGGTCTAC	63	65	191 bp
	R	GGGCAGGCCCCAGTATTC	61	67	
NTRK2_Exon4_1	F	AAAGCGGCCGGTGCAG	57	69	192 bp
	R	CTGCACCAGATCCGAGAGG	61	63	
NTRK2_Exon4_2	F	GGTTGTGGGCTTCTGGAGG	61	63	189 bp
	R	GGGCAAGGAGAAAAAGGAGGAAA	61	48	
NTRK2_Exon5_1	F	TGAGGTGGATGGGAGTTCTTCAT	61	48	188 bp
	R	TCTCTGAGATAATGTGCCCTGGT	61	48	
NTRK2_Exon6_1	F	ATTTTCCTGTTGTCTGCTCTGGT	59	43	192 bp
	R	TAAAATGGGTCCTGGGAAGCAAA	59	43	
NTRK2_Exon7_1	F	CTCTATTTGAATACTGTGTTCCTAAAATGT	60	30	172 bp
	R	TTCCCCAAATGCCACACAAAATC	59	43	
NTRK2_Exon8_1	F	ACAAGCACTAATGTAGCTAAAATGGAA	59	33	169 bp
	R	TCAGGCAGTACAAATCCTGAGTG	61	48	
NTRK2_Exon8_2	F	TGCTCCTGTGACATTATGTGGAT	59	43	192 bp
	R	CGCACCAAGGCAATGAGAATAA	58	45	
NTRK2_Exon9_1	F	TGCTTTTATTTTGATACTGCATTTAACTATT	58	23	192 bp
	R	AAACCAGGTTACCAACATCCCAA	59	43	
NTRK2_Exon9_2	F	TGTTCCATAGGTTTGCCATCTGC	61	48	175 bp
	R	TTAAGACACAGCCAAACACAAGC	59	43	
NTRK2_Exon10_1	F	AGTTAGGGGAAGAAACCCCAAAT	59	43	176 bp
	R	CAAGATTTTCCGCCACACAAGAG	61	48	
NTRK2_Exon10_2	F	GAATGAAACAAGCCACACACAGG	61	48	169 bp
	R	TGCTATTAAAAACACATGCCAGTC	58	38	
NTRK2_Exon11_1	F	TCCCTATCAATGACACAGACATC	59	43	191 bp
	R	CCGTTATAGAACCACTGAAGCG	60	50	
NTRK2_Exon11_2	F	TGCACCAACTATCACATTTCTCG	59	43	175 bp
	R	GTGGTACTCCGTGTGATTGGTAA	61	48	
NTRK2_Exon11_3	F	CAGTGGTTCTATAACGGGGCAAT	61	48	173 bp
	R	TGTTTCTCATCCTTCCCATACTCA	59	42	
NTRK2_Exon11_4	F	GTTACCAATCACACGGAGTACCA	61	48	186 bp
	R	TCTCCCCACATACAAAAGTGTCAG	61	46	
NTRK2_Exon12_1	F	GCAAAACTTCAGTGTATGTCTAGCTTAT	61	36	189 bp
	R	ACACAAACATTTTGAAAAAGAAATACAAAGT	58	23	
NTRK2_Exon13_1	F	GTTGGCAGCTTAATGACAACTTCA	59	42	189 bp
	R	ACCAATTCAGACACCTATTTATTCCA	58	35	
NTRK2_Exon14_1	F	ATAACCACCCTCCCTTCCTTTC	60	50	176 bp
	R	AGCCAAAAATGATCCACATAAGAAGC	60	38	
NTRK2_Exon15_1	F	TGTTAATTTTCATTGATTTTTCTTTTGAGCAT	58	22	164 bp
	R	CTTACATGGCAGCATCAACCAAC	61	48	
NTRK2_Exon16_1	F	CACCTCCGGTTTCTACTTCTCTT	61	48	184 bp
	R	AGAGGGTCTAAGCATTTTCATCCG	61	46	
NTRK2_Exon17_1	F	ACAGCTCAATAAAGCCATTGATTAC	58	36	190 bp
	R	TGACAGGGATCTTGGTCATTCC	60	50	
NTRK2_Exon17_2	F	CCCACTCCATCACATCTCCAA	60	52	199 bp
	R	GATACAGCTATGCAGCAAATGGG	61	48	
NTRK2_Exon18_1	F	ATGGTTTGCAGGATTGTAGAGCA	59	43	182 bp
	R	CAGGCATGGATTTAGCCTCCTTT	61	48	
NTRK2_Exon19_1	F	CCTTCACCTCCACATGCTTCAAT	61	48	189 bp
	R	CTTACCTTCACTGCCACCAAGAT	61	48	

NTRK2_Exon19_2	F	TGAAAAGGGAGCTAGGCGAAG	60	52	192 bp
	R	CCTGCATTGGCCACCAAAATATAA	59	42	
NTRK2_Exon20_1	F	TATCTCAGTATCATAGGGCCCAC	61	48	165 bp
	R	ACGCAGACGCCATAGAACTTG	60	52	
NTRK2_Exon20_2	F	GACAATGCACGCAAGGACTTC	60	52	190 bp
	R	TCCCTCCTGGAGCCCAC	60	71	
NTRK2_Exon21_2	F	AGCTTCATTCTCCATGTCCTTCC	61	48	184 bp
	R	GCAGTTCCTGGTGGCCAAATC	62	57	
NTRK2_Exon21_3	F	CCGCGGGCATGGTCTAC	60	71	170 bp
	R	GGGTCTCTGATCTGCACAGCTA	62	55	
NTRK2_Exon22_1	F	CAGCTCCCTTCCACACCTG	61	63	190 bp
	R	GCCATAGGTGAAAATCTCCCACA	61	48	
NTRK2_Exon22_2	F	CACACAATGCTGCCCATTCG	59	55	173 bp
	R	TCTTGGCCAGACCCATTGC	59	58	
NTRK2_Exon23_1	F	CTTCGATGTGCATTGCTTTTCCT	59	43	181 bp
	R	GATGCCCTTGATGTTCTTCCTCA	61	48	
NTRK2_Exon23_2	F	GCCCCCAGGAGGTGTATGA	61	63	179 bp
	R	CTGAGGAGTACGTTGGGAAGGAT	62	52	

Table 6: LNA primers

Primer Name	Oligo name	Sequence (5'-3')
FL1	CS1	A+CA+CTG+ACGACATGGTTCTACA
	CS2	T+AC+GGT+AGCAGAGACTTGGTCT
FL2	CS1rc	T+GT+AG+AACCATGTCGTCAGTGT
	CS2rc	A+GAC+CA+AGTCTCTGCTACCGTA

LNA nucleotides are preceded by a "+"

Table 7: Primers used for the validation of the Amplicon Sequencing data

Primer	No.		Sequence	°C T_m	% GC	Products Length
IGF1R_1_S	1	F	AGTATTGTTTCCTTCGCCCTTGT	61	43	296 bp
	2	R	GCCCCTCGGAGGAAAAGTTC	61	60	
IGF1R_2_S	7	F	CATAAACAACCCACGGTGCC	60	55	397 bp
	8	R	AAGGAGTCCGTGCACTCAAG	60	55	
IGF1R_3_S	9	F	GCTTGTATGCGGGAAACCACT	61	52	345 bp
	10	R	TTGTGTCCTGAGTGTCTGTCG	60	52	
IGF1R_4_S	11	F	GAGAACATGGAGAGCGTCCC	60	60	440 bp
	12	R	AGTTAAGGGTTTGGGCAGGG	60	55	
NTRK2_1_S	13	F	AAGCATTGCTGGCTAGAAAGA	58	43	331 bp
	14	R	GACTACCGCACCAAGGCAAT	61	55	
EGFR_Amo1_S	13S	F	AGTGATTCTACAAACCAGCCAGCC	63	50	374 bp
	14S	R	TGCAAGACTGTCCTTCACCTACTGG	64	52	
NTRK2_2_S	15	F	TCTATGAAGCTGATCAAAGTAGCAC	59	40	583 bp
	16	R	CACAGGGAAAGTCACTCGCT	60	55	
EGFR_1_S	19	F	TGCTGTGACCCACTCTGTC	59	58	282 bp
	20	R	CCAAAAGCCAAGGGCAAAGAA	60	48	
NTRK1_1_S	27	F	CTGACCTGTTTCTCCCAGGC	60	60	444 bp
	28	R	TCGGGGTTGAACTCGAAAGG	60	55	
ERBB3_1_S	33	F	TCTCCTTATTCTCAGCCGGG	59	55	319 bp

	34	R	TCCCTCAACCCTACTCCCAC	60	60	
ERBB3_2_S	35	F	GGGTTGAGGGATGGAACCAA	60	55	319 bp
	36	R	GAACAGTTCCATTGCAGGGC	60	55	
ERBB3_3_S	39	F	CTACCTTGAGGAACATGGTATGG	59	48	266 bp
	40	R	GCCTTCTCTCCTTGAACTTACC	58	50	
ERBB3_4_S	41	F	GCATCTGGATGCCCTCTCTAC	60	57	346 bp
	42	R	TTGGGCTCAGCAGGTAACTC	60	55	
EPHA2_1_S	45	F	CGCTGAACTCGCCATCCTTC	51	60	395 bp
	46	R	CCATACCTCTGCCCACTCCT	51	60	
EPHA2_2_S	47	F	CCAGGGAAGGTGCATCAGAG	60	60	288 bp
	48	R	TGGACTACGGCACCAACTTC	60	55	
EPHA2_3_S	51	F	GTGCTGCCTTGGGAGATGTAA	60	52	394 bp
	52	R	TGAAAGAATCTGGGCTGTGGAG	60	50	
EPHA2_4_S	53	F	CTCCTACAGGTGTTCTGCCT	59	55	424 bp
	54	R	CGGGTAAGGATGTGGGTTGT	60	55	
EGFR_2_S	55	F	CCCCTGACTCCGTCCAGTAT	60	60	288 bp
	56	R	GCGCAGCTGATCTCAAGGA	60	58	
EGFR_1_HRM	57	F	GGCCTAAGATCCCGTCCATC	60	60	198 bp
	58	R	CCTTGTTCCTGTCGGGGTG	60	63	
IGF1R_1_HRM	73	F	ACCGAGTACTTGCTGCTGTT	60	50	114 bp
	74	R	GATGACCAGGGCGTAGTTGT	60	55	
NTRK1_MM905_S	81	F	GATCCAGGAGATAGTCAACGAACA	60	46	730 bp
	82	R	ATCTAGAGAAATTAGGCAGCGAGC	61	46	
IGF1R_R1	93	F	AGGGAAATGTTGGCATTTATAGTAG	57	36	364 bp
	94	R	CCTTACCTTTGGAGCAGTAATTGT	59	42	
IGF1R_R2	95	F	CGCTAGCCTTCCCAATCAAATAAG	60	46	468 bp
	96	R	CAAACCTCCTTCCTTTCCCAAATTA	59	40	
NTRK2_R1	97	F	TGAGTGCTAACTGGGTGATGAA	59	45	557 bp
	98	R	CACACCCGGAGAATTCCATAAG	59	50	
EPHA2_R1	99	F	GACCAAGCTGAAACCGCTTAT	59	48	476 bp
	100	R	CAGGGCATGAATGAACAGGAG	59	52	
ERBB3_R1	101	F	CCAGATTTAGGTTGGTCCCTTC	58	50	584 bp
	102	R	CCGAGGCACAGAGAAGATAAG	58	52	
EPHA2_R1.2	121	F	GACACCAGGTAGGTTCCAAAGTT	60	48	335 bp
	122	R	TCACCCAACTTCCATTAAGGACTC	60	46	
EPHA2_dbSNP126	133	F	GTCCACACATAACCTCTTAGCC	58	50	371 bp
	134	R	TCAGTGGCTTTCTGCAACA	58	47	
EPHA2_dbSNP120	135	F	GTCTGGTTGATGCTGACACT	58	50	430 bp
	136	R	CCTTGCACACGTGAGTCTT	58	52	
EGFR_dbNSP98	137	F	ACTTTGTCCTTCCAGTCACG	58	50	486 bp
	138	R	TCAAACAACTTCCCGTCTCC	58	50	
NTRK1_dbSNP52	139	F	GCCTCTACTGTTCTCTCAATCC	58	50	380 bp
	140	R	CGGTAATAGTCGGTGCTGTAG	58	52	
NTRK1_dbSNP_126	141	F	ACTGTGTCCATTCGGGTTATTAG	58	43	454 bp
	142	R	CACATGCTGAGGGTGAATTAGA	58	45	
ERBB3_dbSNP86	143	F	AGGCAGTGAACAACCCAATA	57	45	412 bp
	144	R	GAAGAGTCAGGCACCTTTGA	57	50	
IGF1R_dbSNP126_1	145	F	CAGCAACTGTCTGTTCTCCTAT	58	45	312 bp
	146	R	CACTTCCTCCATGCGGTAAA	58	50	

IGF1R_dbSNP126_2	147	F	AGTAGCCAGCGTAACTGATTG	58	48	512 bp
	148	R	GGGTGCATGAGGATGAAGTAG	58	52	
NTRK1_Ex12	149	F	GTGAGTAGCCCAAGGTGGAG	60	60	403 bp
	150	R	GTCTCCAGACCTGCCTCATC	60	60	
EGFR_Ex2	151	F	GAGAGTGAAGAAACTGCTACC	56	48	395 bp
	152	R	CTCTCGTTTGTAGCTCTGTAAG	56	45	
EGFR_Ex6	153	F	GGGCATGGTTTGACTTAGTTTG	58	45	401 bp
	154	R	AGGGCAATATCCTGTCTGTTATG	58	43	
EGFR_Ex3	155	F	TTAGGGTTCAACTGGGCGTC	60	55	509 bp
	156	R	GTAAACACTGGTACCCCGCT	60	55	
EGFR_Ex4	157	F	TGGGCTAATTGCGGGACTCTTGTT	65	50	535 bp
	158	R	CAGGACACAAGTGCTCTGCT	60	55	
EGFR_Ex7	159	F	TAACTTGGGCTTTCTGACGGGAGT	64	50	369 bp
	160	R	TCCAAGCAAGGCAAACACATCCAC	64	50	
EGFR_Ex8	161	F	AAAGCCAAAGGAGGATGGAGCCTT	64	50	456 bp
	162	R	GGCTCTGTGACTGTTCTCATC	59	52	
EGFR_Ex9	163	F	ACTATAGGTCCTGGTGTCCCC	60	57	453 bp
	164	R	TCCAGAGGAGGAGTATGTGTGAAGGA	64	50	
EGFR_Ex4	165	F	AACTGCACCTCCATCAGTGG	60	55	399 bp
	166	R	CCCTTTTGCCTGCAGGAGAAACT	63	52	
EGFR_Ex11	167	F	CCTGCGCATGTACACTCAGAGAAG	63	54	504 bp
	168	R	TGGGATCTGGAGTGGACACA	60	55	
EGFR_Ex12	169	F	TCCCACAGCATGACCTACCATCAT	64	50	562 bp
	170	R	TGGTAGCCTAAACCTCAGGG	58	55	
EGFR_Ex20	171	F	AGAAGGCGTACATTTGTCCTTCC	61	48	534 bp
	172	R	AGGTCAATGGCCCCTTTCAT	59	50	
EGFR_Ex21	173	F	TAATCAGTGTGATTCGTGGAGCC	61	48	544 bp
	174	R	GATGCCAGTAATTGCCTGTTTC	58	45	
EGFR_Ex22	175	F	ACAGCTTTTCCTCCATGAGTACG	61	48	519 bp
	176	R	TCCACATGCAGATGGGACAG	60	55	
EGFR_Ex23	177	F	TTCATGCGCCTTTCCATTCTTTG	61	43	505 bp
	178	R	GCTCTGGCTCACACTACCAG	60	60	
EGFR_Ex24	179	F	CTGAACTCCGTCAGACTGAAATCC	61	50	432 bp
	180	R	ATTTCCTCTGCCGTGTTTTCTCA	61	43	
EGFR_Ex25	181	F	CTTGCTGGGCATTGCACTAAGCAT	65	50	542 bp
	182	R	TGTTTCTGGATTTGTGTGCCTGCC	64	50	
EGFR_Ex26	183	F	CATCCCCTCAGGCGTAACAC	60	60	532 bp
	184	R	GCCTTACTGAGGCTTGCTCTAAT	60	48	
EGFR_Ex27	185	F	TCATGAGGGGAGGCAGCTATAA	60	50	537 bp
	186	R	GGACCTAAAAGGCTTACAATCAAG	58	42	
EPHA2_XII_1	242	F	AGCATCCCTGGTCATCTCCT	60	55	500 bp
	243	R	TTGGCAAGCTTCTAGGCTGT	60	50	
EPHA2_XII_2	244	F	GTAGGAAATGGCCTCCGGG	60	63	445 bp
	245	R	GATGGCGAGTTCAGCGTGC	62	63	
EPHA2_XII_3	246	F	TGACACTGGCAGTACGGAAG	60	55	622 bp
	247	R	GTGGGGTGGAAGCAGATTGA	60	55	
EPHA2_XII_4	248	F	GCCATGTCTTCTCTCGTACAAA	58	45	449 bp
	249	R	AGAGCGAGATCCTGTCTCAA	58	50	
EPHA2_XII_5	250	F	GGGCACTTCTTGTAGTAGACAC	58	50	338 bp

	251	R	GAGGCTGAGCGTATCTTCATT	58	48	
EGFR_XII_1	252	F	TCCAGGCCTAAGATCCCGTC	61	60	235 bp
	253	R	CACAACTGCTAATGGCCCGT	61	55	
EGFR_XII_2	254	F	CCGTCCAGTATTGATCGGGAG	60	57	316 bp
	255	R	ACGAAACGTCCCGTTCCTC	58	60	
EGFR_XII_3	256	F	TTAGGGTTCAACTGGGCGTC	60	55	269 bp
	257	R	CAGCTCCTTCAGTCCGGTTT	60	55	
EGFR_XII_4	258	F	AGTCCCTGAGAGTCTAGAGTAATG	58	46	383 bp
	259	R	CGCTGAGAAGTCTGTGGTTTAG	59	50	
EGFR_XII_5	260	F	TCTCTTGCAGTCGTCAGCCT	61	55	422 bp
	261	R	ATTGGTAGCCTAAACCTCAGGG	59	50	
EGFR_XII_6	262	F	GGTAGACTGAGGCTTCCAGC	60	60	328 bp
	263	R	CAGACCCACCAGTCACTCAC	60	60	
EGFR_XII_7	264	F	TCAGTTTCCGCAGCTGACAT	60	50	489 bp
	265	R	AGCTCCCAAAATAGCCCACC	60	55	
ERBB3_XII_1	266	F	AGGGAAAGGGTCTGCTAGGT	60	55	317 bp
	267	R	ACAGACACCTCCTCGGCTAT	60	55	
ERBB3_XII_2	268	F	GTCTCCTTATTCTCAGCCGGG	60	57	520 bp
	269	R	TTTCGACAGGACAAGCACTGA	60	48	
ERBB3_XII_3	270	F	GGAACATGGTATGGTGCATAGA	58	45	366 bp
	271	R	CTCCCGAAGTGTTGGGATTAC	58	52	
ERBB3_XII_4	272	F	TCAAAGGTGCCTGACTCTTC	57	50	669 bp
	273	R	AGCCTGCTATGCCAGTAATC	57	50	
IGF1R_XII_1	274	F	GCGTGCACCGAGAACAATG	60	58	426 bp
	275	R	AGCCCTCTCAAAATGACCCAC	60	52	
IGF1R_XII_2	276	F	CGGAGTATTGTTTCCTTCGCC	59	52	556 bp
	277	R	CACCAACTTCCCTACCGAGTC	60	57	
IGF1R_XII_3	278	F	ATAAACAACCCACGGTGCCC	61	55	445 bp
	279	R	CGTGCCAGGTTTGTGACCAT	61	55	
IGF1R_XII_4	280	F	GTGTCTTGGCTGCAGGTTTG	60	55	439 bp
	281	R	GTGCGCACACGTTACTGTTT	60	50	
NTRK1_XII_1	282	F	ACTTGAGGTGCGTCTCTGTG	60	55	549 bp
	283	R	AGGATCAGTCCCCAGGTCTC	60	60	
NTRK1_XII_2	284	F	TGTGTCTCCTCTCTAGGCCC	60	60	381 bp
	285	R	GGTTTGGGCTAGCTGTGACT	60	55	
NTRK1_XII_3	286	F	CTGGGTCTTTAACACCGCCC	61	60	412 bp
	287	R	CTGCCTGACCAGCAAACAAG	60	55	
NTRK1_XII_4	288	F	GTGAGTAGCCCAAGGTGGAG	60	60	453 bp
	289	R	GCCTCCTGTAGTAAGCCATTT	58	48	
NTRK2_XII_1	290	F	AACAGGAAAAGAGGTGGAAGACAG	61	46	458 bp
	291	R	AGCCAAACACAAGCCTTACCA	60	48	
NTRK2_XII_2	292	F	GTGTGAGGTTTGGGACCATTC	59	52	484 bp
	293	R	ACGTTGGGAAGGATCGGTCT	61	55	
EGFR_MM1S	414	F	CTTGCTGGGCATTGCACTAAGCAT	65	50	542 bp
	415	R	TGTTTCTGGATTTGTGTGCCTGCC	64	50	
AA_EGFR_21	523	F	TAATCAGTGTGATTCGTGGAGCC	61	48	370 bp
	524	R	CATGAGAAAAGGTGGGCCTGA	60	52	
AA_EGFR_27	527	F	TCATGAGGGGAGGCAGCTATAA	60	50	379 bp
	528	R	TGAGTAGACACAGCTTGAGAGAG	59	48	

EGFR_8_HRM_F	587	F	CGACAGCTATGAGATGGAGGAAGA	62	50	152 bp
	588	R	AGATGTGTTCCTTTGGAGGTGG	60	50	

Table 8: Primer used for the validation of mutations on cDNA level

Primer	No.		Sequence	°C T_m	% GC	Products Length
IGF1R_cDNA882	187	F	ACGGGGCGATCTCAAAAGTT	60	50	490 bp
	188	R	GCGCATCAGTTCAAACAGCA	60	50	
IGF1R_cDNA925	189	F	GCTTGTCCAACGAGCAAGTC	60	55	396 bp
	190	R	CGTAAGGCTGTCTCTCGTCG	60	60	
IGF1R_cDNA891	191	F	AGGCCTTCCTTCCTGGAGAT	60	55	339 bp
	192	R	TCAGCAGGTCGAAGACT	54	53	
IGF1R_cDNA_MM220	193	F	GAAGTCTGGCTCCGGAGGAG	62	65	497 bp
	194	R	TATTGGACACCGCATCCAGG	60	55	

Table 9: Primers used for mutagenesis PCR

Primer	No.		Sequence	°C T_M	% GC
IGF1R_L363_Mut_G/A	109	F	GCATGGTAGCCGAAAATTTCACAGTC	59	46
	110	R	GACTGTGAAATTTTCGGCTACCATGC	59	46
IGF1R_MM882_Mut_A/G	197	F	CATACCTCAACGCCAGTAAGTTCG	58	50
	198	R	CGAACTTACTGGCGTTGAGGTATG	58	50

Table 10: Primers used for cloning of expression and donor vectors

Primer	No.		Sequence	°C T_M	% GC
IGF1R_NotI	199	F	ACGGCGGCCGCACC ATGAAGTCTG	67.9	67
IGF1R_EcoRI_Stop	200	R	ACGCGAATTCTCAGCAGGTCGAA	60.9	52
IGF1R_NheI	240	F	ACGGCTAGCACCATGAAGTCTG	61.9	55
IGF1R_NotI	241	R	ACGCGCGGCCGCTCAGCAGGTCGAA	72.4	72

Table 11: Primer used for Sanger sequencing of ligated plasmids

Primer	No.	Sequence	°C T_M	% GC
IGF1R_seq_1_fw	111	CTGACAACGACACGGCCT	57.9	61
IGF1R_seq_2_fw	112	ATCATCATAACCTGGCACCG	54.9	50
IGF1R_seq_3_fw	113	CCTTTCTTTGAGAGCAGAGTGG	55.5	50
IGF1R_seq_4_fw	114	CATGCGTGAAAGGATTGAGTT	53.6	43
IGF1R_seq_5_fw	115	CTCCTCGTCCTCCCTGCC	60.1	72
IGF1R_seq_1_rv	116	CAAACCTGTAGGTGTTGGGC	56.3	55
IGF1R_seq_2_rv	117	GCATCCTGCCCATCATACTC	55.6	55
IGF1R_seq_3_rv	118	TGGATATCGATGCGGTACAA	53.5	45
IGF1R_seq_4_rv	119	GACACCACACCCAGCAATC	56.4	58
IGF1R_seq_5_rv	120	CTCTCGTCGAAGCTGGCG	58.5	67
M13_fw	-	GTAAAACGACGGCCAGT	52.6	53
M13_rv	-	AACAGCTATGACCATG	45.4	44
CMV_fw	-	CGCAAATGGGCGGTAGGCGTG	63.9	67

5.4.2 RNA

crRNA and tracRNA were purchased from Integrated DNA Technologies (Leuven, Belgium).

Table 12: crRNA used for CRISPR/Cas9 experiments

Name	Sequence
IGF1R_crRNA	GGACGAACTTATTGGCGTTG *AGG*

5.5 Plasmids

Table 13: Plasmids

Name	Resistance	Manufacturer
pCR-XL-TOPO-IGF1-R_WT	Kan	Source Bioscience, Berlin, Germany
pCR-XL-TOPO-IGF1-R-D1146N	Kan	Institute for Pathology Würzburg, Germany
pCR-XL-TOPO-IGF1-R-N1129S	Kan	Institute for Pathology Würzburg, Germany
pSF-CMV-Puro-COOH-GST	Kan	Oxford Genetics, Oxforshire, United Kingdom
pSF_IGF1-R-WT	Kan	Institute for Pathology, Würzburg, Germany
pSF_IGF1-R-D1146N	Kan	Institute for Pathology, Würzburg, Germany
pSF_IGF1-R-N1129S	Kan	Institute for Pathology, Würzburg, Germany
TST206-pT2SVPuroCMV	Amp	Thorsten Stühmer, CCC MF, Würzburg, Germany
TST206-pT2SVPuroCMV_IGF1R	Amp	Institute for Pathology, Würzburg, Germany
TST206_pT2SVPuroCMV_IGF1R-D1146N	Amp	Institute for Pathology, Würzburg, Germany
TST206-pT2SVPuroCMV_IGF1R-N1129S	Amp	Institute for Pathology, Würzburg, Germany
TST-212-pT2BN-SVpuroCAG	Amp	Thorsten Stühmer, CCC MF, Würzburg, Germany
TST_212_T2BN_SVpuroCAG_IGF1R	Amp	Institute for Pathology, Würzburg, Germany
TST-212-pT2BN_SVpuroCAG_IGF1R-D1146N	Amp	Institute for Pathology, Würzburg, Germany
TST-212-pT2BN_SVpuroCAG_IGF1R-N1129S	Amp	Institute for Pathology, Würzburg, Germany
pCMV(CAT)T7-SB100_Transposase	Chl	Thorsten Stühmer, CCC MF, Würzburg, Germany
pmax_GFP	Kan	Lonza, Basel, Switzerland

5.6 Enzymes

5.6.1 Polymerases

Table 14: DNA polymerases

Name	Manufacturer
Taq DNA Polymerase, native, without BSA	Thermo Fisher, Darmstadt, Germany
Phusion High-Fidelity DNA Polymerase	New England Biolabs, Frankfurt, Germany
Q5 High Fidelity DNA Polymerase	New England Biolabs, Frankfurt, Germany

5.6.2 Nucleases

Table 15: Nucleases

Name	Manufacturer
DpnI	New England Biolabs, Frankfurt, Germany
EcoRI-HF	New England Biolabs, Frankfurt, Germany
FspI	New England Biolabs, Frankfurt, Germany
HindIII-HF	New England Biolabs, Frankfurt, Germany
NotI-HF	New England Biolabs, Frankfurt, Germany
NheI-HF	New England Biolabs, Frankfurt, Germany
Cas9 Nuclease 3NLS	Integrated DNA Technologies, Leuven, Belgium
T7 Endonuclease I	New England Biolabs, Frankfurt, Germany

5.6.3 Ligases

Table 16: Ligases

Name	Manufacturer
T4 DNA Ligase	New England Biolabs, Frankfurt, Germany

5.7 Antibodies

5.7.1 Primary antibodies

Table 17: Primary antibodies

Primary Antibody	Size [kDa]	Species	Manufacturer
Akt (pan) (C67E7)	60	rabbit	Cell Signaling, Frankfurt, Germany
Anti-c-Myc antibody (Y69)	57	rabbit	Abcam, Cambridge, United Kingdom
Anti-RAS	21	mouse	Thermo Fisher, Darmstadt, Germany
B-Raf (55C6)	86	rabbit	Cell Signaling, Frankfurt, Germany
BrdU Antibody (BU20A), FITC	-	mouse	Thermo Fisher, Darmstadt, Germany
FAK (D2R2E)	125	rabbit	Cell Signaling, Frankfurt, Germany
IGF-I Receptor β (D23H3) XP	95	rabbit	Cell Signaling, Frankfurt, Germany

IGF-IRβ Antibody (F-1)	95	mouse	Santa Cruz, Heidelberg, Germany
IGF1R antibody [alphaIR3]	95	mouse	GeneTex, Inc., Irvine, USA
Integrin beta-1/CD29 Antibody (7F10)	130	mouse	Thermo Fisher, Darmstadt, Germany
MEK1/2	45	rabbit	Cell Signaling, Frankfurt, Germany
mTOR	289	rabbit	Cell Signaling, Frankfurt, Germany
p44/42 MAPK (Erk1/2)	42, 44	rabbit	Cell Signaling, Frankfurt, Germany
Phospho_IGF-I Receptor β (Y1135)	95	rabbit	Cell Signaling, Frankfurt, Germany
Phospho_IGF-I Receptor β (Y980)	95	rabbit	Cell Signaling, Frankfurt, Germany
Phospho-Akt (Ser473) (D9E) XP	60	rabbit	Cell Signaling, Frankfurt, Germany
Phospho-c-Raf (Ser338) (56A6)	74	rabbit	Cell Signaling, Frankfurt, Germany
Phospho-FAK pTyr397 (141-9)	125	rabbit	Thermo Fisher, Darmstadt, Germany
Phospho-MEK1/2 (Ser217/221) (41G9)	45	rabbit	Cell Signaling, Frankfurt, Germany
Phospho-mTOR (Ser2448)	289	rabbit	Cell Signaling, Frankfurt, Germany
Phospho-p44/42 MAPK (Erk1/2) (Thr202/Tyr204)	42, 44	rabbit	Cell Signaling, Frankfurt, Germany
Phospho-Pyk2 (Tyr402)	116	rabbit	Cell Signaling, Frankfurt, Germany
Pyk2 (H364)	116	rabbit	Cell Signaling, Frankfurt, Germany
Raf-1 Antibody (C-12)	80	rabbit	Santa Cruz, Heidelberg, Germany
Ras Antibody (D2C1)	21	rabbit	Cell Signaling, Frankfurt, Germany
Tubulin-α AB-2 (DM1A)	57	mouse	Neomarkers, Freemont, USA
β-Tubulin	55	rabbit	Cell Signaling, Frankfurt, Germany

5.7.2 Secondary antibodies

Table 18: Secondary antibodies

Antibody	Manufacturer
Anti-rabbit IgG, HRP-linked Antibody	Cell Signaling, Frankfurt, Germany
Anti-mouse IgG, HRP-linked Antibody	Cell Signaling, Frankfurt, Germany
Peroxidase AffiniPure F(ab')$_2$ Fragment Goat Anti-Rabbit IgG (H+L)	Jackson Immuno Research Europe Ltd, Newmarket, United Kingdom
Goat anti-Mouse IgG (H+L) Cross-Adsorbed Secondary Antibody, Alexa Fluor 647	Thermo Fisher, Darmstadt, Germany

5.8 Molecular weight size marker

Table 19: Molecular weight size marker

Name	Manufacturer
GeneRuler 100 bp DNA Ladder	Thermo Fisher, Darmstadt, Germany
GeneRuler 1 kb DNA Ladder	Thermo Fisher, Darmstadt, Germany
PageRuler Plus Prestained Protein Ladder	Thermo Fisher, Darmstadt, Germany
PageRuler Prestained Protein Ladder	Thermo Fisher, Darmstadt, Germany

5.9 Protease Inhibitors

Table 20: Protease inhibitors

Name	Manufacturer
Aprotinin	AppliChem, Darmstadt, Germany
Pefabloc SC	Sigma-Aldrich, Munich, Germany
PMSF	Carl Roth, Karlsruhe, Germany
Sodium orthovanadate	AppliChem, Darmstadt, Germany
PhosSTOP	Roche, Mannheim, Germany
cOmplete ULTRA Tablets	Roche, Mannheim, Germany

5.10 Kits

Table 21: Kits

Name	Manufacturer
Abi Prism BigDyeTerm v3.1 CycleSeq Kit	Thermo Fisher, Darmstadt, Germany
Access Array 48.48 Loading Reagent Kit	Fluidigm, Munich, Germany
Agilent DNA 1000 Kit	Agilent, Waldbronn, Germany
AllPrep DNA/RNA Mini Kit	Qiagen, Hilden, Germany
CelLytic NuCLEAR Extraction Kit	Sigma-Aldrich, Munich, Germany
Cell Proliferation ELISA, BrdU (colorimetric)	Roche, Mannheim, Germany
Cell Proliferation Kit I (MTT)	Roche, Mannheim, Germany
FastStart High Fidelity PCR System, dNTPack	Roche, Mannheim, Germany
First Strand cDNA Synthesis Kit	Thermo Fisher, Darmstadt, Germany
LightCycler 480 High Resolution Melting Master	Roche, Mannheim, Germany
MinElute Gel Extraction Kit	Qiagen, Hilden, Germany
Nucleo Bond Xtra Midi	Macherey-Nagel, Düren, Germany
NucleoSpin Plasmid Kit (NoLid)	Macherey-Nagel, Düren, Germany
Qubit dsDNA HS Assay Kit	Thermo Fisher, Darmstadt, Germany
Rapid PCR Cleanup Enzyme Set	New England Biolabs, Frankfurt, Germany
VenorGeM OneStep	Minerva Bioloabs, Berlin, Deutschland

5.11 Solutions and Buffers

Table 22: Solutions and buffers

Name	Ingredients	Concentration
2x Lysis buffer	Hepes pH 8.0	40 mM
	NaCl	700 mM
	MgCl	2 mM
	EDTA pH 8.0	1 mM
	EGTA pH 8.0	0.2 mM

Lysis buffer	2x lysis buffer	1x
	PMSF	0.6 µg/ml
	Pefabloc	0.1 mM
	Aprotinin	1 µg/ml
	Na-O-Vandat	1 mM
	DTT	0.5 %
	Igepal	1 %
4x Loading dye	Tris-HCl pH 6.8	200 mM
	SDS	8 %
	Glycerol	40 %
	β-mercaptoethanol	4 %
	EDTA	50 mM
	Bromophenol blue	0.08 %
50x TAE	Tris (ultrapure)	2 M
	EDTA pH 8.0	0.05 M
	Acetic acid	5.71 %
10x TBS	Tris (ultrapure)	200 mM
	NaCl	1.37 M
1x TBS-T	10x TBS	1x
	Tween-20	0.1 %
10x PBS	KCl	27 mM
	K_2HPO_4	20 mM
	NaCl	13.7 M
	$Na_2HPO_4x2H_2O$	80 mM
1x PBS-T	10x PBS	1x
	Tween-20	0.1 %
10x Western blot buffer	Glycine	1.92 M
	Tris (ultrapure)	250 mM
1x Running buffer	10x Western blot buffer	1x
	SDS	0.1 %
1x Blot buffer	10x Western buffer	1x
	Methanol	20 %
	SDS	0.03 %
1x Separation-gel buffer pH 8.8	Tris	1.5 M
	SDS	15 mM

1x Stacking-gel buffer pH 6.8	Tris	0.5 M
	SDS	15 mM
FACS buffer	PBS	1x
	BSA	1 %
Annexin-FACS buffer pH 7.4	NaCl	140 mM
	$CaCl_2$	2.5 mM
	Hepes	10 mM
DNase I for FACS	DNAse I	0.5 U
	10x DNAse buffer	1x
	FACS buffer	add 100 µl
Ponceau S staining solution	Ponceau S	0.1 %
	Acetic acid	5 %
1x DNA-Lysis buffer	Tris-HCl pH 7.6	10 mM
	NaCl	50 mM
	$MgCl_2$	6.25 mM
	Igepal	0.045 %
	Tween-20	0.45 %
Cas9 storage buffer	HEPES 1M, pH 7.5	20 mM
	KCl	150 mM
Fixation buffer for FACS	PBS	1x
	Formaldehyde	4 %
Permeabilization buffer	Methanol	90 %

5.12 Chemicals

Table 23: Chemicals

Name	Manufacturer
10 x CutSmart buffer	New England Biolabs, Frankfurt, Germany
10 x Taq Buffer with KCl	Thermo Fisher, Darmstadt, Germany
Access Array Harvest Solution 1X	Fluidigm, Munich, Germany
Access Array Loading Reagent 20X	Fluidigm, Munich, Germany
AccuGene Molecular Biology Water	Lonza, Verviers, Belgium
AccuGene NaCl 5 M	Cambrex, Wiesbaden, Germany
Acetic acid 100 %	Merck Chemicals GmbH, Darmstadt, Germany
Agarose GTQ	Carl Roth, Karlsruhe, Germany

Albumin fraction V (pH 7.0)	AppliChem, Darmstadt, Germany
Ammonium persulfate >98 %	Sigma-Aldrich, Munich, Germany
Bradford reagent	Sigma-Aldrich, Munich, Germany
BrdU	Sigma-Aldrich, Munich, Germany
Brilliant Blue R	Sigma-Aldrich, Munich, Germany
Bromophenol blue sodium salt	Carl Roth, Karlsruhe, Germany
Calcium chloride dehydrate	AppliChem, Darmstadt, Germany
Dimethyl sulfoxide 99.5 %	Carl Roth, Karlsruhe, Germany
Dipotassium phosphate	AppliChem, Darmstadt, Germany
Disodium hydrogen phosphate	AppliChem, Darmstadt, Germany
Dithiothreitol	AppliChem, Darmstadt, Germany
DNA Gel Loading Dye (6X)	Thermo Fisher, Darmstadt, Germany
Dulbecco's Phosphate Buffered Saline	Sigma-Aldrich, Munich, Germany
EDTA 0.5 M pH8.0	AppliChem, Darmstadt, Germany
EGTA pH 8.0	AppliChem, Darmstadt, Germany
Ethanol absolute	AppliChem, Darmstadt, Germany
Formaldehyde solution 37 %	Carl Roth, Karlsruhe, Germany
Gel Loading Dye, Purple (6X), no SDS	New England Biolabs, Frankfurt, Germany
GelRed	Genaxxon Bioscience, Ulm, Germany
Glycerol	Carl Roth, Karlsruhe, Germany
Glycine for analysis	AppliChem, Darmstadt, Germany
Hepes 1 M pH 8.0	AppliChem, Darmstadt, Germany
Hi-Di Formamide	Thermo Fisher, Darmstadt, Germany
Hydrogen chloride	AppliChem, Darmstadt, Germany
Igepal	Sigma-Aldrich, Munich, Germany
IGF-1	Immunotools, Friesoythe, Germany
IL-6	Immunotools, Friesoythe, Germany
Isopropanol, technical grade	AppliChem, Darmstadt, Germany
Proteinase K	Roche, Mannheim, Germany
Low fat milk powder	Heirler Cenovis, Radolfzell, Deutschland
Magnesium chloride 1M	AppliChem, Darmstadt, Germany
Methanol for analysis	AppliChem, Darmstadt, Germany
$MgCl_2$ 25 mM	Thermo Fisher, Darmstadt, Germany
Nocodazole	Sigma-Aldrich, Munich, Germany
Normal mouse IgG	Santa Cruz, Heidelberg, Germany
Normal rabbit IgG	Santa Cruz, Heidelberg, Germany
OptiPrep	Progen, Heidelberg, Germany
Ponceau S	Sigma-Aldrich, Munich, Germany
Potassium chloride	AppliChem, Darmstadt, Germany
Propidium iodide	Sigma-Aldrich, Munich, Germany
Protein A/G PLUS-Agarose	Santa Cruz, Heidelberg, Germany
Rotiphorese Gel 30 (37,5:1)	Carl Roth, Karlsruhe, Germany
Sephadex G-50	Sigma-Aldrich, Munich, Germany
Sodium chloride for analysis	AppliChem, Darmstadt, Germany
Sodium dodecyl sulfate	Sigma-Aldrich, Munich, Germany

Sodium hydroxide	Sigma-Aldrich, Munich, Germany
SYBR Safe DNA Gel Stain	Thermo Fisher, Darmstadt, Germany
TEMED	AppliChem, Darmstadt, Germany
TNF-α	Immunotools, Friesoythe, Germany
Tris ultrapure	AppliChem, Darmstadt, Germany
Tris-hydrochloride	AppliChem, Darmstadt, Germany
Triton X-100	AppliChem, Darmstadt, Germany
Trypan blue, cell culture tested	Sigma-Aldrich, Munich, Germany
Tween-20	AppliChem, Darmstadt, Germany
Urea	AppliChem, Darmstadt, Germany
VEGF-A	Immunotools, Friesoythe, Germany
Water bidistilled	AppliChem, Darmstadt, Germany
β-mercaptoethanol	AppliChem, Darmstadt, Germany

5.13 Consumption items

Table 24: Consumption items

Name	Manufacturer
0.2ml thin wall tubes, strips of 8	Starlabs, Hamburg, Germany
96-Well PCR-plate, non-skirted	Hartenstein, Würzburg, Germany
Access Array 48.48 IFC for Targeted Sequencing	Fluidigm, Munich, Germany
Amersham Hyperfilm ECL	Fisher Scientific, Schwerte, Germany
Autoclavable disposal bags	Hartenstein, Würzburg, Germany
Biosphere SafeSeal Tube 1.5ml	Sarstedt, Nümbrecht, Germany
Biosphere SafeSeal Tube 2ml	Sarstedt, Nümbrecht, Germany
Blotting paper, 0.35 mm, medium absorbency	Hartenstein, Würzburg, Germany
Cell culture flasks, CellStar TC	Greiner Bio-One, Frickenhausen, Germany
Cell lifter	Hartenstein, Würzburg, Germany
Cell scraper	Hartenstein, Würzburg, Germany
CellStar tubes 15ml, PP, graduated	Greiner Bio-One, Frickenhausen, Germany
CellStar tubes 50 ml, PP, graduated	Greiner Bio-One, Frickenhausen, Germany
CryoS 2 ml PP	Greiner Bio-One, Frickenhausen, Germany
CryoS 5 ml PP	Greiner Bio-One, Frickenhausen, Germany
Disposal bags	Brand, Wertheim, Germany
Electroporation cuvettes, 2 mm	Peqlab, Erlangen, Germany
Electroporation cuvettes, 4 mm	Peqlab, Erlangen, Germany
Filter tips, sterile	Nerbe Plus, Winsen, Germany
Flow cytometry tubes	Sarstedt, Nümbrecht, Germany
Identitape	Hartenstein, Würzburg, Germany

LightCycler 480 Multiwell Plate 96, white	Roche, Mannheim, Germany
LightCycler 480 Sealing Foil	Roche, Mannheim, Germany
MicroAmp Optical 96-Well Reaction Plates	Thermo Fisher, Darmstadt, Germany
Microseal 'B' Adhesive Seals	Bio-Rad, Munich, Germany
Microtubes with thread	Hartenstein, Würzburg, Germany
Multiply-Pro 0.5ml Biosphere tubes	Sarstedt, Nümbrecht, Germany
Neoject needles, for single use	Dispomed, Gelnhausen, Germany
Pasteur pipettes, 230 mm	Hartenstein, Würzburg, Germany
Petri dishes	Hartenstein, Würzburg, Germany
Pierce concentrators	Thermo Fisher, Darmstadt, Germany
Pipette tips	Sarstedt, Nümbrecht, Germany
Pipette tips, sterile, wide bore	VWR, Darmstadt, Germany
Protran Nitrocellulose Transfer Membrane, 0.45µM	Hartenstein, Würzburg, Germany
SafeSeal Tube 1.5ml, blue	Sarstedt, Nümbrecht, Germany
Scalpel blades	Bayha, Tuttlingen, Germany
Screw caps for microtubes	Hartenstein, Würzburg, Germany
Serological pipettes	Sarstedt, Nümbrecht, Germany
SuperSignal West Pico Chemiluminescent Substrate	Thermo Fisher, Darmstadt, Germany
Syringe filters, Minisart, High Flow Rate	Sartorius Stedim, Göttingen, Germany
Syringes, single use	Dispomed, Gelnhausen, Germany
TC Dish 100, Standard	Sarstedt, Nümbrecht, Germany
Tube 13 ml, with ventilation cap	Sarstedt, Nümbrecht, Germany
Tube 15 ml, PP	Sarstedt, Nümbrecht, Germany
Tube 50 ml, PP	Sarstedt, Nümbrecht, Germany
Well-plates	Greiner Bio-One, Frickenhausen, Germany
X-ray cassettes	Hartenstein, Würzburg, Germany

5.14 Laboratory equipment

Table 25: Laboratory equipment

Type	Name	Manufacturer
Access Array System	IFC Controller AX	Fluidigm, Munich, Germany
	FC1 Cycler	Fluidigm, Munich, Germany
Benchtop centrifuges	Centrifuge 5415D	Eppendorf, Hamburg, Germany
	Centrifuge 5415R	Eppendorf, Hamburg, Germany
	Centrifuge 5417R	Eppendorf, Hamburg, Germany
	Centrifuge 5424	Eppendorf, Hamburg, Germany
Capillary Electrophoresis	2100 Bioanalyzer	Agilent, Waldbronn, Germany
Cell counter	Countess FL II	Thermo Fisher, Darmstadt, Germany

Centrifuges	J2-HS Centrifuge	Beckmann Coulter, Krefeld, Germany
	Megafuge 1.0, Heraeus	Thermo Fisher, Darmstadt, Germany
	Megafuge 16R	Thermo Fisher, Darmstadt, Germany
DNA gel electrophoresis system	MIDI-1 Electrophoresis Unit	Carl Roth, Karlsruhe, Germany
DNA sequencer	ABI Prism 3130-Avant	Thermo Fisher, Darmstadt, Germany
Electroporation device	Gene Pulser II	Bio-Rad, Munich, Germany
FACS	BD FACS Canto II	BD Bioscience, Heidelberg, Germany
Fluorometer	Qubit	Thermo Fisher, Darmstadt, Germany
Fluorospectrophotometer	Fluostar Omega	BMG Labtech, Ortenberg, Germany
Freezer (-80°C)	Herafreeze HFU 686 Basic	Thermo Fisher, Darmstadt, Germany
Gel Documentation System	Gel Doc XR+	Bio-Rad, Munich, Germany
Heating blocks	Thermomixer comfort	Eppendorf, Hamburg, Germany
	Thermostat plus	Eppendorf, Hamburg, Germany
	Hybex Microsample Incubator	SciGene, Sunnyvale, USA
Hemocytometer	Neubauer chamber, bright-lined	Hartenstein, Würzburg, Germany
Incubator (bacteria)	Model U10	Memmert, Schwabach, Germany
Incubator (cell culture)	Hera Cell 150	Thermo Fisher, Darmstadt, Germany
Incubator shaker (bacteria)	New Brunswick Scientific G25	Eppendorf, Hamburg, Germany
Magnetic separator	MagnaRack	Thermo Fisher, Darmstadt, Germany

Magnetic stirrer	M3001K	Heidolph, Schwabach, Germany
Micropipettes	Eppendorf research PIPETMAN Classic	Eppendorf, Hamburg, Germany Gilson, Limburg-Offheim, Germany
Microscopes	Wilovert (Inverted Phase) Fluovert (Inverted Phase)	Leica, Wetzlar, Germany Leica, Wetzlar, Germany
Microwave	NN3256	Panasonic, Hamburg, Germany
Multichannel pipette	Discovery comfort	HTL Lab Solutions, Warszawa, Poland
Multipipette	Multipipette plus	Eppendorf, Hamburg, Germany
Orbital shaker	Unimax 1010	Heidolph, Schwabach, Germany
pH meter	Inolab pH Level 1	WTW, Weilheim, Germany
Pipet aid	accu-jet pro pipetboy acu	Brand, Wertheim, Germany Integra, Biebertal, Germany
Power supplies	E835 Power Pac 200	Consort, Turnhout, Belgium Bio-Rad, Munich, Germany
Protein gel electrophoresis system	Mini-PROTEAN Tetra System	Bio-Rad, Munich, Germany
qPCR analyzer	Cobas Z480	Roche, Mannheim, Germany
Scales	LC 1500 P1200	Labor Center, Fürth, Germany Mettler-Toledo, Gießen, Germany
Sequencer	ABI Prism 3130-Avant Genetic Analyzer	Thermo Fisher, Darmstadt, Germany
Spectrophotometer	Nanodrop ND-1000	Peqlab, Erlangen, Germany
Thermal cyclers	Mastercycler Gradient Mastercycler Personal GeneAmp PCR System 9700 SimpliAmp Thermal Cycler	Eppendorf, Hamburg, Germany Eppendorf, Hamburg, Germany Thermo Fisher, Darmstadt, Germany Thermo Fisher, Darmstadt, Germany

Tilting table	Platform mixer	Ratek, Melbourne, Australia
Tissue culture hood	HeraSafe KS12	Thermo Fisher, Darmstadt, Germany
Vacuum pump	LABOPORT N 86 KT.18	KNF, Freiburg, Germany
Vortexer	Vortex Genie 2 GLW L46	Scientific Industries, Bohemia, USA Hartenstein, Würzburg, Germany
Water baths	Model 1003, 14 L Model S and F3	GFL, Burgwedel, Germany Haake, Osterode am Harz, Germany
Western blot transfer system	PerfectBlue Tank-Electroblotter	peQLab, Erlangen, Germany

5.15 Software

Table 26: Software

Name	Manufacturer/ URL
Adobe Illustrator CS2	Adobe Systems Incorporated, San Jose, USA
ChromasLite (version 2.6.2)	Technelysium Pty Ltd, South Brisbane, Australia
ClustalX2	Conway Institute, University College Dublin, Ireland
CRISPR Design	Zhang Lab, McGovern Institute, MIT, Cambridge, USA http://crispr.mit.edu/
Flowing software (version 2.5.1)	Turku Centre for Biotechnology, University of Turku, Finland
GraphPad Prism	GraphPad Software, Inc., La Jolla, USA
Jalview 2.10.1	http://www.jalview.org RIKEN Yokohama Institute, Yokohama, Japan
LightCycler 480 Gene Scanning Software	Roche, Mannheim, Deutschland
Microsoft Office 2013	Microsoft, Redmond, USA
NCBI BLAST	NCBI, Bethesda, USA http://blast.ncbi.nlm.nih.gov/Blast.cgi
NCBI PrimerBLAST	NCBI, Bethesda, USA http://www.ncbi.nlm.nih.gov/tools/primer-blast/
OligoAnalyzer 3.1	Integrated DNA Technologies, Leuven, Belgium http://eu.idtdna.com/calc/analyzer
SnapGene	GSL Biotech LLC, Chicago, USA

5.16 Databases

Table 27: Databases

Database	URL
1000 genomes project	http://www.internationalgenome.org/
Catalogue of somatic mutations in cancer (Cosmic)	http://cancer.sanger.ac.uk/cancergenome/projects/cosmic/
dbSNP	http://www.ncbi.nlm.nih.gov/projects/SNP/
Exome Aggregation Consortium (ExAC)	http://exac.broadinstitute.org/
UCSC Genome Browser	http://genome.ucsc.edu/

6 Methods

6.1 Targeted resequencing of the RTKs *EGFR, EPHA2, IGF1R, ERBB3, NTRK1 and NTRK2*

6.1.1 Library preparation using the 48.48. Access Array

Amplicons of the coding DNA sequences of the RTKs *EGFR*, *ERBB3*, *IGF1R*, *EPHA2*, *NTRK1* and *NTRK2* were generated in a multiplex PCR approach with sample specific barcodes to distinguish samples. Tumor and normal samples of MM patients were kindly provided by the DSMM, cell line specific DNA was isolated using the AllPrep DNA/RNA Mini Kit and quantified using the Nanodrop ND-1000. 20 ng DNA was used for target enrichment in a multiplex PCR approach with 255 tagged primer pairs. For the multiplex PCR the 48.48. Access Array together with the FC1 cycler system (Fluidigm) was used according to manufacturer's specifications. Amplified products were diluted 1:30 and barcoded with the Access Array barcode library designed for the Illumina system according to manufacturer's manual. The barcoded products were analyzed for size and quality using the DNA 1000 Kit (Agilent) and the 2100 Bioanalyzer (Agilent). After barcoding, samples were pooled (Harvest sample pool) and purified using AMPure XP beads (BeckmanCoulter). For this purpose, 20 ng of each barcoded sample were combined in a harvest sample pool. Next, 12 µl of this harvest sample pool, 25 µl TE buffer and 36 µl AMPure XP beads were mixed, vortexed and incubated at RT for 10 min. Tubes were placed into a magnetic separator (Thermo Fisher) for 1 min before the supernatant was removed. Beads were washed twice with 180 µl freshly prepared 70% ethanol using the magnetic separator. Supernatant was removed and beads air-dried for 15 min at RT. 20 µl DNA suspension buffer was added to the dried beads and vortexed for 5 s before tube was placed into the magnetic separator for 1 min. Supernatant was placed into a new tube and 1 µl purified sample was analyzed using a DNA 1000 chip and the 2100 Bioanalyzer. The concentration of the PCR product library was determined using the Qubit dsDNA HS Assay Kit according to manufacturer's specifications.

6.1.2 Amplicon sequencing and data analysis

Library preparation and amplicon sequencing were performed using the Access Array platform from Fluidigm for amplicon generation (6.1.1) and the MiSeq for paired-end sequencing as

described previously [124]. An equimolar amount of each purified harvest sample pool of the six performed Access Arrays was pooled and 300 ng of this DNA pool was subsequently used for paired end sequencing on the MiSeq platform (Illumina, Eindhoven, Netherlands). Sequencing was performed with custom-specific LNA-primers (Table 6) according to the "Access Array System for Illumina Sequencing Systems" manual (Fluidigm). Bioinformatics data analysis was performed by Dr. Jordan Pischimarov using Cutadapt, BWA, GATK and SeattleSeqAnnotation 137 as described previously [124, 127]. The identified mutations were furthermore manually filtered for non-synonymous mutations in exonic regions.

6.1.3 Validation of detected mutations

All mutations detected by the amplicon sequencing approach were validated using PCR and Sanger sequencing. Therefore, tumor samples containing a possible mutation as well as the corresponding normal samples were used as templates for a 25 µl PCR reaction (Table 28, Table 29). Specific primers were designed using NCBI Primer BLAST and checked for hairpins, self- and heterodimers using OligoAnalyzer 3.1 (IDT) (Table 7).

Table 28: Standard PCR components

Component	Volume [µl]	Final concentration
DNA template	1	5 ng
Primer (forward) 10 µM	0.5	0.2 µM
Primer (Reverse) 10 µM	0.5	0.2 µM
Taq buffer with KCl 10x	2.5	1x
$MgCl_2$ 25 mM	2.5	2.5 mM
dNTPs 2 mM	2.5	0.2 mM
Taq DNA polymerase 5U/µl	0.2	1 U
H_2O	15.3	

Table 29: Standard PCR program

Temperature	Time	No. of cycles
95°C	3 min	1
95°C	30 s	45
55-65 °C	30 s	
72°C	1 min/kb	
72°C	10 min	1
4°C	∞	

To visualize the generated PCR products, 5µl of each reaction were mixed with 1µl 6x loading dye (LD) and applied to a 1.5 % agarose gel stained with GelRed (Genaxxon). The agarose gel ran at 140 V for approximately 25 min before DNA bands were visualized under UV light using the Gel Doc XR+ (Bio-Rad). For Sanger sequencing samples were purified using the Rapid PCR Cleanup Enzyme Set (NEB) according to manufacturer's protocol. Purified samples were used for a sequencing PCR with either the forward or reverse primer (Table 30, Table 31).

Table 30: Sequencing PCR components

Component	Volume [µ]
Purified PCR product	3.5
BigDye Terminator v3.1 Ready Reaction Mix	1
Primer (forward or reverse) 10 µM	1.6
H_2O	3.9

Table 31: Sequencing PCR program

Temperature	Time	No. of cycles
94°C	2 min	1
94°C	20 s	
50 °C	20 s	50
60°C	2 min	
4°C	∞	

After the sequencing PCR, samples were purified using sephadex columns. 22 µl Hi-Di Formamide were added to the purified sample and the samples were sequenced using the ABI Prism 3130-Avant Genetic Analyzer (Thermo Fisher). The generated sequences were evaluated using ChromasLite and ClustalX2.

To validate mutations with variant allele frequencies lower than 20 % a high resolution melting assay (HRM) was performed using the LightCycler 480 High Resolution Melting Master Kit (Roche) according to the manufacturer's specifications. Specific primers were designed using NCBI Primer BLAST (Table 7). Briefly, DNA isolated from HMCLs was used to adjust the primer-specific $MgCl_2$ concentration. No secondary products should be created and the C_p-value should be below 30. Three HMCLs (here: AMO1, L363 and INA6) with no mutations in the generated amplicons were used as controls in HRM assays with tumor and normal patient samples to distinguish between mutation and no mutation. The Cobas Z480 was used to amplify the product and to record the fluorescence signal (Table 33). The HRM was analyzed

using the LightCycler 480 Gene Scanning Software with the Comn/Vars settings and a sensitivity of 0.6.

Table 32: HRM components

Component	Volume [µl]	Final concentration
DNA template	1	5 ng
HRM master mix 2x	10	1x
Primer mix 4 µM	1	0.2 µM
$MgCl_2$ 25 mM	0.8 – 2.8	1 - 3.5 mM
H_2O	*Ad* 20	

Table 33: HRM program

T [°C]	Time	Cycles	Acquisition Mode	Ramp rate [°C/s]	Acquisition [per °C]	Sec T [°C]	Step size [°C]	Step delay [cycles]
Pre-Incubation								
95	10 min	1	none	4.4	none	0	0	0
Amplification								
95	10 s		none	4.4	none	0	0	0
65	15 s	45	none	2.2	none	53	0.5	1
72	10 s		single	4.4	none	0	0	0
HRM								
95	1 min		none	4.4	none			
40	1 min	1	none	2.2	none			
65	1 s		none	1	none			
95			continues	0.2	25			
Cooling								
40	10	1	none	2.2	None	0	0	0

6.1.4 Statistical analysis

Statistical analysis was done using SPSS statistics software (version 23) or GraphPad Prism (version 7) with *p*-values < 0.05 being considered statistically significant. Correlations of RTK mutations with cytogenetics and response to therapy were done with cross tabulations in combination with Pearson chi-square and Fisher's exact-test for significance. Monovariate survival statistics were done using Kaplan-Meier curves with log-rank tests for significance. For comparison of cell proliferation a Student's *t*-test was performed.

6.1.5 Validation of mutations on cDNA level

For the validation of mutations on cDNA level, RNA was isolated using the AllPrep DNA/RNA Mini Kit (Qiagen) according to the manufacturer's manual. 1 µg isolated RNA was reversely transcribed using the First Strand cDNA Synthesis Kit (Thermo Fisher) according to the manufacturer's specifications. The synthesized cDNA was used as template in a standard PCR reaction. PCR products were visualized on an agarose gel and Sanger sequenced as described previously (6.1.3).

6.2 Prokaryotic cell methods

6.2.1 Culturing of *E. coli*

The *E. coli* strains NEB10β and α-Select Silver were cultivated on either LB-agar plates containing the appropriate selection antibiotic at 37°C or in LB-broth containing the appropriate selection antibiotic at 37°C and 250 rpm.

6.2.2 Transformation of *E. coli*

For each transformation 50 µl *E. coli* were used and thawed on ice. Either 5 µl of newly ligated or 5 ng of previously purified plasmid was added to the cells and mixed carefully. Samples were incubated on ice for 30 min before a heat shock at 42°C for 45 s. After the heat shock samples were incubated on ice for 2 min. 200 µl SOC medium was added to the samples. If the plasmids used for the transformation had an AMP resistance gene, 10 µl and 100 µl of the samples were directly plated on LB-Amp plates. For all other resistance genes, samples were incubated for 1h at 37°C and 220 rpm before 10 µl and 100 µl were plated on the appropriate LB selection plates. Plates were incubated overnight at 37°C. Single colonies were picked, streaked onto LB selection plates, incubated overnight at 37°C and plasmids isolated from grown clones using the NucleoSpin Plasmid Kit (Macherey Nagel) according to the manufacturer's manual.

6.3 Molecular biology methods

6.3.1 Mutagenesis PCR

IGF1R mutations validated on cDNA level (here: N1129S and D1146N) were introduced into the coding DNA sequence (CDS) of IGF1R using a mutagenesis PCR. For this purpose specific

mutagenesis primers were designed (Table 9) and used in a mutagenesis PCR with the Q5 polymerase (Table 34, Table 35).

Table 34: Mutagenesis PCR components

Component	Volume [µl]	Final concentration
pCR-XL-TOPO-IGF1-R	1	100 ng
Primer (forward) 10 µM	0.5	0.5 µM
Primer (Reverse) 10 µM	0.5	0.5 µM
Q5 buffer 5x	5	1x
dNTPs 10 mM	0.5	0.2 mM
Q5 High-Fidelity DNA Polymerase 2U/µl	0.2	0.4 U
H_2O	17.3	

Table 35: Mutagenesis PCR program

Temperature	Time		No. of cycles
98°C	30 s		1
98°C	10 s	⎡	
69 °C	20 s	⎢	50
72°C	2 min	⎣	
4°C	∞		

To remove the plasmid template, the PCR product was digested with DpnI at 37°C overnight, followed by heat inactivation at 80°C for 30 min (Table 36).

Table 36: DpnI digestion components

Component	Volume [µl]	Final concentration
PCR amplified plasmid	10	
CutSmart Buffer 10x	2	1x
DpnI (20 U/µl)	1	20 U
H_2O	7	

E. coli NEB10β were transformed with digested plasmids (6.2.2). Following transformation and plasmid isolation plasmids were sequenced at GATC Biotech to review for undesired mutations. Accurate plasmids were subsequently used for cloning of overexpression plasmids.

6.3.2 Cloning of overexpression plasmids

A restriction digestion approach was used for the cloning of the overexpression plasmids. Previously constructed pCR-XL-TOPO-IGF1-R-WT and pCR-XL-TOPO-IGF1-R-mut plasmids were used as templates in a PCR with Phusion polymerase to introduce restriction digestion sites (Table 10, Table 37 Table 38).

Table 37: Phusion High-Fidelity Polymerase PCR components

Component	Volume [µl]	Final concentration
Plasmid (100 ng/µl)	1	100 ng
Primer (forward) 10 µM	1.25	0.5 µM
Primer (Reverse) 10 µM	1.25	0.5 µM
Phusion High-Fidelity Master Mix 2x	12.5	1x
DMSO	1.25	5 % (optional)
H_2O	*ad* 25	

Table 38: Phusion High-Fidelity polymerase PCR program

Temperature	Time	No. of cycles
98°C	3 min	1
98°C	10 s	40-50
70 °C	30 s	
72°C	2 min 30 s	
72°C	10 min	1
4°C	∞	

PCR products and the empty mammalian pSF-CMV-Puro-COOH-GST expression vector were digested with NotI-HF and EcoRI-HF for 1h at 37°C followed by heat inactivation at 60°C for 20 min.

Table 39: Restriction digestion components

Component	Volume [µl]	Final concentration
PCR product/Expression vector	20	
CutSmart Buffer 10x	5	1x
EcoRI-HF (20 U/µl)	1	20 U
NotI-HF (20 U/µl)	1	20 U
H_2O	23	

Digested PCR products (=inserts) and vectors were applied to a 1% agarose gel stained with SYBR Safe (Thermo Fisher), ran at 140 V for approximately 30 min and were visualized using blue light. The desired DNA was purified using the MinElute Gel Extraction Kit (Qiagen) according to the manufacturer's specifications and the DNA concentration was determined using the Nanodrop ND-1000. Vector and insert were ligated using the T4 ligase in a 1:3 (vector:insert) ratio. The amounts of vector and insert needed for ligation were calculated (Equation 1) and the ligation occurred at RT for 2 h (Table 40).

Equation 1: Calculation of DNA amount needed for ligation approaches

$$Amount\ [g] = amount\ [mol] * Molecular\ mass\ 1bp\ \left[660\ \frac{g}{mol}\right] * number\ bases$$

Table 40: T4 DNA ligase approach

Component	Volume [µl]	Final concentration
Vector	variable	10 fmol
Insert	variable	30 fmol
T4 DNA ligase buffer 10x	2	1x
T4 DNA ligase	1	
H_2O	ad 20 µl	

Ligated plasmids were transformed into *E.coli* strain NEB10β as described previously (6.2.2). To confirm successful integration of the insert into the plasmid, isolated plasmids were digested using NotI-HF and EcoRI-HF for 1h at 37°C. Digested plasmids were applied to an agarose gel and visualized using UV light. Plasmids containing an insert were sent to GATC for sequencing (for primer information see Table 11). Plasmids containing no undesired mutations were stored at -20°C.

Table 41: Components for digestion of ligated plasmids

Component	Volume [µl]	Final concentration
Ligated plasmid	5	
CutSmart Buffer 10x	1	1x
EcoRI-HF (20 U/µl)	0.5	10 U
NotI-HF (20 U/µl)	0.5	10 U
H_2O	3	

6.4 Eukaryotic cell culture methods

6.4.1 Culturing of human cell lines

The HMCL AMO1, L363, OPM2, JJN3, MOLP8, KMS11, KMS12BM, U266, NCIH-929, RPMI8226, MM1.S and INA 6 were cultivated in RPMI1640 medium containing 10 % FBS and 2 mM L-glutamine. NCIH929 cells were supplemented with 0.05 mM 2-mercapto-ethanol, INA 6 cells were supplemented with 2 ng/ml human recombinant IL-6. Cells were passaged every 3-4 days. For electroporation experiments cells were cultivated in RPMI1640 medium containing 15 % fetal bovine serum (FBS) and 2 mmol/L L-glutamine. Every 3-4 months fresh cells in low passage numbers were thawed from liquid nitrogen.

HEK293FT cells were cultivated in DMEM supplemented with 10 % FBS, 0.5 mg/ml Geneticin, 6 mM L-Glutamine, 1 mM Sodium Pyruvate und 1x MEM Non-Essential Amino Acids containing 0.1 mM Glycine, 0.1 mM L-Alanine, 0.1 mM L-Asparagine, 0.1 mM L-Aspartic acid, 0.1 mM L-Glutamic acid, 0.1 mM L-Proline and 0.1 mM L-Serine. Cells were passaged every 3-4 days.

Therefore, medium was removed, cells were washed with 1x PBS and 1 ml trypsin-EDTA was added per 10 cm dish. Cells were removed and centrifuged at 111 relative centrifugal force (rcf) for 4 min. The cell pellet was resuspended in 10 ml complete DMEM medium. 1 ml of the resuspended cells was added to 9 ml fresh complete DMEM in a new 10 cm dish. After 16 passages cells were discarded and fresh cells were thawed from liquid nitrogen.

All cell lines were cultivated at 37°C and 5 % CO_2 and regularly checked for mycoplasma contamination using the VenorGEM One-Step kit according to manufacturer's manual.

6.4.2 Transfection of HEK293FT cells

HEK293FT cells were transfected using Lipofectamin 2000. One day before transfection 6 x 10^5 cells/well were seeded into a 6 well plate and incubated at 37°C and 5 % CO_2. Before transfection, medium was removed, the cells were carefully washed with 1x PBS and 500 µl Opti-MEM with 10 % FBS was added to the cells. For each approach 12 µl Lipofectamin 2000 was mixed with 150 µl Opti-MEM and incubated at RT for 5 min. Meanwhile, 2.5 µg plasmid was mixed with 150 µl Opti-MEM and added to the Lipofectamin 2000 following incubation. The Lipofectamin-plasmid mix was incubated at RT for 20 min and added dropwise to the cells. After 24 h medium was removed and whole cell lysates (WCL) were prepared (6.5.1).

6.4.3 Stimulation experiments using IGF1

To detect the influence of IGF1R WT, IGF1R D1146N and IGF1R N1129S on the downstream signaling of MM cells stimulation experiments using IGF-1 were performed. For this purpose, 3 x 10^6 cells per stimulation were used. The appropriate amount of cells was centrifuged for 4 min at 111 rcf. The cell pellet was washed with 1x PBS, centrifuged again, resuspended in 3 ml starvation medium and put into a 6 well plate. Cells were starved for 18 h at 37°C and 5 % CO_2 before they were stimulated with 20 ng/ml IGF-1 for 10 min at 37°C and 5 % CO_2. Unstimulated cells were carried along as negative controls. Immediately after stimulation cells were transferred to a 15 ml falcon tube and put on ice. Used wells were washed with 1 ml cold 1x PBS and added to the corresponding samples. Cells were centrifuged at 250 rcf for 5 min. The cell pellets were resuspended in 1 ml cold 1x PBS, put into a 1.5 ml tube and centrifuged again. WCL of stimulated and unstimulated cell pellets were prepared using 50 µl lysis buffer (6.5.1). Stimulation experiments were performed twice.

6.4.4 Analysis of cell proliferation

To analyze cell proliferation of MM cells BrdU assays were performed. The Cell Proliferation ELISA, BrdU (colorimetric) kit in combination with FACS analysis was used to measure BrdU integration into the cellular DNA. BrdU integration was measured after 0 h, 12 h, 24 h and 48 h. For this purpose, cells were counted using the Countess II FL (Thermo Fisher) and 5 x 10^4 cells for each approach were seeded into a 6-well plate (total cell number: 4 x 10^5 cells in 4.8 ml medium) and incubated in complete medium. After incubation, 600 µl of cells were removed and centrifuged at 390 rcf for 5 min. The cell pellet was resuspended in 1 ml fixation buffer and incubated at 37°C for 10 min, followed by an incubation on ice for 1 min. Fixed cells were centrifuged for 5 min at 390 rcf, the cell pellet resuspended in 90 % methanol, incubated on ice for 10 min and stored at -20°C until all approaches were completed. For FACS analysis, cells were centrifuged for 5 min at 250 rcf and washed twice with FACS buffer. Cells were resuspended in 100 µl FACS buffer containing 0.5 U DNase I and incubated at 37°C for 1 h. After DNase I treatment cells were washed twice with FACS buffer and cells resuspended in 100 µl FACS buffer containing 2 µl BrdU-FITC antibody followed by an incubation for 1 h at RT in the dark. Afterwards, cells were once more washed with FACS buffer, the washed cells were resuspended in 200 µl FACS buffer and measured using the BD FACS Canto II. FACS results were analyzed using Flowing Software. BrdU assays were performed in three independent experiments.

Additionally, cells were counted manually using a Neubauer chamber to monitor cell proliferation. For this purpose, 1.5 x 10^6 cells were seeded in 3 ml cell culture medium in a 6 well plate. After 24 h, 48 h and 72 h cells were counted and the total number of cells determined. All assays were performed in triplicates.

6.5 Protein work

6.5.1 Preparation of whole cell lysates

Before the preparation of WCL, cells were counted using trypan blue and a Neubauer chamber. 1 x 10^7 cells were centrifuged at 111 rcf for 4 min and the cell pellet was resuspended in 1 ml cold 1x PBS. Cells were centrifuged again and the pellet was resuspended in 250 µl lysis buffer. The resuspended pellet was incubated on ice for 20 min before being centrifuged at 16000 rcf and 4°C for 15 min. The supernatant was transferred into a new 1.5

ml tube and either used immediately for the determination of the protein concentration and sample preparation or stored at -80°C.

6.5.2 Determination of protein concentration

To determine the protein concentration of the WCL a Bradford assay was applied. For this purpose, the WCLs were diluted 1:20 in H_2O and standards with known BSA concentrations were prepared. Each lysate as well as the standards and the blank were measured in triplicates. For each sample 290 µl Bradford solution was put in a well of a 96 well plate and either 10 µl diluted protein or standard was added. 300 µl Bradford without a sample served as the blank measurement. After addition of the samples the plate incubated at RT in the dark for 5 min before being measured at a wavelength of 595 nm. Using the known BSA concentrations a standard curve was determined and used to calculate the protein concentrations of the WCL.

6.5.3 Sample preparation

To prepare samples for Western blot analysis 40 µg of WCL were diluted with 4x loading dye (LD) and heated at 95°C for 5 min. Prepared samples were either used for SDS-PAGE immediately or stored at -20°C.

6.5.4 SDS-PAGE and Western blot

Prepared Western blot samples were subsequently used for sodium dodecyl sulfate polyacrylamide gel electrophoresis (SDS-PAGE) to separate the proteins by size using an electric current. For this purpose, SDS gels, consisting of stacking (6%) and separation gel (10%) (Table 42), were poured and the previously prepared samples as well as 2.5 µl prestained protein ladder were applied. The gel was run for 10 min at 90 V and for approximately 70 min at 140 V.

Table 42: Components of stacking and separation gel for SDS-PAGE

Stacking gel		Separation gel	
Component	**Volume**	**Component**	**Volume**
Stacking gel buffer	875 µl	Separation gel buffer	1.38 ml
Acrylamide (30 %)	700 µl	Acrylamide (30 %)	1.85 ml
APS (10 %)	42 µl	APS (10 %)	93.5 µl
TEMED	3.5 µl	TEMED	7.7 µL
H_2O	1.9 ml	H_2O	2.3 ml

Following SDS-PAGE proteins were transferred to nitrocellulose membranes using the PerfectBlue Tank-Electroblotter, a wet blotting transfer system. Proteins were transferred for 90 min at 400 mA and 90 V. Afterwards the membranes were reversibly stained with Ponceau S and subsequently washed with deionized H_2O to ensure successful protein transfer.

6.5.5 Immunodetection of proteins

After successful transfer of proteins to nitrocellulose membranes, the membranes were blocked with either 5 % MP in TBS-T or 5 % BSA in TBS-T for 1 h at RT. After blocking of the membrane, the primary antibody was added in the indicated dilution (Table 43) and incubated at 4°C overnight.

Table 43: Dilutions of used primary antibodies

Antibody	Dilution	Diluent
IGF1R	1:5000	MP
phospho-IGF1R_Y980	1:1000	BSA
phospho-IGF1R_Y1135	1:1000	BSA
AKT	1:4000	MP
phospho-AKT_S473	1:1000	BSA
ERK1/2	1:2000	BSA
phospho-ERK1/2	1:5000	BSA
MEK	1:2000	BSA
phospho-MEK	1:2000	BSA
FAK	1:1000	BSA
phospho-FAK_Y397	1:500	BSA
mTOR	1:1000	BSA
phospho-mTOR	1:1000	BSA
BRAF	1:1000	BSA
CRAF (raf-1)	1:2000	BSA
phospho-CRAF	1:1000	MP
RAS	1:1000	BSA
PYK2	1:8000	BSA
phospho-PYK2	1:1000	BSA
ITGB1	1:500	BSA
c-myc	1:25 000	MP
GAPDH	1:100 000	MP

After incubation, the membrane was washed 3x 10 min with TBS-T before the corresponding secondary antibody was added in the indicated dilution (Table 44) for 1-2 h at RT. Following the incubation with secondary antibody, the membrane was washed 3x 10 min with TBS-T. SuperSignal West Pico Chemiluminescent Substrate was added to the membrane for approximately 1 min followed by the visualization of protein signals using X-ray films. Western blots were usually performed twice.

Table 44: Dilutions of used secondary antibodies

Antibody	Dilution	Diluent
Anti-rabbit IgG, HRP-linked Antibody	1:2000	TBS-T
Anti-mouse IgG, HRP-linked Antibody	1:3000	TBS-T
Peroxidase AffiniPure F(ab')$_2$ Fragment Goat Anti-Rabbit IgG (H+L)	1:10000	5 % MP/TBS-T

6.6 CRISPR/Cas9

For CRISPR/Cas9 experiments the Alt-CRISPR-Cas9 System from IDT was used.

6.6.1 Preparation of RNP complex

In a first step, the ribonucleoprotein (RNP) complex consisting of the crRNA:tracrRNA complex and the Cas9 nuclease was assembled. Therefore, 5 µl crRNA (200 µM) and 5 µl tracrRNA (200 µM) were mixed, incubated at 95°C for 5 min and cooled to RT. Afterwards, the components needed for the formation of the RNP complex (Table 45) were mixed and incubated at RT for 5 min. For each transfection approach 10 µl RNP complex were required.

Table 45: Components for RNP complex formation

Component	Volume [µl]
crRNA:tracrRNA 100µM	2.4
Nuclease-free IDT Buffer	2.6
Cas9 61 µM	3.34
Cas9 Storage buffer	1.66

6.6.2 Transfection of HMCL

One day before transfection MM cells were counted using trypan blue and a Neubauer counting chamber. For each electroporation approach 1 x 10^6 cells were required. The necessary amount of cells was centrifuged at 111 rcf for 4 min and the cell pellet resuspended in electroporation medium without P/S. Cells were cultivated at 37°C and 5 % CO_2 overnight. Directly before transfection, cells were counted again and the necessary amount of cells was centrifuged at 250 rcf for 5 min. The cell pellet was resuspended in 1ml 1x PBS per approach and distributed equally into one 1.5 ml tubes per approach. Cells were centrifuged again and the supernatant was removed. 40 µL RPMI and 10 µl RNP complex were added to each CRISPR/Cas9 approach, 50 µl RPMI was added to control electroporation approaches. Cells were resuspended right before electroporation and put into a 2 mm electroporation cuvette. Each approach was electroporated using a single electric pulse with HMCL dependent voltages (Table 46).

Table 46: Voltages used for electroporation (2 mm cuvettes)

Cell line	Voltage
L363	190 V
U266	230 V

Right after the electric pulse cells were removed from the cuvette using 200 µl RPMI 1640 and incubated at RT for 5 min. After incubation cells were put into 7 ml electroporation medium and incubated at 37°C and 5 % CO_2 for 24 h. To separate dead cells, cell debris and living cells an Optiprep assay was used. For each approach an optimix containing 2.5 ml RPMI 1640 and 750 µl Optiprep was prepared. Cells were centrifuged at 250 rcf for 5 min and the pellet was resuspended in the prepared optimix. This suspension was overlaid using 200 µl PBS and centrifuged for 7 min at 2122 rcf. The white layer of living cells was removed, put into 500 µl electroporation medium and centrifuged at 175 rcf for 3 min. The cell pellet was resuspended in 100 µl electroporation medium and incubated at 37°C and 5% CO_2 for 48 h.

6.6.3 Analysis of transfected cells

To analyze the cells transfected with the RNP complex a PCR followed by a T7 endonuclease digestion was performed. To isolate genomic DNA from the cells, cells were counted and $1x10^4$ cells were centrifuged at 250 rcf for 5 min. The pellet was washed using 100 µl 1x PBS, centrifuged again and dissolved in 20 µl DNA-lysis buffer. Subsequently, 1 µl Proteinase K was added and the whole mixture incubated at 56°C for 1h, followed by an incubation at 95°C for 15 min[128]. Isolated DNA was used to amplify the target region using specific primers (Table 7) and the Q5 polymerase (Table 47, Table 48).

Table 47: Components of a PCR with the Q5 polymerase

Component	Volume [µl]	Final concentration
Isolated genomic DNA	5	
Primer (forward) 10 µM; #7	1.25	0.5 µM
Primer (Reverse) 10 µM; #8	1.25	0.5 µM
Q5 buffer 5x	5	1x
dNTPs 10 mM	0.5	0.2 mM
Q5 High-Fidelity DNA Polymerase 2U/µl	0.25	0.5 U
H_2O	11.75	

Table 48: Q5 polymerase PCR program

Temperature	Time	No. of cycles
98°C	30 s	1
98°C	10 s	
68 °C	20 s	45
72°C	30 s	
72°C	2 min	1
4°C	∞	

PCR products were visualized on a 1.5 % agarose gel and ran for approximately 30 min at 140 V. For T7 endonuclease digestion the PCR products were first heteroduplexed. Therefore, the components needed for heteroduplex formation (Table 49) were mixed and incubated at 95°C for 10 min before the mixture was cooled down in 10°C intervals with a ramp rate of -2°C/s (Table 50). The heteroduplexed PCR products were subsequently digested using the T7 endonuclease for 1 h at 37°C (Table 51). Digested products were visualized on a 1.5 % agarose gel and the ratio (%) of cut DNA was calculated (Equation 2).

Table 49: Components for heteroduplex formation

Component	Volume [µl]
PCR product	10
10x NEBuffer2	1.5
H_2O	2.5

Table 50: Thermocycler program for heteroduplex formation

Temperature	Time	Ramp rate
95°C	10 min	
95-85°C		-2°C/s
85°C	1 min	
85-75°C		-2°C/s
75°C	1 min	
75-65°C		-2°C/s
65°C	1 min	
65-55°C		-2°C/s
55°C	1 min	
55-45°C		-2°C/s
45°C	1 min	
45-35°C		-2°C/s
35°C	1 min	
35-25°C		-2°C/s
25°C	1 min	
4°C	∞	

Table 51: Components for T7 endonuclease digestion

Component	Volume [µl]
PCR heteroduplex	14
T7 endonuclease (10 U/µl)	1

Equation 2: Calculation of ratio of cut DNA

$$cut\ DNA\ (\%) = \left(1 - \left(1 - \left(\frac{b+c}{a+b+c}\right)\right)^{\frac{1}{2}}\right) * 100$$

$$a\text{: intensity of DNA substrate}$$

$$b, c\text{: intensity of cleaved products}$$

6.6.4 Single cell selection and confirmation of genome editing

For the establishment of stable knockdown clones, single cells had to be selected. Therefore, cells were counted using a Neubauer chamber and 1 cell/100 µl was plated in each well of a 96 well plate. To enhance cell growth complete medium was supplemented with 2 ng/ml IL-6, 2 ng/ml VEGF-A and 100 U/ml TNF-α. After 48h at 37°C and 5 % CO_2 wells were checked for single cells. Cells were incubated at 37°C and 5 % CO_2 until cell colonies were visible. To confirm successful genome editing, genomic DNA was isolated as described previously (6.6.3) and used for a PCR with the Q5 Polymerase. PCR products were sequenced as described previously (6.1.3) and sequences analyzed using ChromasLite, ClustalX2 and Jalview 2.10.1 [129].

6.6.5 Confirmation of protein knockdowns using Western blot

Cells with an altered sequence were further cultivated and used to prepare WCL to confirm protein knockdown by Western blot (6.5). Cells with a successful protein knockdown were frozen in liquid nitrogen. For this purpose, cells were centrifuged for 5 min at 111 rcf and the cell pellet resuspended in freezing medium. Cells were stored at -80°C for 24 h before being transferred into liquid nitrogen.

6.7 Sleeping beauty transposase system

6.7.1 Cloning and purification of vectors

Sleeping Beauty donor vectors (kindly provided by Dr. Thorsten Stühmer) were cloned using restriction digestion and ligation. For this purpose, previously cloned pSF-IGF1R-WT and pSF-IGF1R-N1129S/D1146N (6.3.2) were used as templates for a PCR to introduce NheI and NotI restriction sites with previously designed primers (Table 10, Table 37 and Table 38). As

described previously, PCR products were subjected to an agarose gel electrophoresis and desired DNA was purified using the MinElute Gel Extraction Kit (Qiagen).

The DNA concentrations of the purified PCR products (=inserts) were determined using the Nanodrop ND-1000 (Peqlab) and digested with NheI-HF and NotI-HF for 1 h at 37°C (Table 52).

Table 52: NheI/NotI-restriction digestion components

Component	Volume [µl]	Final concentration
PCR product	10	
CutSmart Buffer 10x	1.5	1x
NheI-HF (20 U/µl)	0.5	10 U
NotI-HF (20 U/µl)	0.5	10 U
H_2O	2.5	

Vectors (TST-206-pT2-SVPuroCMV; TST-212-pT2BN-SVPuroCAG) were digested with NheI-HF and NotI-HF for 1 h at 37°C (Table 53). Digested vectors were applied to an agarose gel stained with SYBR Safe, ran at 140 V for 30 min and were visualized using blue light. Linearized vectors were cut from the agarose gel, purified using the MinElute Gel Extraction Kit (Qiagen) and the DNA concentration was determined.

Table 53: Components for restriction digestion of vectors

Component	Volume [µl]	Final concentration
Vector (1 µg/µl)	10	10 µg
CutSmart Buffer 10x	2	1x
NheI-HF (20 U/µl)	3	60 U
NotI-HF (20 U/µl)	3	60 U
H_2O	2	

Digested vector and insert were used for a ligation with T4 ligase in a ratio 1:3 (vector:insert). The amounts of vector and insert needed for ligation were calculated (Equation 1) and used for an overnight ligation at 19°C (Table 40).

The next day, ligated plasmids were used for transformation of *E. coli* NEB10β (6.2.2) and incubated overnight at 37°C. Single colonies were picked, grown overnight at 37°C and plasmids were isolated using the Nucleo Spin Kit (Macherey Nagel) according to the manufacturer's instructions. Isolated plasmids were digested for 1 h at 37°C (Table 54) before being applied to a 1 % agarose gel. Plasmids containing the desired inserts were sequenced at GATC to ensure no undesired mutations were present in the open reading frame (ORF).

Table 54: Components for restriction digestion of cloned plasmids

Component	Volume [µl]	Final concentration
Plasmid	5	
CutSmart buffer 10x	1	1x
FspI-HF	0.5	10 U
H_2O	3.5	

Bacterial colonies containing plasmids with no undesired mutations were grown overnight at 37°C and 225 rpm. Plasmids were isolated using the NuceloBond Xtra kit (Macherey Nagel) according to the manufacturer's instructions. Plasmids were diluted to a concentration of 1 µg/µl and stored at -20°C. Cloning was done in cooperation with Marlene Schwarzfischer [130].

6.7.2 Determination of lethal puromycin concentration

As part of the sleeping beauty transposase system a puromycin resistance gene is integrated into the genome of successfully transfected cells. Therefore, it had to be determined which puromycin concentration is lethal to MM cells without a resistance gene. 5 x 10^5 cells were plated into the wells of a 12 well plate. Cells were treated with 0.1 µg/ml, 0.25 µg/ml, 0.5 µg/ml, 0.75 µg/ml, 1.0 µg/ml, 1.5 µg/ml, 2 µg/ml and 3 µg/ml puromycin and incubated at 37°C and 5 % CO_2. After incubation for 72 h, cells were centrifuged at 250 rcf for 5 min, resuspended in medium and treated with puromycin again. Additionally, a blank control (only medium), alive control (no treatment) and a dead control (treated with H_2O_2) were carried along. After an additional incubation for 72 h at 37°C, cells were used for a MTT test using the Cell Proliferation Kit I (MTT) (Roche) according to the manufacturer's specifications.

6.7.3 Transfection of HMCL

The day before transfection, cells were centrifuged at 111 rcf for 4 min, the cell pellet resuspended in electroporation medium and cultivated at 37°C and 5% CO2 overnight. Directly before transfection, cells were counted using a Neubauer counting chamber and trypan blue. For each approach 1 x 10^7 cells were needed. The required amount of cells was centrifuged at 250 rcf for 5 min. The cell pellet was resuspended in 1 ml 1x PBS/approach and distributed equally into one 1.5 ml tubes per approach. Cells were centrifuged again and 500 µl RPMI containing the required plasmids were added to the cell pellet. For each approach 10 µg donor vector (TST206-pT2SVPuroCMV-IGF1R-WT, TST206-pT2SVPuroCMV-IGF1R-D1146N, TST206-pT2SVPuroCMV-IGF1R-N1129S, TST-212-T2BN-SVpuroCAG-IGF1R, TST-212-pT2BN-

SVpuroCAG-IGF1R-D1146N or TST-212-pT2BN-SVpuroCAG-IGF1R-N1129S), 15 µg transposase vector (pCMV(CAT)T7-SB100-Transposase) and 2.5 µg GFP vector (pmax-GFP) were used. Control reaction only contained 2.5 µg GFP vector. Right before electroporation, cells were resuspended and transferred into a 4 mm electroporation cuvette. For each approach, cells were electroporated with a single electric pulse and HMCL dependent voltages (Table 55).

Table 55: Voltages used for electroporation (4 mm cuvettes)

Cell line	Voltage
L363	300 V
AMO1	300 V

Cells were removed from the cuvette using 500 µl RPMI, incubated at RT for 5 min and added to 7 ml electroporation medium. Cells were incubated at 37°C and 5% CO_2 for 24 h. Following this incubation, living cells were separated from dead cells and cell debris using Optiprep (6.6.2). Living cells were resuspended in 5 ml electroporation medium and incubated at 37°C.

6.7.4 FACS analysis of transfected cells

To monitor electroporation efficiency, cells were subjected to FACS analysis 48 h after electroporation. For this purpose, 250 µl of each approach were centrifuged at 250 rcf for 5 min. Cell pellets were washed twice with 500 µl Annexin-FACS buffer and centrifuged at 250 rcf for 5 min. After washing, cell pellets were resuspended in 52 µl Annexin-FACS buffer containing 1 µl Annexin-V and 1 µl Propidium iodide and incubated for 30 min in the dark. After incubation 200 µl Annexin-FACS buffer were added to cell pellets and cells were measured using BD FACS Canto II. FACS results were analyzed using Flowing software 2.

6.7.5 Puromycin treatment

After FACS analysis of transfected cells, remaining cells were treated with puromycin. Cells were centrifuged at 111 rcf for 5 min and the cell pellet was resuspended in electroporation medium and cell-line dependent concentrations of puromycin (Table 56). Additionally, medium was supplemented with IL-6, VEGF-A and TNF-α to increase cell proliferation.

Table 56: Puromycin concentrations for cell selection

Cell line	Puromycin concentration
L363	1 µg/ml
AMO1	1.5 µg/µl

Every third day cells were centrifuged at 111 rcf for 5 min to remove dead cells. Cell pellets were resuspended in fresh medium containing puromycin. Control cells (untransfected/ transfected with pmax-GFP) were checked for living cells using Trypan blue and a Neubauer chamber. Cells were treated with puromycin until no living cells were detected in the control cells.

6.7.6 Overexpression analysis

To see if integration of IGF1R WT and IGF1R mut into the genome of host cells was successful, cells were subjected to FACS and Western blot analyses. For FACS analysis 500 µl of cells were centrifuged at 390 rcf for 5 min and washed with 1x PBS. Washed cells were resuspended in 500 µl FACS buffer and again centrifuged at 390 rcf for 5 min. The cell pellet was resuspended in 100 µl FACS buffer containing 5 µl IGF1R (alphaIR3) antibody (1:20 dilution) and incubated at RT for 15 min followed by incubation with secondary antibody (Goat anti-Mouse IgG (H+L) Cross-Adsorbed Secondary Antibody, Alexa Fluor 647; 1:200 in FACS buffer) for 15 min in the dark. Cells were measured using the BD FACS Canto II and analyzed using Flowing software. WCL were prepared and Western blot and immunodetection of proteins was performed as described previously (6.5). Western blots were performed in duplicates.

7 Results

7.1 Characterization of novel RTK mutations in the DSMM XI cohort

7.1.1 RTK mutations mainly affect the ligand-binding and tyrosine-kinase domains

In a first amplicon sequencing approach the CDS of the RTKs *EPHA2, EGFR, ERBB3, IGF1R, NTRK1* and *NTRK2* of 75 MM patients of the DSMM XI was sequenced using the Illumina MiSeq and the 454 GS Junior platforms. [124] After initial filtering steps 31 mutations remained. To exclude false positive mutations due to technical error, all mutations had to be validated by Sanger sequencing or HRM. This validation step resulted in the elimination of 11 mutations previously detected by amplicon sequencing. Nine out of these 11 mutations had very low variant allele frequencies (VAFs) (8-19%) and low quality parameters compared to validated mutations, indicating false positive hits. After the elimination of these mutations 9 of the remaining mutations were present in HMCL and 11 mutations were present in 10 patient samples (Table 57). The validated patient-specific mutations were neither listed in the 1000 genomes database nor in the dbSNP database and were all located in conserved domains according to PhastCons and GERP. Additionally, 36.3 % of mutations (4/11) led to structural changes according to Polyphen2. Interestingly, 5 mutations (45.5%) were not only present in the tumor, but also in the corresponding normal sample. These mutations were defined as rare SNPs which correlates to the low allele frequency (0- 8.241×10^{-5}) received from the ExAC browser. One mutation (9%) was a tumor-associated SNV and the remaining 5 mutations (45.5%) were specified as mutations-not otherwise specified (NOS) due to the lack of available normal sample. [124]

The 11 verified mutations were not previously reported in the Cosmic database and were present in a total of 13 % (10/75) of primary MM cases. These mutations affected mainly the tyrosine-kinase domain (4 rare SNPs, 2 mutations-NOS) as well as the ligand-binding domain (1 SNV, 2 mutations-NOS). One rare SNP was located in the furine-like domain and 1 mutation-NOS was located downstream of the tyrosine-kinase domain. Mutations in the HMCL AMO1, L363, MM1.S and U266 were previously reported in a whole-exome sequencing approach [39] and could be confirmed by the present amplicon study (Figure 7 A-F). The most affected RTK was IGF1R (4/75 patients, 5.3 %), followed by ERBB3 (3/75 patients, 4%), EGFR (2/75, 2.7%), EPHA2 and NTRK1 (1/75, 1.3% each). While NTRK2 was mutated in the HMCL L363, none of the patients harbored a mutation in this RTK (Figure 7 A-F) [124].

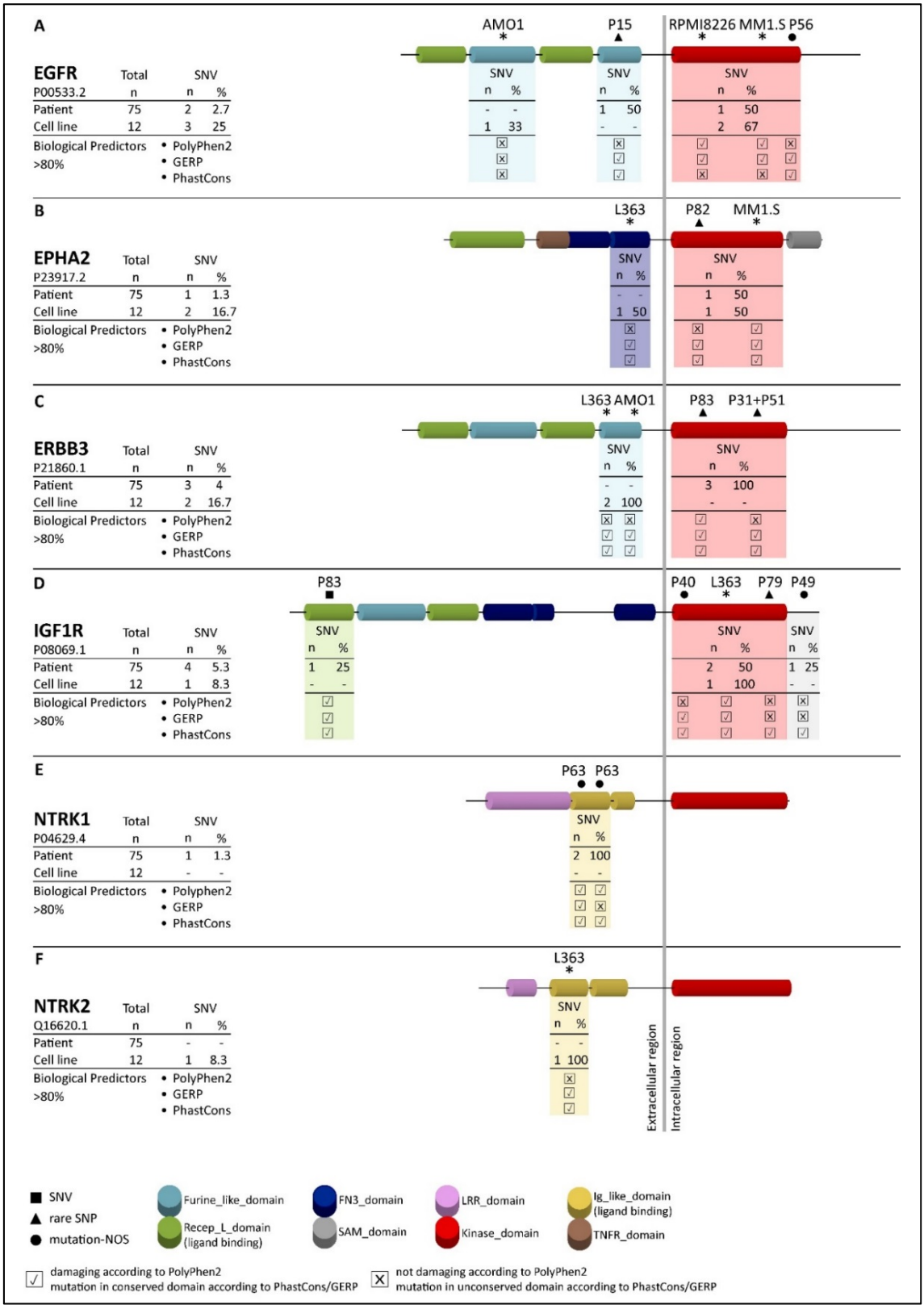

Figure 7: Frequency of mutations and affected regions in receptor tyrosine kinases

Mutations detected by amplicon sequencing were validated using Sanger sequencing. Patient-specific mutations were detected in EGFR (**A**), EPHA2 (**B**), ERBB3 (**C**), IGF1R (**D**) and NTRK1 (**E**). SNVs, rare SNPs and mutations-not otherwise specified (mutations-NOS) are indicated by a square (■), triangle (▲) and circle (●) and the respective patient assigned. HMCL specific mutations are indicated by asterisks and were detected in EGFR (**A**), EPHA2 (**B**), ERBB3 (**C**), IGF1R (**D**) and NTRK2 (**F**). Functional predictions are based on PhastCons, GERP (predicting the level of conservation) and PolyPhen2 (predicting structural changes). [124]

Table 57: Novel RTK mutations detected in the DSMM XI cohort [124]

Gene	Chr.	Exon	position (hg19)	Ref Base	sample Alleles	patient	VAF	cDNA Pos.	amino acids	PolyPhen2	grantham	Phast Cons	GERP
EPHA2	1	6	16458908	A	A/G	P82	49.75	2080	TYR,HIS	benign	83	0.824	4.95
NTRK1	1	9	156841538	A	A/C	P63	53.29	751	ASN,HIS	probably-damaging	68	1	4.97
NTRK1	1	9	156841540	C	C/G	P63	54.21	753	ASN,LYS	probably-damaging	94	0.998	1.05
EGFR	7	13	55229263	G	G/C	P15	49.16	1570	VAL,LEU	benign	32	0.902	4.08
EGFR	7	27	55268938	A	A/G	P56	42.86 F 35.42 R	3004	MET,VAL	benign	21	1	5.65
ERBB3	12	21	56491703	G	G/T	P83	49.17	2595	GLN,HIS	probably-damaging	24	0.997	2.59
ERBB3	12	23	56492567	C	C/G	P31	24.38	2717	THR,SER	benign	58	0.999	5.29
ERBB3	12	23	56492567	C	C/G	P51	24.77	2717	THR,SER	benign	58	0.999	5.29
IGF1R	15	2	99251007	C	C/T	P83	9.24	311	THR,MET	probably-damaging	81	0.998	5.36
IGF1R	15	18	99482518	A	A/G	P40	26.43	3386	ASN,SER	benign	45	1	3.61
IGF1R	15	21	99500419	G	G/T	P79	65.62	3852	GLU,ASP	benign	98	1	0.576
IGF1R	15	21	99500663	A	A/C	P49	55.04	4096	THR,PRO	benign	74	1	2.46

7.1.2 RTK mutations do not correlate with cytogenetic events commonly found in MM

In a previously conducted study the DSMM XI dataset showed a significant correlation of del13q14, del17p13 and gain1q21 with an adverse clinical outcome [40]. To see if there is an association of these adverse prognostic factors and RTK mutations, a correlation of the validated RTK mutations of the DSMM XI with adverse and other cytogenetic events commonly found in MM was prepared. The validated RTK mutations were neither correlated with chromosomal gains 1q21, 9q34, chromosomal losses 13q14, 17p13 nor with translocations t(4;14), t(11;14), t(14;16), t(8;14) and t(14;20) (Table 58). Moreover, correlations of the rare RTK SNPs with the cytogenetic events showed also no association (Table 59). [124] Interestingly however, men were significantly more affected by RTK mutations compared to women (8/39 cases vs. 1/33 cases, p=0.033).

Table 58: Correlation of RTK mutations with common cytogenetic events [124]

Cytogenetic Parameters	WT, n=65	RTK_mut, n=10	*p*
13q deletion: no; yes	28;37	7;3	0.174
17p deletion: no; yes	53;12	8;2	1
1q gain: no; yes	42;23	6;4	1
9q gain: no; yes	38;27	3;7	0.17
t(4;14): no; yes	45;20	9;1	0.266
t(11;14): no; yes	50;15	7;3	0.695
t(14;16): no; yes	62;3	10;0	1
t(8;14): no; yes	62;3	9;0	1
t(14;20): no; yes	65;0	9;0	-

Table 59: Correlation of rare RTK SNPs with common cytogenetic events [124]

Cytogenetic Parameters	WT, n=63	rare RTK SNP, n=6	*p*
13q deletion; no, yes	27;36	4;2	0.397
17p deletion; no, yes	51;12	5;1	1
1q gain; no, yes	41;22	2;4	0.189
9q gain; no, yes	37;26	2;4	0.392
t(4;14); no, yes	43;20	5;1	0.659
t(11;14); no, yes	48;15	5;1	1
t(14;16); no, yes	60;3	6;0	1
t(8;14); no, yes	60;3	5;0	1
t(14;20); no, yes	63;0	5;0	-

7.1.3 RTK mutations have a negative impact on the clinical progression of MM patients

While the validated RTK mutations of the DSMM XI study did not correlate with previously detected adverse prognosis factors, a significant correlation of RTK mutations with overall survival (OS), event-free survival (EFS) and progression-free survival (PFS) was observed [40, 124]. Patients harboring a RTK mutation (n=8) had a significantly worse OS (26 months vs. 56 months, *p*=0.002), a significantly worse EFS (19 months vs. 36 months, *p*=0.005) and a trend towards a significantly worse PFS (26 months vs. 36 months, *p*=0.054) (Figure 8 A-C)[124]. After limiting the analysis to patients affected by a rare SNP, a significantly lower OS (31 months vs. 56 months, *p*=0.011), EFS (21 months vs. 35 months, *p*=0.009) and PFS (27 months vs. 36 months, *p*=0.025) was observed (Figure 8 D-F). To ensure that the RTK mutations are responsible for the significantly worse survival and this observation is not due to the adverse prognostic factors del13q14 and del17p13 [40], correlations were performed disregarding cases with these deletion. Survival statistics still showed a significantly lower OS and EFS and a trend towards a lower PFS (del17p13: 30.5 months vs. 60.5 months, *p*=0.003; 20.5 months vs. 36 months, *p*=0.009; 30 months vs. 36 months *p*=0.118, del13q14: 30.5 months vs. 63 months, *p*=0.003; 25.5 months vs. 36 months, *p*=0.043; 27 months vs. 36 months, *p*=0.129, respectively)(Figure 9).[124] Rare SNPs that were validated in the current dataset were neither present in the dbSNP database nor in the 1000 genomes database. It was therefore analyzed whether common SNPs, SNPs in conserved regions or SNPs in 2 samples or less (meeting the criteria of a rare SNP) influence the clinical outcome of MM patients of the DSMM XI. These analyses, however, showed no significant difference in OS, EFS or PFS (OS: *p*=0.641, *p*=0.667 and *p*=0.532; EFS: *p*=0.717 , *p*=0.516 and, *p*=0.953; PFS: *p*=0.980 , *p*=0.786 and *p*=0.739, respectively)(Figure 10 A-I).[124]

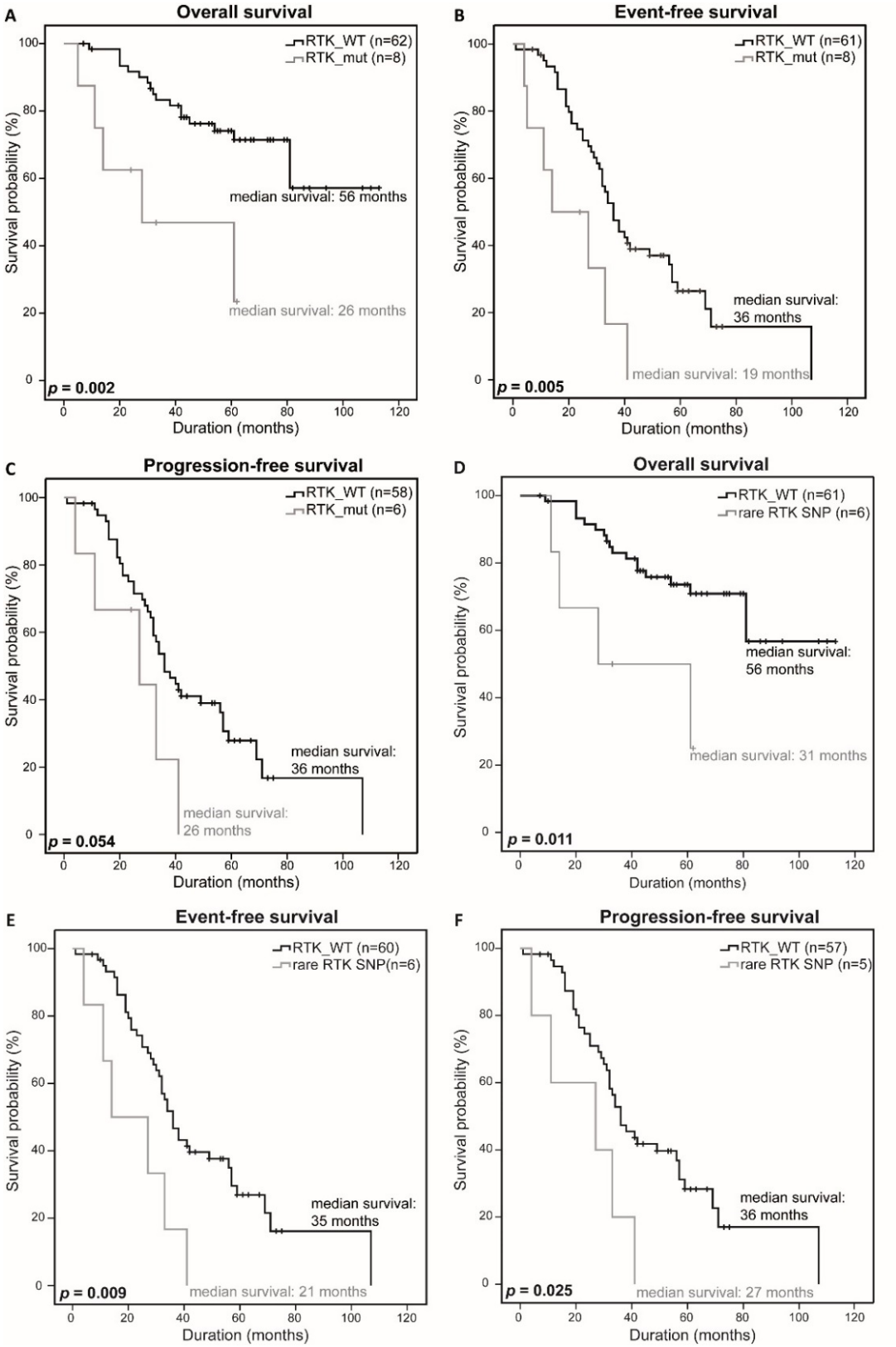

Figure 8: Clinical impact of RTK mutations and rare RTK SNP

Survival of patients with (RTK_mut) and without (RTK_WT) a RTK mutation were compared using a univariate analysis with log-rank test for significance. *P*-values <0.05 were considered statistically significant. (**A-C**) Overall (OS), event-free (EFS) and progression-free (PFS) survival of all patients with an RTK_mut independent of mutation type were compared to RTK_WT patients (OS: RTK_WT n=62, RTK_mut n=8; EFS: RTK_WT n=61, RTK_mut n=8; PFS: RTK_WT n=58, RTK_mut n=6) (**D-F**) Overall (OS), event-free (EFS) and progression-free (PFS) survival of patients with a rare SNP were compared to RTK_WT patients (OS: RTK_WT n=61, rare RTK SNP n=6; EFS: RTK_WT n=60, rare RTK SNP n=6; PFS: RTK_WT n=57, rare RTK SNP n=7).

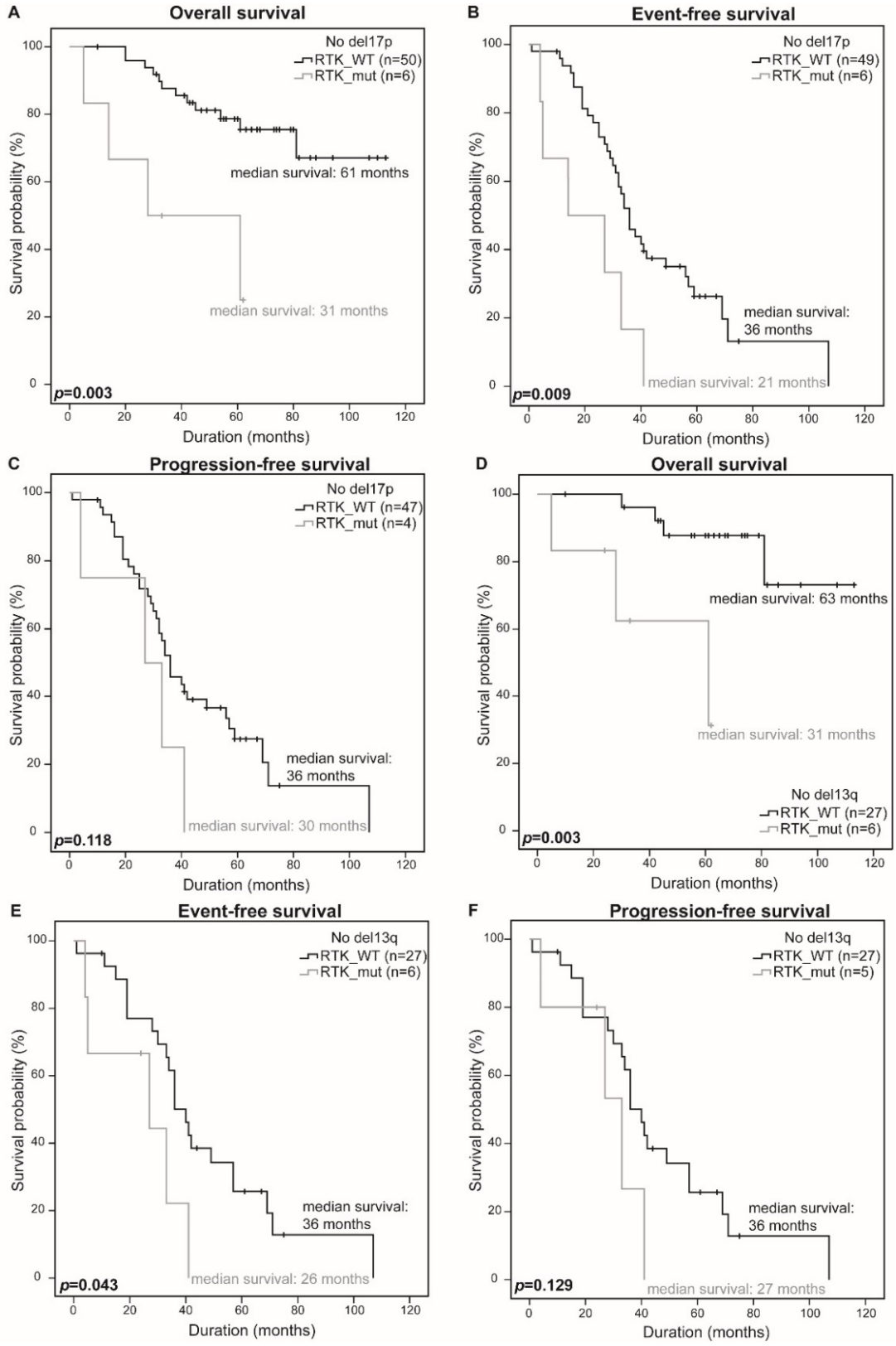

Figure 9: Clinical impact of RTK mutations without del13q or del17p

(**A-C**) Overall (OS), event-free (EFS) and progression-free (PFS) survival of patients with an RTK mutation and without the adverse prognostic marker del17p were compared to RTK_WT patients (OS: RTK_WT n=50, RTK_mut n=6; EFS: RTK_WT n=49, RTK_mut n=6; PFS: RTK_WT n=47, RTK_mut n=4) (**D-F**) Overall (OS), event-free (EFS) and progression-free (PFS) survival of patients with a RTK mutation and without the adverse prognostic marker del13q were compared to RTK_WT patients (OS: RTK_WT n=61, rare RTK SNP n=6; EFS: RTK_WT n=60, rare RTK SNP n=6; PFS: RTK_WT n=57, rare RTK SNP n=7). Survival was compared using a univariate analysis with log-rank for significance and *p*-values <0.05 were considered statistically significant. [124]

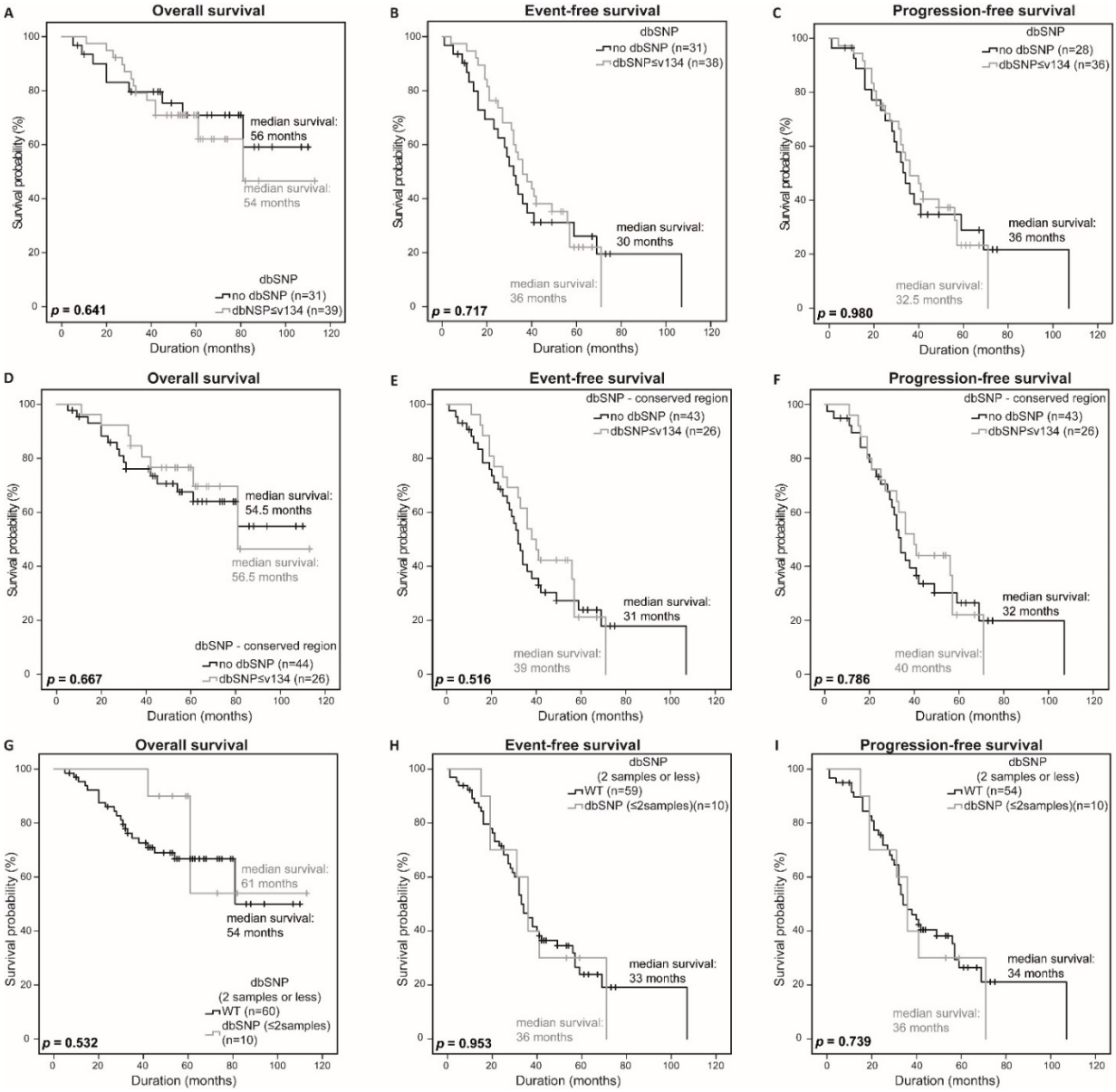

Figure 10: Clinical impact of mutations listed in dbSNP

Patient survival was compared using a univariate analysis with log-rank for significance and *p*-values <0.05 were considered statistically significant (**A-C**) Overall (OS), event-free (EFS) and progression-free (PFS) survival of patients with a general SNP listed in dbSNPv134 were compared to patients without a SNP (OS: no dbSNP n=31, dbSNP n=39; EFS: no dbSNP n=31, dbSNP n=38; PFS: no dbSNP n=28, dbSNP n=36) (**D-F**) Overall (OS), event-free (EFS) and progression-free (PFS) survival of patients with a SNP in a conserved region and listed in dbSNPv134 were compared to patients without a SNP in a conserved region (OS: no dbSNP n=44, dbSNP n=26; EFS: no dbSNP n=43, dbSNP n=26; PFS: no dbSNP n=43, dbSNP n=26). (**G-I**) Overall (OS), event-free (EFS) and progression-free (PFS) survival of patients with a general SNP present in 2 patients or less were compared to patients without a SNP (OS: no dbSNP n=60, dbSNP in 2 or less patients n=10; EFS: no dbSNP n=59, dbSNP in 2 or less patients n=10; PFS: no dbSNP n=54, dbSNP in 2 or less patients n=10).

7.2 Identification and characterization of rare RTK SNPs in the DSMM XII cohort

In the previously conducted amplicon sequencing approach in a patient cohort of the DSMM XI a significant correlation of rare RTK SNPs with a worse clinical outcome was observed (Figure 8 D-F) [124]. To further elucidate the role of rare RTK SNPs in MM, a second amplicon approach in a different clinical cohort of the DSMM XII was therefore conducted. The DSMM XII cohort contained 75 tumor as well as 184 normal samples. The CDS of *EPHA2*, *EGFR*, *ERBB3*, *IGF1R*, *NTRK1* and *NTRK2* were covered on average with 947, 714, 821, 1103, 871 and 641 reads/sample, respectively. Mutations with a coverage ≤10 were removed from further analyses. After initial filtering steps 31 mutations were detected (Figure 11, Table 60). Out of these 31 mutations, 8 mutations were exclusively detected in HMCL and served as technical controls. The remaining 23 mutations were detected in a total of 24 MM patient samples (Figure 11, Table 60). These mutations could be identified as either rare RTK SNPs (20 mutations) affecting all sequenced RTKs or SNVs (3 mutations) affecting *EPHA2*, *EGFR*, *IGF1R* and *NTRK1*. The rare RTK SNPs were either not listed in the common databases dbSNP and 1000 genomes, or had a minor allele frequency (MAF) below 1%. All rare SNPS were located in conserved domains according to the bioinformatics predictors GERP and/or PhastCons and 55 % of rare SNPs (11 out of 20) led to structural changes according to PolyPhen2. The three identified SNVs were not listed in the COSMIC database at time of analysis. Bioinformatic analysis revealed that 2 out of 3 SNVs (67%) were defined as damaging to the protein structure according to Polyphen2 and all SNVs were located in conserved domains according to PhastCons and/or GERP (Figure 11 A, B and D).

Interestingly, in contrast to the previously conducted study, no accumulation of patient-specific mutations/rare SNPs in the tyrosine-kinase domain was observed and only six mutations were located in the intracellular domains of the investigated RTKs (26.1 %). The patients P69 and P76 were affected by a rare SNP in the tyrosine-kinase domain of *ERBB3* and *NTRK2*, respectively (Figure 11 C, F). Moreover, patients P18, P81, P127, P142 and P161 were all affected by the same mutation located in the SAM domain of *EPHA2* (Figure 11 A). Although this mutation was listed in the dbSNP database the observed MAF was determined to be 0.21 % (ExAC) and 0.06 % (1000 genomes) in population-wide studies. This low MAF still allows the classification of this variant as a rare SNP. Moreover, the patients P73, P81 and P129 were affected by rare SNPs in the intracellular parts of *ERBB3*, *IGF1R* and *NTRK1*, respectively,

outside of defined protein domains or regions (Figure 11 C-E). Most mutations (16/23; 69.5 %), however, were located in the extracellular region of the sequenced RTKs with an accumulation of mutations in the signaling peptide (5/16) of *EGFR* and *IGF1R* (Figure 11 B, D) and the ligand-binding domain (4/16) of *EPHA2* and *EGFR* (Figure 11A, B,). Two patients (P36, P101) were affected by mutations in the furin-like domain of *IGF1R* (Figure 11 D) and four mutations affecting *EPHA2*, *ERBB3* and *NTRK1* were located between different domains (Figure 11 A; C; E). Additionally; patient P75 was affected by a mutation in the transmembrane domain of *EGFR* (Figure 11 B). Taken together, the RTKs affected by the most patient-specific rare SNPs/SNVs were *EGFR* and *IGF1R* (6 each), followed by *EPHA2* (4), *NTRK1* and *ERBB3* (3 each) and *NTRK2* (1). The HMCL specific mutations were already reported previously and served as technical control (Figure 11, Table 60) [39, 124]. However, the mutation affecting *EGFR* in the HMCL RPMI8226 identified in the previous amplicon approach (Figure 7, [124]) could not be validated in the current sequencing study.

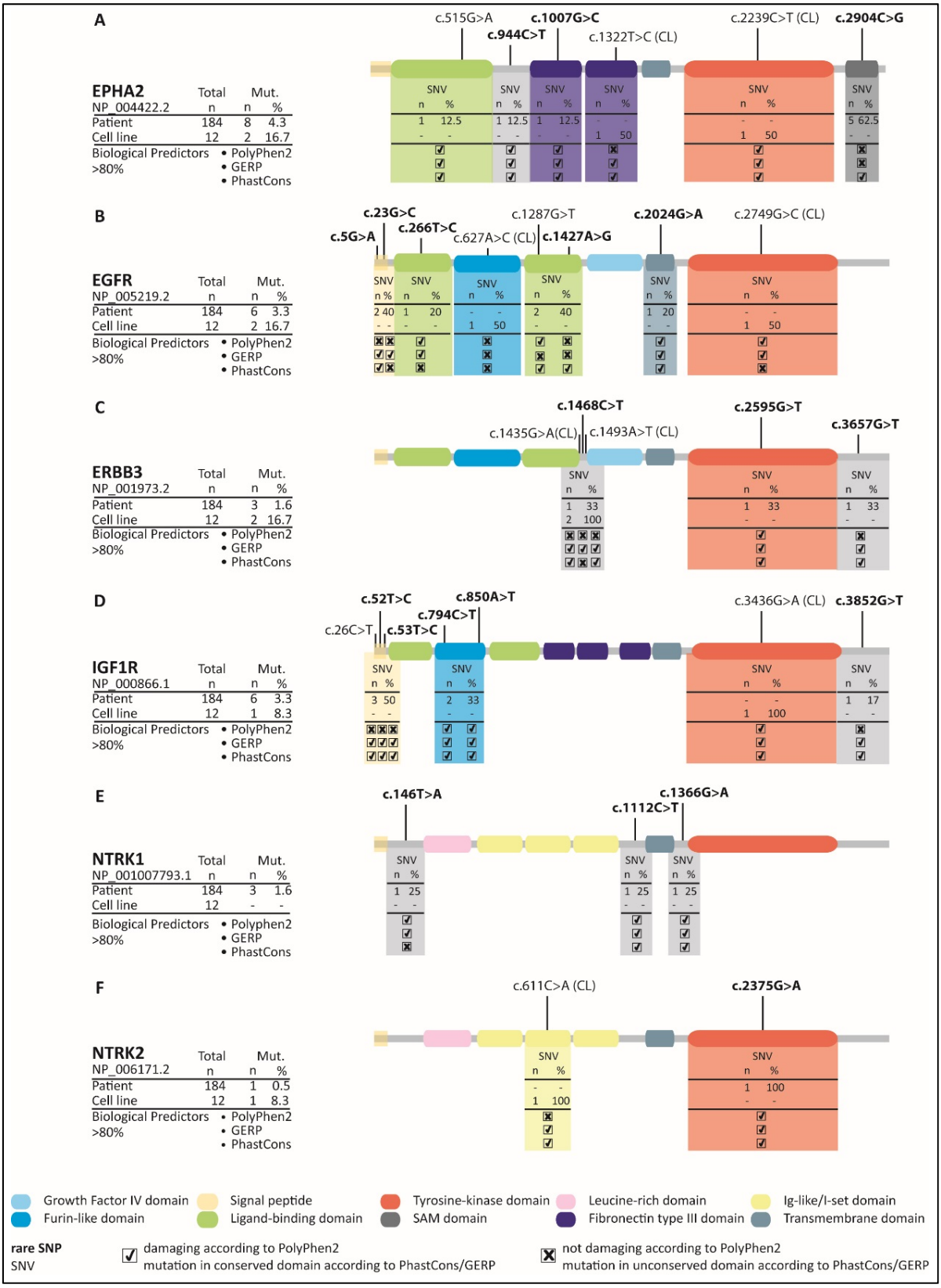

Figure 11: Affected regions and frequency of mutations identified in patients of the DSMM XII
Amplicon sequencing of patients of the DSMM XII trial identified mutations in receptor-tyrosine kinases. All detected mutations were validated by Sanger sequencing. Patient-specific mutations were detected in EPHA2 (**A**), EGFR (**B**), ERBB3 (**C**), IGF1R (**D**), NTRK1 (**E**) and NTRK2 (**F**). Rare SNPs are illustrated in bold letters. CL indicates a HMCL specific mutations HMCL specific mutations detected in EPHA2 (**A**), EGFR (B), ERBB3 (**C**), IGF1R (**D**) and NTRK2 (**F**). Bioinformatics analysis predicted the level of conservation (PhastCons, GERP) as well as structural changes (PolyPhen2).

Table 60: Mutations detected in MM patients of the DSMM XII trial

Gene	Chr	Position (hg19)	Ref.Base	Sample Alleles	Patient	Mut. type	cDNA Pos.	amino acids	PolyPhen2	grantham	Phast Cons	GERP
EPHA2	1	16451737	C	C/G	P18	rare SNP	2904	GLN,HIS	benign	24	0,989	-2,16
EPHA2	1	16451737	C	C/G	P81	rare SNP	2904	GLN,HIS	benign	24	0,989	-2,16
EPHA2	1	16451737	C	C/G	P127	rare SNP	2904	GLN,HIS	benign	24	0,989	-2,16
EPHA2	1	16451737	C	C/G	P142	rare SNP	2904	GLN,HIS	benign	24	0,989	-2,16
EPHA2	1	16451737	C	C/G	P161	rare SNP	2904	GLN,HIS	benign	24	0,989	-2,16
EPHA2	1	16458645	C	C/T	MM1S	cell line	2239	VAL,ILE	probably-damaging	29	0,979	6,07
EPHA2	1	16462256	T	T/C	L363	cell line	1322	LYS,ARG	benign	26	1	4,15
EPHA2	1	16464653	G	G/C	P171	rare SNP	1007	THR,ARG	possibly-damaging	71	0,969	4,97
EPHA2	1	16464805	C	C/T	P95	rare SNP	944	ARG,GLN	probably-damaging	43	1	5,3
EPHA2	1	16475181	G	G/A	P92	SNV	515	PRO,LEU	possibly-damaging	98	1	5,14
NTRK1	1	156834169	T	T/A	P83	rare SNP	146	LEU,GLN	probably-damaging	113	0,193	4,61
NTRK1	1	156844387	C	C/T	P3	rare SNP	1112	PRO,LEU	probably-damaging	98	0,958	5,39
NTRK1	1	156845431	G	G/A	P149	rare SNP	1366	GLU,LYS	possibly-damaging	56	0,992	4,72
EGFR	7	55240780	G	G/A	P75	rare SNP	2024	ARG,GLN	probably-damaging	43	1	5,96
EGFR	7	55086975	G	G/A	P78	rare SNP	5	ARG,GLN	benign	43	0,88	4,3
EGFR	7	55086993	G	G/C	P75	rare SNP	23	GLY,ALA	benign	60	0,005	3,4
EGFR	7	55211023	T	T/C	P112	rare SNP	266	VAL,ALA	probably-damaging	64	0,618	4,15
EGFR	7	55219054	A	A/C	AMO1	cell line	627	LYS,ASN	benign	94	0,193	-0,95
EGFR	7	55225435	G	G/T	P143	SNV	1287	ARG,SER	probably-damaging	110	0,986	-0,05
EGFR	7	55227960	A	A/G	P66	rare SNP	1427	ASN,SER	benign	46	0,977	2,11
EGFR	7	55266457	G	G/C	MM1S	cell line	2749	GLY,ARG	probably-damaging	125	0,095	4,25
NTRK2	9	87338515	C	C/A	L363	cell line	611	PRO,HIS	benign	77	0,987	4,62
NTRK2	9	87636210	G	G/A	P76	rare SNP	2327	ARG,HIS	probably-damaging	29	1	5,75
ERBB3	12	56487560	A	A/T	AMO1	cell line	1493	LYS,ILE	benign	102	1	2,87
ERBB3	12	56487289	G	G/A	L363	cell line	1435	GLU,LYS	benign	56	0,829	4,24
ERBB3	12	56487322	C	C/T	P112	rare SNP	1468	ARG,CYS	benign	180	0,618	4,1

Gene	Chr.	Position (hg19)	Ref.Base	Sample Alleles	sample	Mut. type	cDNA Pos.	amino acids	PolyPhen2	grantham	Phast Cons	GERP
ERBB3	12	56491703	G	G/T	P69	rare SNP	2595	GLN,HIS	possibly-damaging	24	0,997	2,59
ERBB3	12	56495467	G	G/T	P73	rare SNP	3657	GLU,ASP	benign	45	1	3,78
IGF1R	15	99192836	C	C/T	P155	SNV	26	SER,PHE	benign	155	1	3,72
IGF1R	15	99192862	T	T/C	P183	rare SNP	52	PHE,LEU	benign	22	0,992	2,51
IGF1R	15	99192863	T	T/C	P57	rare SNP	53	PHE,SER	benign	155	0,991	3,76
IGF1R	15	99434707	C	C/T	P36	rare SNP	794	PRO,LEU	probably-damaging	98	0,997	5,28
IGF1R	15	99434763	A	A/T	P101	rare SNP	850	ASN,TYR	possibly-damaging	143	1	4,87
IGF1R	15	99482568	G	G/A	L363	cell line	3436	ASP,ASN	probably-damaging	23	0,997	5,9
IGF1R	15	99500419	G	G/T	P81	rare SNP	3852	GLU,ASP	benign	45	1	3,61

7.2.1 Rare SNPs detected in patients of the DSMM XII are significantly associated with the cytogenetic abnormality del17p13

Identical to the first amplicon study, identified SNVs and rare SNPs of the second study were correlated with the common cytogenetic event such as chromosomal gains 1q21, 9q34, chromosomal losses 13q14, and 17p13 as well as translocations t(4;14), t(11;14), t(14;16). In comparison to the previous correlation, the RTK mutations identified in the patient cohort of the DSMM XII trial were significantly associated with the adverse prognostic factor del17p13 (Table 61). Additionally, restricting the analysis to the detected rare SNPs an even higher level of significance was reached (p=0.024 vs p=0.013, Table 62).

Table 61: Correlation of mutations of the DSMM XII cohort with cytogenetic events

Cytogenetic Parameters	WT, n=150	RTK_mut, n=23	*p*
13q deletion; no, yes	89;61	12;11	0.650
17p deletion; no, yes	137;13	17;6	0.024
1q gain; no, yes	100;36	15;7	0.611
9q gain; no, yes	63;73	8;14	0.490
t(4;14); no, yes	130;21	20;3	1.000
t(11;14); no, yes	116;28	20;3	0.575
t(14;16); no, yes	148;2	23;0	1.000

Table 62: Correlation of rare RTK SNPs of the DSMM XII cohort with cytogenetic alterations

Cytogenetic Parameters	WT, n=150	rare RTK SNP, n=20	*p*
13q deletion; no, yes	89;60	11;9	0.809
17p deletion; no, yes	136;13	14;6	0.013
1q gain; no, yes	99;36	13;6	0.784
9q gain; no, yes	63;72	7;12	0.469
t(4;14); no, yes	129;21	18;2	1.000
t(11;14); no, yes	115;28	17;3	0.768
t(14;16); no, yes	147;2	20;0	1.000

7.3 Functional investigation of IGF1R-mutations

In the first amplicon sequencing approach IGF1R was the most affected RTK [124]. IGF1R plays an important role in tissue development and growth by activating cell proliferation and inhibiting apoptosis [131-133]. In MM high IGF1R expression is an adverse prognostic event and IGF1 is known as an important growth factor [68, 100]. There are, however, no known studies which elucidate the role of mutated IGF1R in the development and progression of MM. This may be partly due to the low transfection efficiency of plasma cells [134, 135] and the large size of the IGF1R cDNA with 4,989 nucleotides [73].

7.3.1 The c.3386A>G and c.3436G>A mutations are present on cDNA level

Four out of 75 patients of the DSMM XI and one HMCL carried mutations in IGF1R (Figure 7D, Table 57)[124]. To see if these mutation are not only present on the genomic DNA, but also transcribed to RNA, the RNA of all respective patients was reversely transcribed into cDNA and used as a template for PCR and Sanger sequencing. The patient-specific mutations c.311C>T (P83) and c.3852G>T (P79) could not be validated on the cDNA level (Figure 12A). Amplification of the DNA region adjoining the mutation c.4096A>C (P49) was not possible due to the mutation's location at the end of the cDNA sequence. The patient-specific mutation c.3386A>G (P40) resulting in the amino acid change p.N1129S, as well as the HMCL specific mutation c.3436G>A (L363) resulting in the amino acid change p.D1146N could be validated on the cDNA level (Figure 12B).

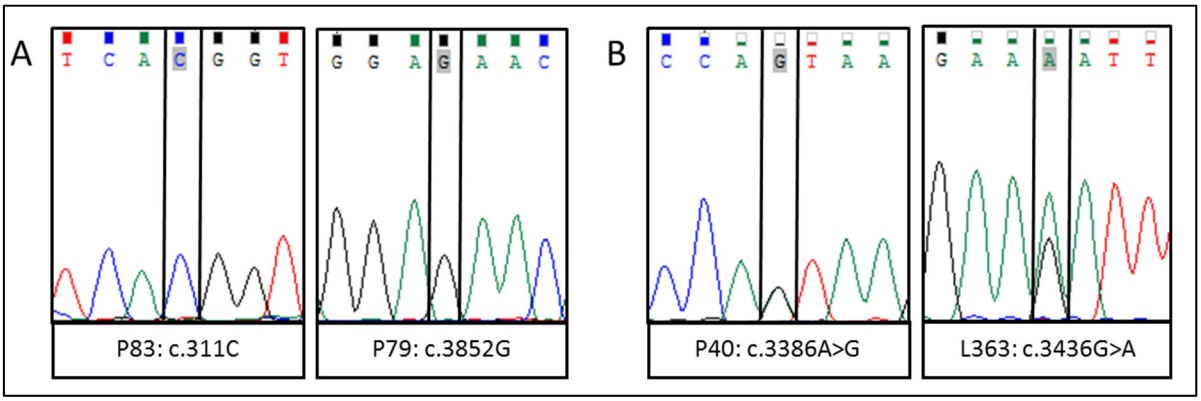

Figure 12: Sanger sequencing of IGF1R cDNA
cDNA of patients harboring a genomic IGF1R mutation was generated and sequenced using specific sequencing primers. **A** Previously detected mutations of patients P83 and P79 could not be validated on cDNA level. **B** Previously detected mutation of patient P40 (c.3386A>G) and HMCL L363 (c.3436G>A) could be validated on cDNA level.

7.3.2 Overexpression of IGF1R WT, IGF1R D1146N and IGF1R N1129S in HEK293FT cells

After successful validation of the IGF1R mutations p.D1146N and p.N1129S on cDNA level, the influence of these mutations on the activity and the downstream signaling of IGF1R ought to be investigated. Due to the hard-to-transfect HMCLs, preliminary experiments were performed in HEK293FT cells. Mutagenesis PCR using the vector pCR-XL-TOPO-IGF1-R containing the complete cDNA of IGF1R as a template was performed. Sequencing revealed that the desired mutations were present in the plasmids and no further mutations were detected. Cloning of these constructs into the pSF-CMV-Puro-COOH-GST expression vector and subsequent control digestion of the cloned expression vectors with NotI and EcoRI resulted in the expected DNA sizes of 6761 bp and 4115 bp (Figure 13). Sanger sequencing of ligated plasmids (pSF-CMV-IGF1R-WT, pSF-CMV-IGF1R-D1146N, pSF-CMV-IGF1R-N1129S) showed no undesired mutations and plasmids were used for overexpression analysis.

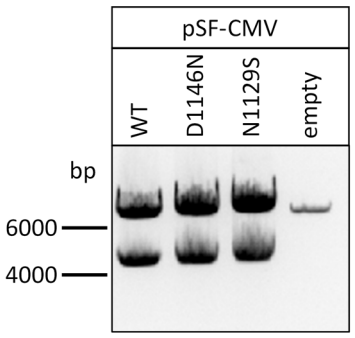

Figure 13: Restriction digestion of cloned pSF-CMV plasmids
Cloned plasmids were transformed in *E. coli* NEB10β, purified and digested using NotI and EcoRI. Digestion of pSF-CMV_IGF1R-WT, pSF-CMV_IGF1R-D1146N and pSF-CMV_IGF1R-N1129S resulted in the expected DNA sizes of 6761bp and 4115bp. Digestion of the empty vector resulted in the expected DNA size of 6761bp.

After the successful cloning of the IGF1R overexpression plasmids, HEK293FT cells were transfected with these plasmids to study the effect of overexpression of IGF1R WT and mutant IGF1R on the expression and activation level of selected IGF1R downstream effectors (Figure 14). The overexpression of IGF1R, independent of mutational status, resulted in the increased phosphorylation of ERK1/2, MEK and AKT. Interestingly, the overexpression of IGF1R N1129S led to an even stronger phosphorylation of ERK1/2, MEK and AKT compared to the overexpression of IGF1R WT and IGF1R D1146N. Moreover, the expression of c-myc was enhanced in cells overexpressing IGF1R N1129S. These results indicate an influence of the

IGF1R N1129S mutation on the downstream signaling and encouraged further analyses in HMCLs.

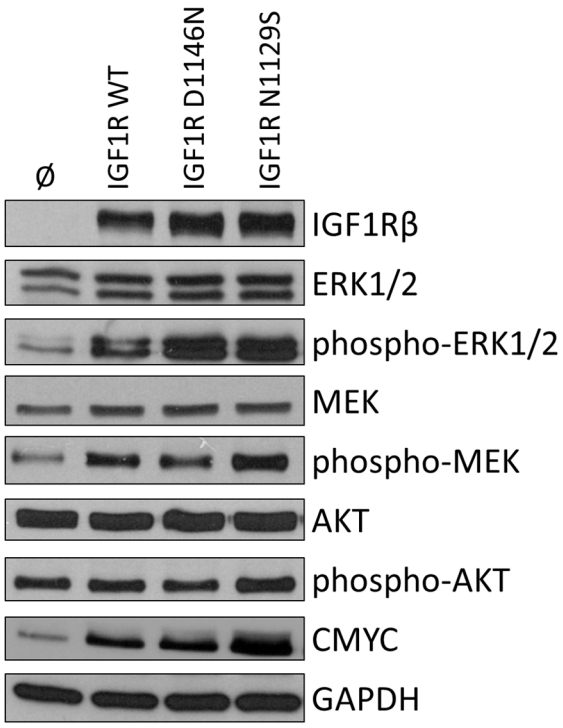

Figure 14: Downstream signaling of HEK293FT cells overexpressing IGF1R WT, IGF1R D1146N or IGF1R N1129S
Western blot analyses of HEK293FT cells transfected with IGF1R-WT, IGF1R-D1146N or IGF1R-N1129S overexpression plasmids. Membranes were incubated overnight with the indicated antibody for proteins of the AKT and MAPK signaling pathways. GAPDH served as loading control.

7.3.3 Determination of suitable HMCL for IGF1R overexpression and knockdown experiments

In order to establish IGF1R knockdown as well as IGF1R overexpression cell lines suitable HMCL had to be identified. For this purpose, the IGF1R protein level was determined using Western blot analysis. IGF1R expression was detectable in all HMCL. The IGF1R protein level was comparable between cell lines with the exception of KMS11, INA6 and AMO1 which was confirmed in three independent experiments. KMS11 showed an elevated IGF1R expression, whereas INA6 and AMO1 exhibited a decreased level. (Figure 15) HEK293 cells were carried along as a positive control.

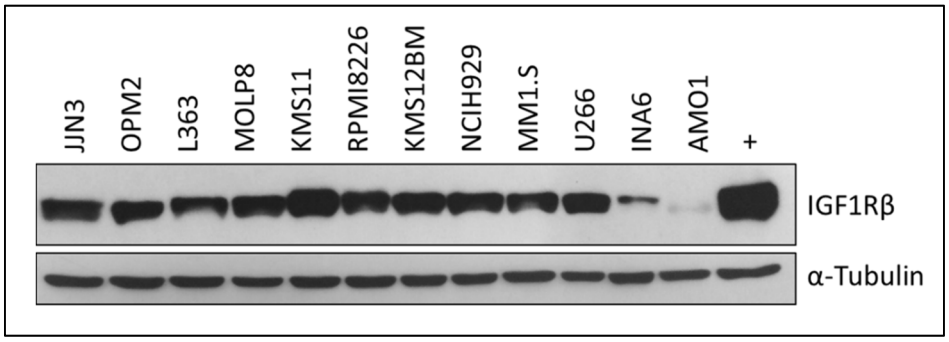

Figure 15: Endogenous IGF1R level in 12 HMCL
WCL were prepared from all HMCLs and used for Western blot analysis with IGF1Rβ antibody. α-tubulin antibody was used as loading control. WCL from HEK293 cells served as positive control (+). All cell lines showed varying endogenous IGF1R expression. KMS11 showed an elevated expression, INA6 and AMO1 exhibited a decreased level.

Additionally, previously published sequencing data of the HMCL AMO1, U266, OPM2, MM1S, JJN3 and L363 was incorporated into the final decision [39]. For IGF1R knockdown experiments, the IGF1R mutant HMCL L363, as well as the IGF1R WT HMCL U266 were chosen. In addition to the high IGF1R expression, the HMCL U266 was only mutated in one downstream effector (BRAF in U266 [39]). For IGF1R overexpression experiments the HMCL AMO1 was chosen due to its low endogenous IGF1R expression (Figure 15).

7.3.4 Successful knockdown of IGF1R in the HMCLs U266 and L363 using CRISPR/Cas9

To further elucidate the role of IGF1R in MM, stable IGF1R-knockdown cell lines were created using the CRISPR/Cas9 system. Using the CRISPR Design software a crRNA was designed that bound specifically to IGF1R exon 18 and contained the PAM site necessary for Cas9 nuclease activity (Figure 16).

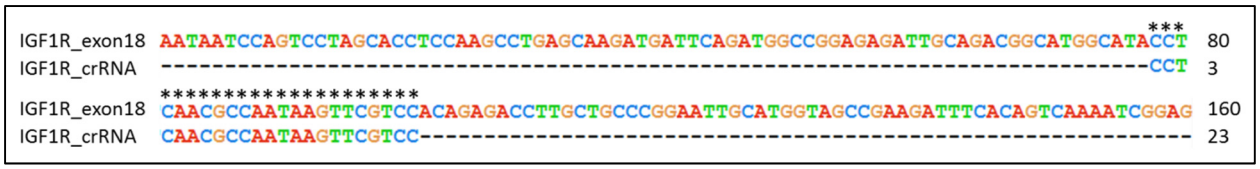

Figure 16: Alignment of IGF1R_exon 18 and IGF1R_crRNA
IGF1R_Exon 18 was aligned with the designed crRNA. The crRNA sequence was detected on the antisense strand, therefore the PAM site is CCT and located at pos. 1-3 of crRNA

For knockdown experiments the IGF1R mutant HMCL L363 as well as the IGF1R WT HMCL U266 were chose. PCR of the isolated DNA from untreated cells (Ø), cells electroporated without the RNP complex (Ø+) and cells electroporated with the RNP complex (C/C9) resulted in the expected DNA band size of 397 bp in both HMCLs (Figure 17 A). Digestion of heteroduplexed dsDNA with T7 endonuclease resulted in cut DNA with the expected size of 197 and 200 bp in both cell lines (Figure 17 B). Due to the similar size of the cut products, only one band is visible on the agarose gel. The CRISPR/Cas9 assay was more successful in the L363 cell line (9.1 % cut product), compared to the U266 cell line (4.2 % cut product).

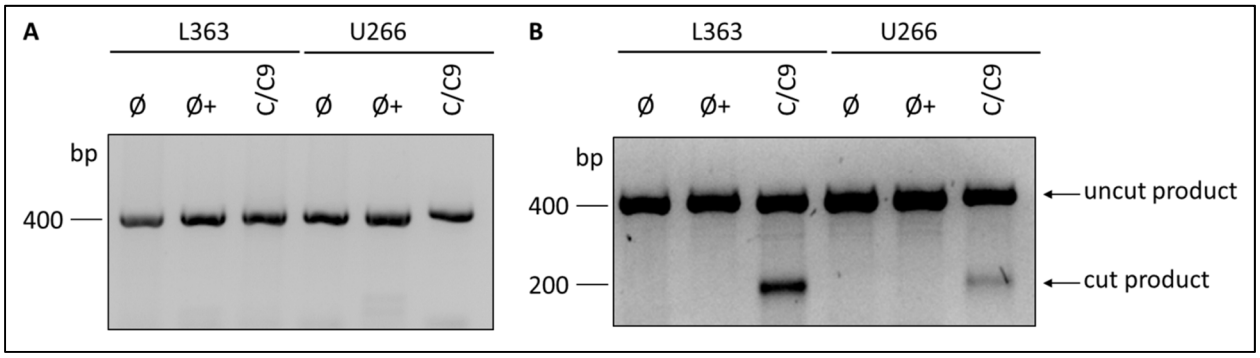

Figure 17: Analysis of CRISPR/Cas9 cells
A DNA from untreated cells (Ø), cells electroporated without RNP complex (Ø+) and cells electroporated with RNP complex (C/C9) were subjected to PCR followed by agarose gel electrophoresis resulting in the expected DNA size of 397 bp. **B** PCR products were heteroduplexed, digested using T7 endonuclease and analyzed using agarose gel electrophoresis. PCR products from cells electroporated with RNP complex (C/C9) show cut DNA at the expected size of 197 and 200 bp.

Following successful T7 endonuclease digestion, single cells were plated into 96-well plates and treated with IL-6, VEGF-A and TNF-α to enhance cell growth (6.6.4). Out of 192 plated L363 single cells, 70 cell clones were growing. Single cell selection for U266 cells was less successful. Only 19 out of 192 plated cells formed distinct cell colonies and showed successful growth. After 2 weeks, DNA was isolated from growing cell clones, amplified using PCR and sequenced. However, PCR revealed amplicons for only 66 of the L363 single cell clones and 15 of the U266 single cell clones (data not shown). Sequenced DNA was aligned and checked for changes in the DNA sequence (Figure 18, Figure 19). Out of the 66 L363 single cell clones, 30

clones showed a clear change in the DNA sequence (Figure 18) and out of the 15 U266 single cell clones, seven clones showed a change in the sequence (Figure 19). To see if these changes in the DNA sequence lead to a reduced IGF1R level, WCL of these clones were prepared and used for Western blot analysis.

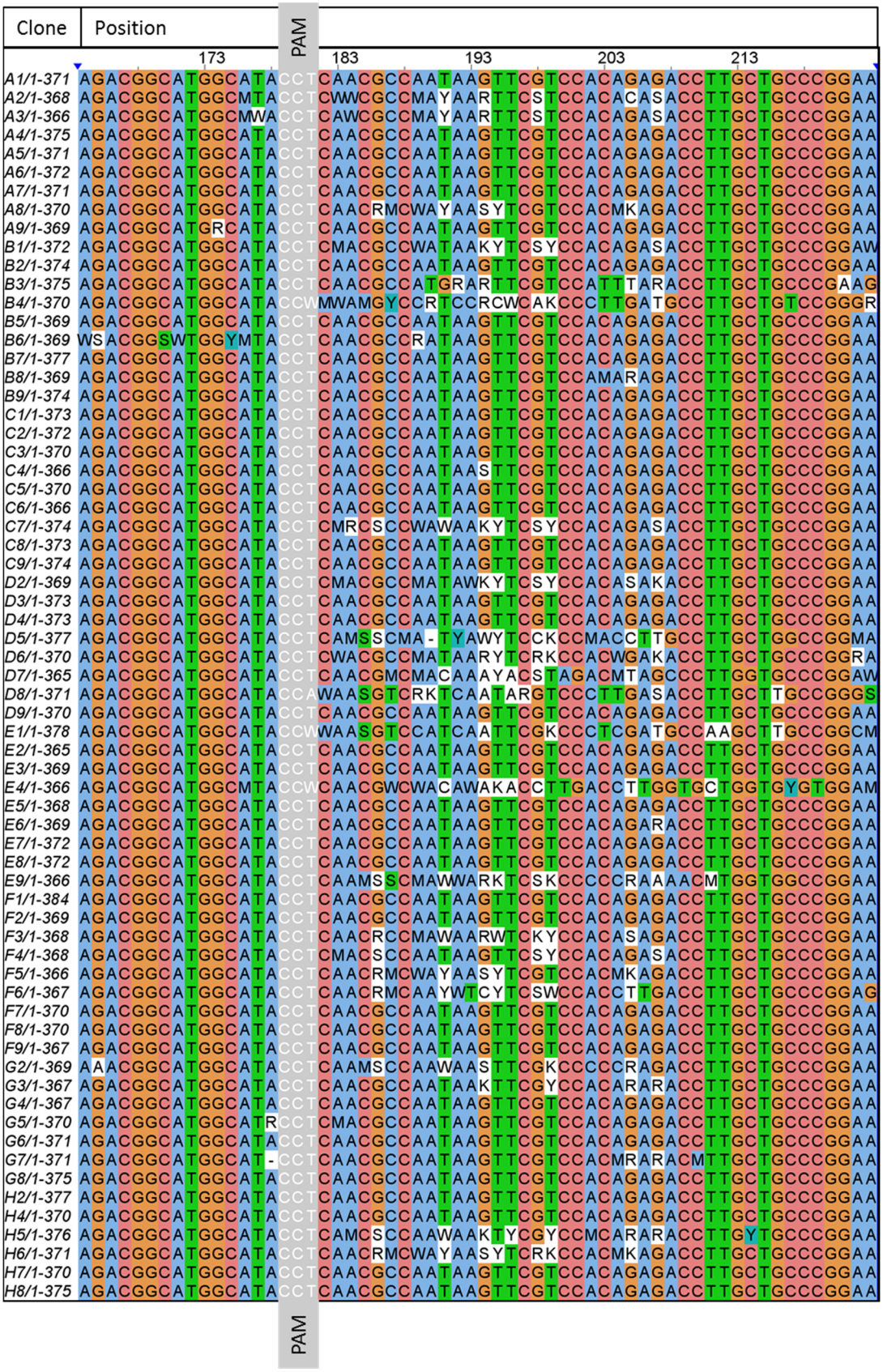

Figure 18: Alignment of L363_C/C9 single cell clones
DNA of growing single cell clones of the L363 cell line previously subjected to CRISPR/Cas9, was isolated and Sanger sequenced. Sequences were aligned and analyzed up- and downstream of indicated PAM site. Cas9 cuts 3 bp away from the PAM site. Nucleotides are according to IUPAC code.

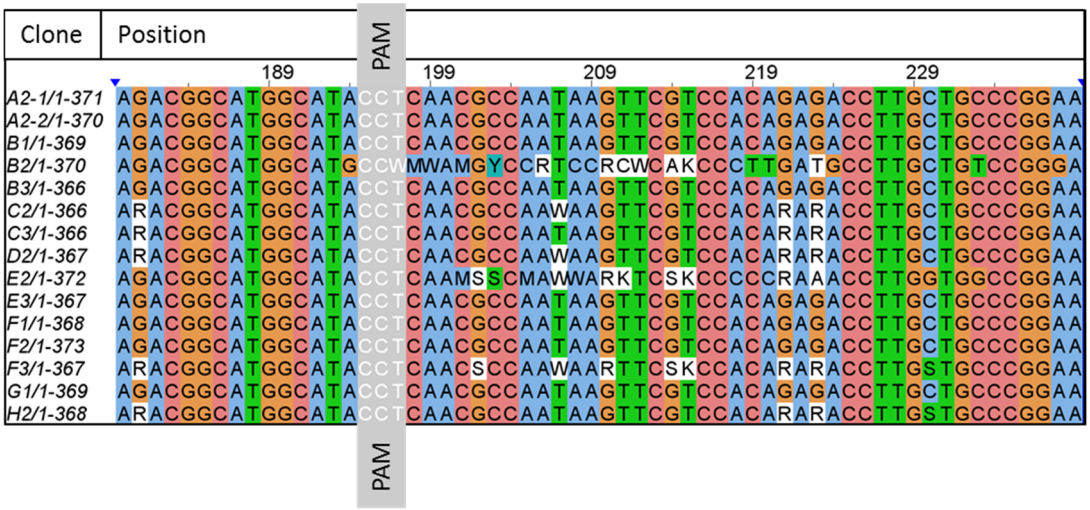

Figure 19: Alignment of U266_C/C9 single cell clones
DNA of growing single cell clones of the U266 cell line previously subjected to CRISPR/Cas9, was isolated and Sanger sequenced. Sequences were aligned and analyzed up- and downstream of indicated PAM site Cas9 cuts 3 bp a. Nucleotides are according to IUPAC code.

Western blot analysis revealed a variable IGF1R expression across the single cell clones. In L363 cells the clones A2, A8, B1, B3, B4, B8, D8, E1 and E9 showed a reduced IGF1R expression level compared to the L363 control lysate (+) (Figure 20 A). In U266 cells all clones with a changed DNA sequence showed a reduced IGF1R level compared to the U266 control lysate (+). However, the strongest IGF1R-knockdown effect was seen in the clones B2, B3 and E2 (Figure 20 B). Cells with an IGF1R-knockdown are called L363-C/C9 and U266-C/C9 from now on.

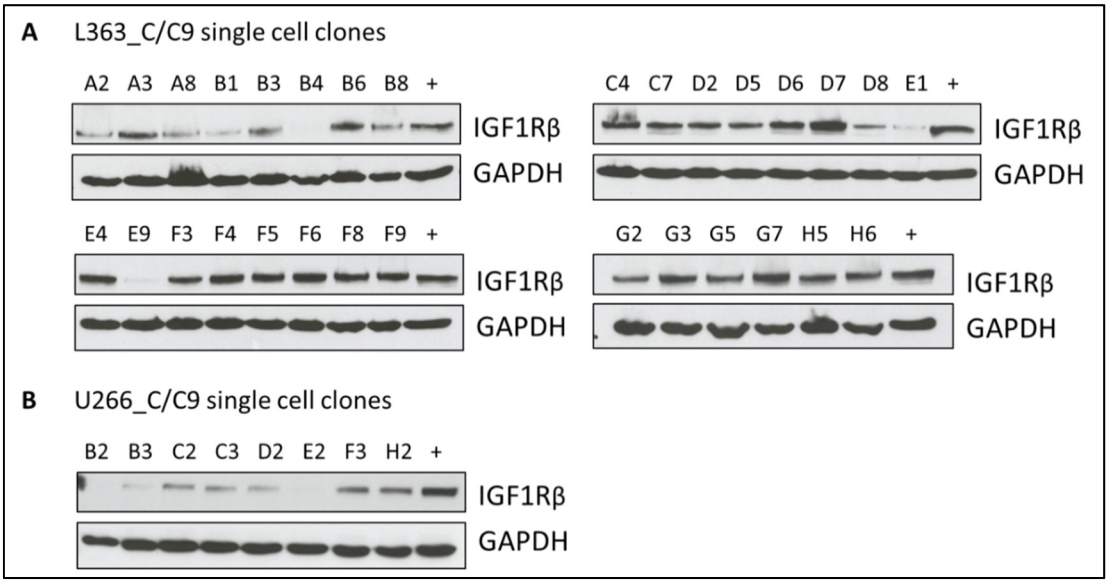

Figure 20: IGF1R expression in L363_C/C9 and U266_C/C9 cells
A WCL of L363_C/C9 single cell clones with changed DNA sequences were prepared and used for Western blot analysis to investigate IGF1R level. A clear knockdown is visible in clones B4, E1 and E9. **B** Growing U266_C/C9 single cell clones with a changed DNA sequence were used to prepare WCL followed by subsequent Western blot analysis to examine IGF1R expression. Clones B2, B3 and E2 showed the strongest IGF1R knockdown. GAPDH served as a loading control for both cell lines.

7.3.5 Knockdown of IGF1R enhances the MEK/ERK pathway but decreases cell proliferation

The successfully engineered HMCLs L363-C/C9 (clone B4) and U266-C/C9 (clone B3) were used for Western blots analyses to examine the effect of IGF1R knockdown on downstream signaling pathways with focus on the PI3K/AKT and the MEK/ERK pathways as well as selected adhesion molecules in two independent experiments (Figure 21). As expected, L363-C/C9 and U266-C/C9 cells showed a clear IGF1R knockdown compared to untreated cells. Knockdown of IGF1R had no effect on the phosphorylation level of AKT in the L363-C/C9 cells, however, the U266-C/C9 cells showed a decrease in the phosphorylation level of AKT. Phosphorylation of ERK1/2 and MEK was increased in both IGF1R knockdown cell lines, however, the expression and activation level of ERK1/2 was higher in U266 C/C9 cells compared to L363 C/C9 cells. No change was observed in the expression and phosphorylation level of MTOR and in the expression level of FAK and BRAF. RAS expression was increased in both IGF1R knockdown cell lines compared to controls. CRAF displayed a higher phosphorylation level in the L363 C/C9 cells compared to untreated L363 control cells. Additionally, the c-myc and integrin β1 level was increased in the L363 cells upon IGF1R knockdown. No c-myc and integrin β1 expression was detected in the U266 cells independent of IGF1R knockdown. PYK2 expression showed no difference between untreated and IGF1R knockdown cells in either cell line, however, the PYK2 level in U266 cells is considerably lower compared to L363 cells. Phosphorylation of PYK2 was only detectable in L363 cells and showed no difference between treated and untreated cells (Figure 21).

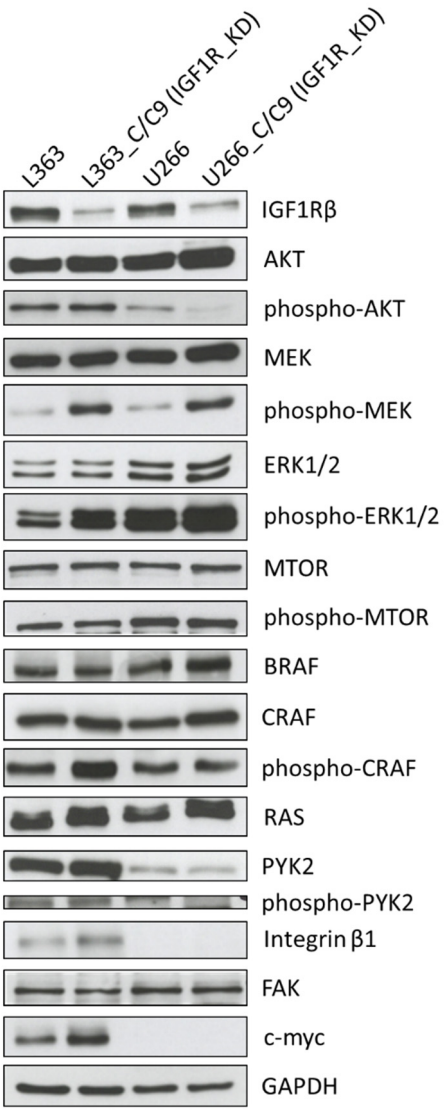

Figure 21: Downstream signaling of IGF1R_KD cell lines
Western blot analysis of L363_C/C9 and U266_C/C9 cell lines in comparison to untreated controls. Membranes were incubated overnight with indicated antibodies for the detection of selected signaling pathway and adhesion proteins. GAPDH served as loading control.

To further elucidate the role of IGF1R in MM, proliferation assays using BrdU incorporation of the untreated and L363-C/C9 cells were performed. Even though the phosphorylation levels of CRAF, MEK and ERK1/2 were increased upon IGF1R knockdown (Figure 21), these cells showed a decrease in cell proliferation compared to untreated cells (Figure 22). In an independent approach the untreated L363 and the L363 C/C9 were manually counted every 24 h using a Neubauer chamber. This approach revealed a significant difference in the amount of cells after 72h (p=0.036) indicating that the IGF1R knockdown leads to a decrease in cell proliferation (Figure 23). The proliferation of the U266 cells could not be evaluated due to stark differences in the performed replicates (data not shown).

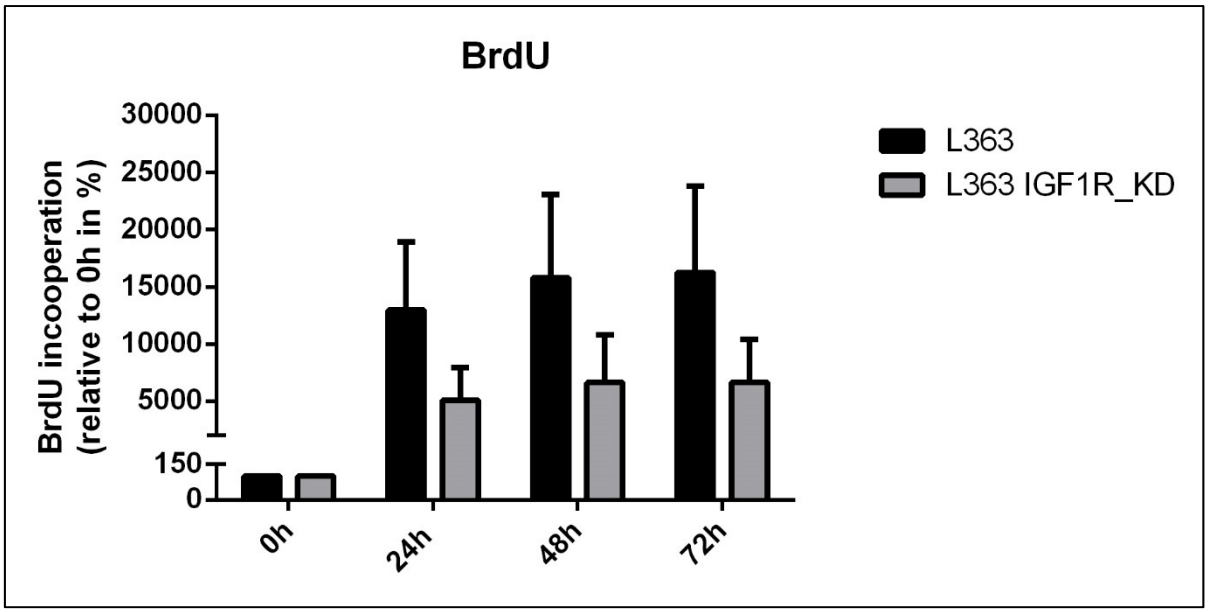

Figure 22: Determination of cell proliferation of L363 and L363 IGF1R_KD cells using a BrdU incorporation assay
Cell proliferation of L363 and L363 IGF1R_KD was measured by BrdU incorporation followed by subsequent FACS analysis using a FITC-coupled BrdU antibody. Values were normalized to 0h control. L363_C/C9 cells with an IGF1R KD show decreased cell proliferation compared to untreated cells.

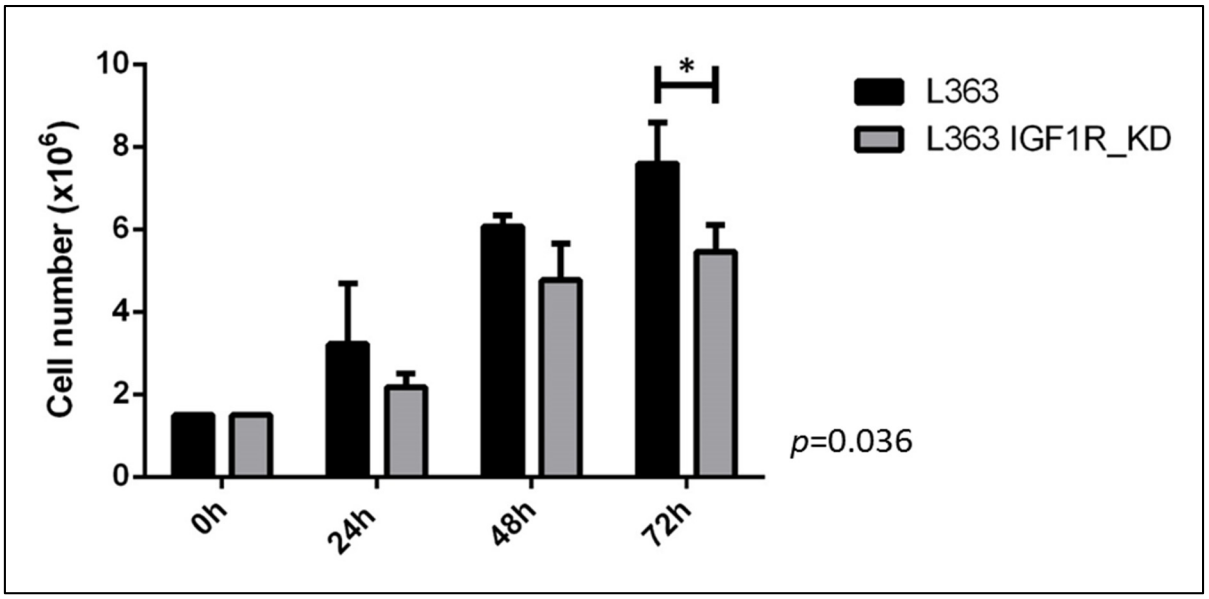

Figure 23: Total cell numbers of L363 and L363 IGF1R_KD cells
An equal amount of L363 and L363 IGF1R_KD cells (1.5 * 10^6 cells) were seeded into a 6-well plate and incubated for a total of 72 h. After 24 h, 48 h and 72 h cells were manually counted using Trypan blue and a Neubauer chamber. After 72 h, a significant difference in the total amount of cells was observed.

7.3.6 Successful overexpression of IGF1R WT, IGF1R D1146N and IGF1R N1129S in the HMCLs L363 and AMO1 using the sleeping beauty system

Initial experiments in HEK293FT cells showed that the overexpression of IGF1R WT, IGF1R D1146N and IGF1R N1129S had an influence on the cellular downstream signaling. To further analyze the effect of IGF1R overexpression as well as the effect of the mutations, stable HMCL had to be established. For this purpose, the transposon-based sleeping beauty system was used. Previously cloned pSF-CMV-IGF1R-WT, pSF-CMV-IGF1R-D1146N and pSF-CMV-IGF1R-N1129S plasmids were used as templates for PCR amplification of ORFs and subsequent cloning into the TST206-pT2-SVPuroCMV and TST212-pT2BN-SVpuroCAG vectors. Test digestion of the cloned expression vectors with FspI resulted in the expected DNA fragment sizes of 4882bp, 3938bp and 1172bp for cloned plasmids with the TST206-pT2-SVPuroCMV backbone. Digested plasmids with the TST212-pT2BN-SVpuroCAG backbone resulted in the expected DNA fragment sizes of 6076bp, 4270bp, 1172bp. Digestion of empty TST206-pT2-SVPuroCMV and TST212-pT2BN-SVpuroCAG vectors resulted in the expected DNA fragment band sizes of 4747bp and 1172bp as well as 6249bp and 1172bp, respectively. (Figure 24)

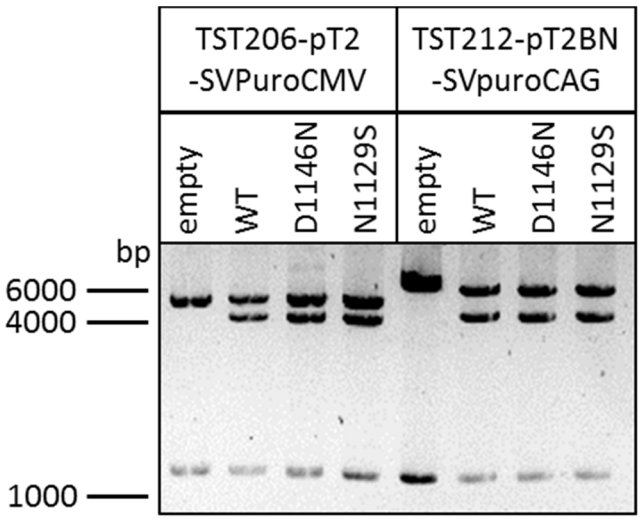

Figure 24: Restriction digestion of cloned TST206-pT2-SVPuroCMV and TST212-pT2BN-SVpuroCAG plasmids
Cloned TST206-pT2-SVPuroCMV and TST212-pT2BN-SVpuroCAG plasmids were transformed in *E. coli* NEB10β, purified and digested using FspI. Digestion of TST206-pT2-SVPuroCMV_IGF1R-WT, TST206-pT2-SVPuroCMV_IGF1R-D1146N and TST206-pT2-SVPuroCMV_IGF1R-N1129S resulted in the expected DNA fragment sizes of 4882bp, 3938bp and 1172bp. Digestion of the empty TST206-pT2-SVPuroCMV vector resulted in the expected DNA fragment sizes of 4747bp and 1172bp. Digestion of TST212-pT2BN-SVpuroCAG _IGF1R-WT TST212-pT2BN-SVpuroCAG _IGF1R-D1146N and TST212-pT2BN-SVpuroCAG _IGF1R-N1129S resulted in the expected DNA fragment sizes of 6076bp, 4270bp, 1172bp. Digestion of the empty TST212-pT2BN-SVpuroCAG vector resulted in the expected DNA fragment sizes of 6249bp and 1172bp.

Sequencing of the ligated plasmids (TST206-pT2SVPuroCMV_IGF1R, TST206_pT2SVPuroCMV_IGF1R-D1146N, TST206-pT2SVPuroCMV_IGF1R-N1129S, TST_212_T2BN_SVpuroCAG_IGF1R, TST-212-pT2BN_SVpuroCAG_IGF1R-D1146N, and TST-212-pT2BN_SVpuroCAG_IGF1R-N1129S) showed no undesired mutations in the IGF1R ORF. All cloned plasmids contained a puromycin resistance gene for selection of positive cells. The HMCL AMO1 showed a significant decrease of viability starting at 0.75 µg/ml puromycin ($p < 0.0001$). At a puromycin concentration of 1 µg/ml nearly all cells were dead (Figure 25 A). To ensure a successful positive selection in further experiments a puromycin concentration of 1.5 µg/ml was used. The HMCL L363 showed a significant decrease of cell viability at a concentration 0.25 µg/ml puromycin ($p < 0.0001$; Figure 25 B), however, in further experiments this concentration was too low to kill all control cells (data not shown). The used puromycin concentration was therefore increased to 1 µg/ml.

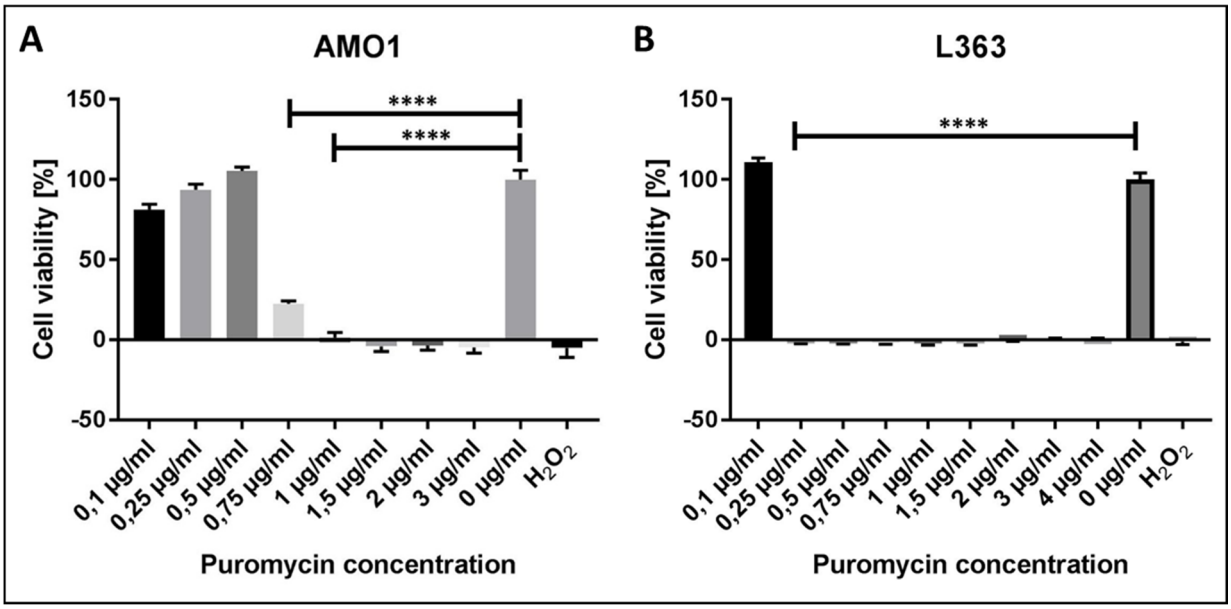

Figure 25: Cell viability after puromycin treatment
Cells were treated with indicated puromycin concentration for 72h. After incubation, cells were washed and treated for a second time with puromycin. After additional 72h, cells were subjected to a MTT assay to determine lethal puromycin concentration. Untreated (0µg/ml) and H_2O_2 treated cells were carried along as positive and negative control cells. Values were normalized to untreated cells.

After the successful determination of the lethal puromycin concentration for the AMO1 and L363 cells, the HMCL AMO1 as well as the HMCL L363 containing a stable IGF1R knockdown by CRISPR/Cas9 (L363_C/C9) were used for the overexpression of IGF1R WT, IGF1R D1146N and IGF1R N1129S using the transposon-based sleeping beauty system. After selection of positive cells using puromycin, cells were analyzed by Western blot using an IGF1Rβ specific antibody as well as FACS analysis. Initially, both HMCLs were transfected using the TST206-pT2SVPuroCMV plasmids. However, FACS analysis of AMO1 cells showed no clear increase in IGF1R expression (data not shown). Transfection of the AMO1 cells was thus repeated using the TST-212-pT2BN-SVpuroCAG plasmids. Transfection of L363-C/C9 cells using the TST206-pT2SVPuroCMV-IGF1R-WT/N1129S/D1146N plasmids resulted in a distinct overexpression of IGF1R WT, IGF1R D1146N and IGF1R N1129S, respectively (Figure 26 A). Transfection of AMO1 cells with the TST-212-pT2BN-SVpuroCAG-IGF1R-WT/N1129S/D1146N plasmids also resulted in a clearly visible overexpression of IGF1R WT, IGF1R D1146N and IGF1R N1129S, however slight differences were observed between IGF1R WT and IGF1R N1129S (Figure 26 B). The overexpression was stable in both HMCLs and still detectable after cells were cultured for 3 months (data not shown). For further downstream analysis only the L363-C/C9 overexpression cell lines were used.

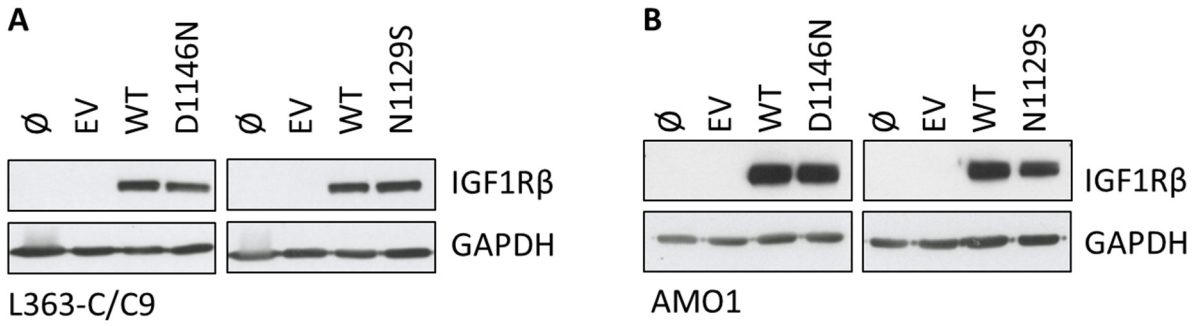

Figure 26: IGF1R overexpression in L363-C/C9 and AMO1 cells
A Western blot analysis of L363-C/C9 cells overexpressing IGF1R WT, IGF1R D1146N and IGF1R N1129S using the TST206_CMV vector backbone. Untreated and EV controls show no IGF1R expression. GAPDH was used as a loading control. **B** Western blot analysis of AMO1 cells overexpressing IGF1R-WT, IGF1R-D1146N and IGF1R-N1129S using the TST212-CAG vector backbone. Untreated and EV control cells show no IGF1R expression. GAPDH served as loading control.

7.3.7 Downstream signaling analysis of genetically engineered L363-C/C9 cells overexpressing WT and mutant IGF1R

After the successful establishment of the IGF1R overexpression in the HMCL L363-C/C9 and AMO1, the L363 cells were subsequently used to study the effect of IGF1R WT and mutant IGF1R overexpression on selected downstream signaling pathways including PI3K/AKT and MAPK as well as selected focal adhesion molecules (Figure 27). Overexpression of IGF1R appeared consistent over the three L363-C/C9 overexpression cell lines and no IGF1R was detected in the empty vector (EV) control. Moreover, the phosphorylation of the IGF1R tyrosine residues 980 and 1135 was observed in all overexpression cell lines independent of the presence of a mutation. Moreover, independent of mutation status, the overexpression of IGF1R led to an increased phosphorylation of the downstream signaling molecules AKT, MEK, EK1/2 and PYK2 compared to the EV control cell line. Interestingly, no change in the expression and/or phosphorylation of MTOR, BRAF, CRAF, integrin β1, FAK and c-myc was observed between the overexpression cell lines and the EV control cell line. Unfortunately, the Ras signal was not evaluable due to a tear in the gel.

The IGF1R N1129S overexpression cell line exhibited the strongest IGF1R phosphorylation compared to the IGF1R WT and IGF1R D1146N cell lines. Furthermore, the IGF1R N1129S cell line exhibited an increase in the downstream signaling pathways compared to the other L363 overexpression cell lines. In this cell line a higher phosphorylation level of AKT, MEK, ERK1/2 and PYK2 was observed whereas the expression levels remained constant across the different overexpression cell lines. In contrast to the situation in HEK293FT cells, the IGF1R N1129S cell line showed no enhanced expression of c-my.

To evaluate the influence of the overexpression of IGF1R WT as well as IGF1R D1146N and IGF1R N1129S the cell proliferation of the different L363 cell lines was evaluated. Therefore, an equal amount of cells was seeded into a 6-well plate and the cells were counted after 72 h in three independent experiments. There was a significant difference in the total cell number between the IGF1R N1129S cell and all other cell lines ($p<0.05$) which is in support of the results seen in the Western blot analyses (Figure 28).

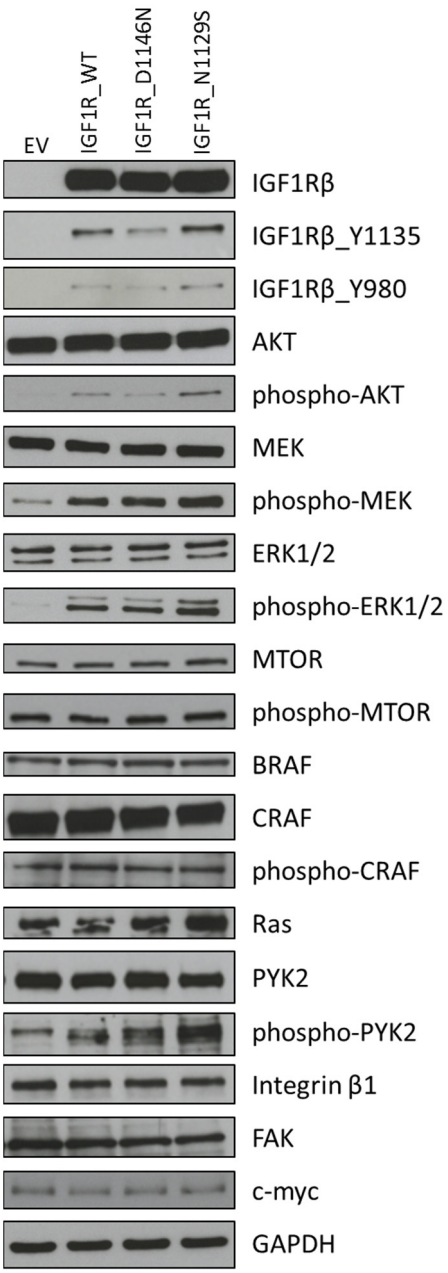

Figure 27: Downstream signaling of the L363 IGF1R overexpression cells
Western blots of L363 C/C9 cells overexpressing either IGF1R WT, IGF1R D1146N or IGF1R N1129S. L363 C/C9 cells transfected with EV served as control. Membranes were incubated overnight with indicated antibodies for the detection of selected signaling pathway and adhesion proteins. GAPDH served as loading control

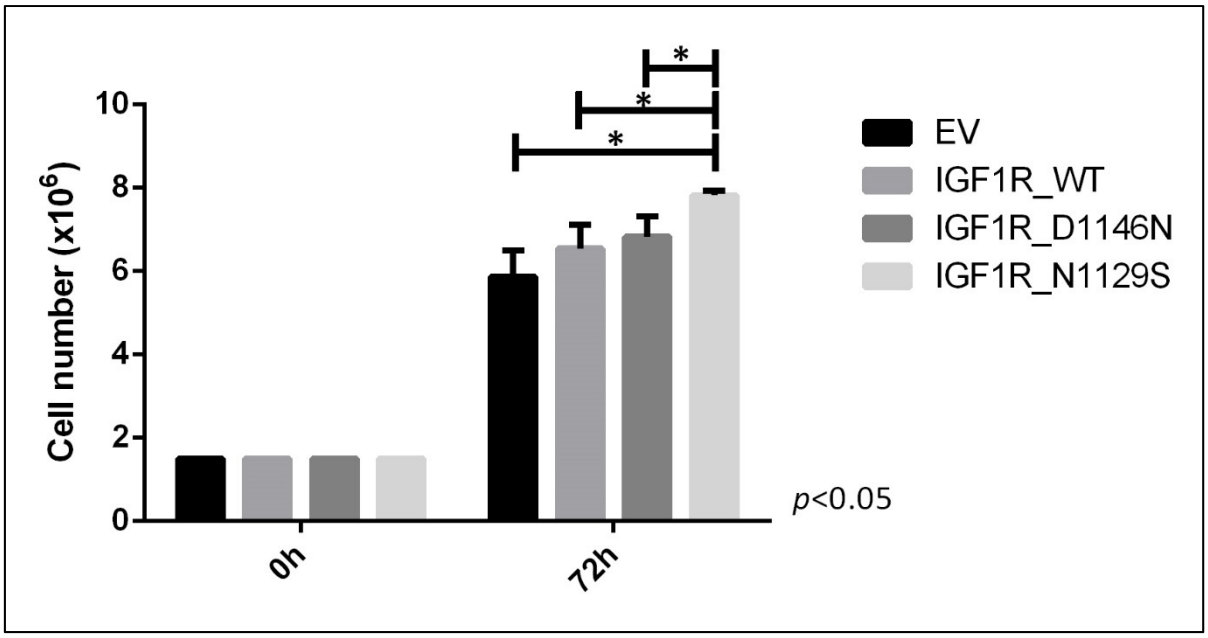

Figure 28: Total amount of cells of the different IGF1R overexpression cell lines after 72 h
An equal amount of the different IGF1R overexpression as well as the EV control cells (1.5 * 10^6 cells) were seeded into a 6-well plate and incubated for a total of 72 h. After 72 h, the cells were manually counted using Trypan blue and a Neubauer chamber. Student t-tests were performed for statistical analyses and $p<0.05$ was considered statistically significant. A significant difference between the IGF1R-N1129S overexpression cell line and the other three cell lines was observed ($p<0.05$).

7.3.8 Stimulation of the L363-C/C9 IGF1R overexpression cell lines with IGF1

MM is characterized by the accumulation of MM cells in the bone marrow. There the cells can interact with bone marrow stromal cells which leads, among others, to an increase in IGF1. [136] To specifically activate IGF1R, the different IGF1R overexpression as well as the EV control cell lines of L363-C/C9 were subjected to stimulation experiments. Briefly, cells were serum-starved for 18 h and stimulated with IGF1 before the preparation of WCL and subsequent Western blot analyses (Figure 29). First Western blot analyses showed a constant expression level of IGF1R in the IGF1R overexpression cell lines and no expression in the EV control, as expected. Moreover the expression levels of AKT, MEK, ERK1/2, MTOR, and BRAF were constant in all cell lines independent of IGF1R status and IGF1 stimulation. However, after IGF1 stimulation the IGF1R overexpression cell lines showed an increase in the phosphorylation of nearly all investigated downstream effectors. The IGF1R N1129S cell line exhibited the strongest IGF1R Y980 and PYK2 phosphorylation level after IGF1 stimulation. This cell line also showed, after stimulation, the highest expression level of integrin β1, an extracellular matrix adhesion molecule. Interestingly, the IGF1R D1146N and IGF1R N1129S overexpression cell lines exhibited a stronger MEK and ERK1/2 phosphorylation level after IGF1 stimulation indicating an increase in the MAPK signaling pathway. All cell lines, including the EV control cell line, showed an increase of AKT phosphorylation after stimulation, however, the level in the IGF1R N1129S cell line was marginally lower compared to the EV control and the L363-C/C9 cells expressing IGF1R WT and IGF1R D1146N. The expression level of BRAF was consistent across the cell lines, the expression level of CRAF, though, was decreased in the stimulated IGF1R N1129S cells compared to all other L363-C/C9 cell lines. Therefore, it is not possible to make a definite statement about the influence of IGF1 stimulation on the CRAF phosphorylation in these cells. IGF1 stimulation, however, led to a slight increase in the CRAF phosphorylation level of the IGF1R WT and IGF1R D1146N cells. Another interesting observation is the fact that the c-myc expression is increased after IGF1 stimulation in the EV control as well as the IGF1R mutant cell lines. Taken together these results show that IGF1 stimulation leads to an increase in IGF1R activity and downstream signaling independent of mutational status. However, the mutant cell lines exhibit an increase in the MAPK pathway compared to the WT cell line (Figure 29).

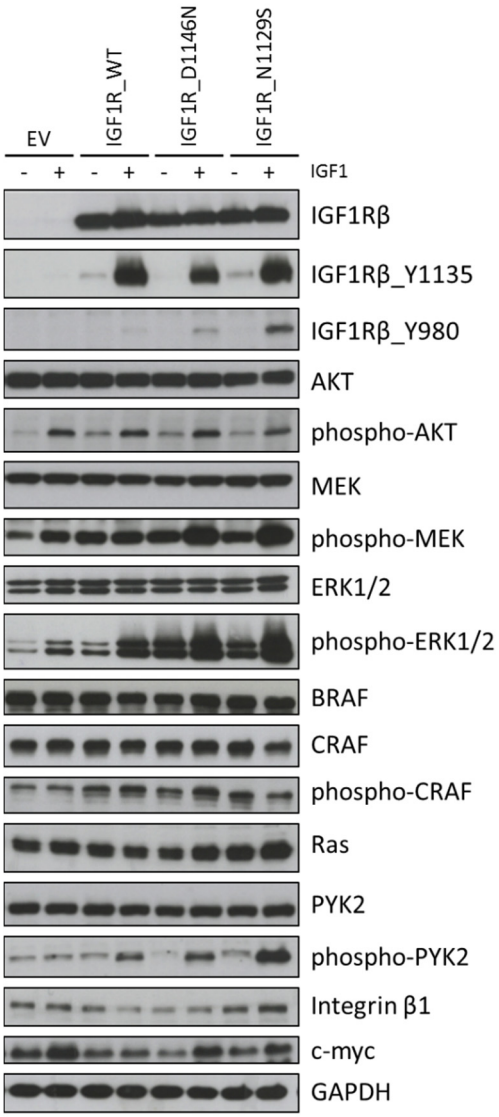

Figure 29: Signaling analysis of L363-C/C9 IGF1R WT/N1129S/D1146N sleeping beauty cell lines after IGF1 simulation
The different L363 C/C9 IGF1R WT/N1129S/D1146N cell lines were serum-starved for 18 h before stimulation with IGF1 for 10 min. Following IGF1 stimulus WCL were prepared and used for Western blot analyses. Membranes were incubated with indicated antibodies overnight. GAPDH served as loading control.

8 Discussion

8.1 RTK mutations identified in the DSMM XI patient cohort are potential novel prognostic markers in MM

RTKs are known to play important roles in cell proliferation and survival and have been shown to be frequently deregulated in different cancer entities [44, 52]. In a recent WES approach an accumulation of mutations in RTKs, adhesion molecules and their downstream signaling effectors in MM was discovered. Almost all analyzed MM patients were affected by at least one mutation and about half of the MM patients were affected by more than one mutation in this defined signaling network [39]. Important downstream targets of RTKs are members of the PI3K/AKT and MAPK pathways, e.g. RAS and RAF [46, 137]. These pathways are often deregulated in MM and key molecules such as *NRAS*, *KRAS* and *BRAF* belong to the most frequently mutated genes in MM [22, 35, 138, 139]. However, new results indicate that the mutational status of *RAS* alone may not always be associated with MAPK pathway activation [140]. Additionally, the activation of the PI3K/AKT pathway in MM can only be explained to some extent by previously obtained results [141-143]. The activation of these pathways in MM may therefore also be explained by activating mutations in upstream molecules such as RTKs. For further investigations of the role of RTK mutations in MM the CDS of the six RTK genes *EGFR*, *ERBB3*, *EPHA2*, *IGF1R*, *NTRK1* and *NTRK2* was deep-sequenced using an amplicon sequencing approach [124]. The validated mutations were furthermore correlated with cytogenetic alterations and survival status of the 75 uniformly treated patients of the DSMM XI. *IGF1R* was the most affected gene in this analysis and most validated mutations (9/11) were detected in the tyrosine-kinase and ligand-binding domains (Figure 7) [124]. Both domains play important parts in the signal transfer from the extracellular space to the nucleus. Ligand binding to the extracellular part of the RTK leads to the dimerization of the receptor or, in the case of IGF1R, to structural changes and subsequent autophosphorylation of the tyrosine-kinase domain and downstream signaling [45, 46]. Mutations in the ligand-binding domain may therefore lead to changes in ligand binding by allowing a better or worse accessibility of the ligand to the binding site. RTK mutations located in the tyrosine-kinase domain have furthermore been shown to lead to the activation of RTKs and subsequent downstream signaling [53, 58, 144]. The validated RTK mutations in the ligand-binding and tyrosine kinase domain may therefore result in an altered downstream signaling and thus may

lead to an increase in cell proliferation, cell survival and a worse clinical outcome. This would also be in accordance with the obtained survival results which suggest a negative influence of RTK mutations on the OS and EFS of the analyzed patient cohort of the DSMM XI (Figure 8). [124] To exclude the possibility that the worse outcome is associated with adverse prognostic factors such as del13q14 and del17p13 [40], cases containing these cytogenetic abnormalities were removed from the analyses. Of note, even after removing these adverse prognostic factors, patients harboring RTK mutations still had a significantly lower OS and EFS (Figure 9) further demonstrating the role of RTK mutations as potential prognostic markers in MM. [124] Especially rare SNPs seem to be adverse prognostic parameters with patients carrying a rare RTK SNP exhibiting a significantly worse OS, EFS and PFS compared to RTK_WT patients (Figure 8 D-F). [124] These rare SNPs seem to be unique for the sequenced RTKs and have not been observed in *DIS3* [40] and *KRAS* (unpublished data) which were sequenced and analyzed in the same patient cohort. Rare RTK SNPs identified in the amplicon sequencing study were the first SNPs associated with a worse OS, EFS and PFS in MM patients treated with bortezomib, ACST and chemotherapy whereas previous studies only found an association between the *TNFα* (-238) polymorphism and improved survival in thalidomide treated patients and a trend towards an increase in PFS in patients harboring the *TNFα*/*LTα* (-308, +252) polymorphism treated with high dose chemotherapy [124, 145, 146]. Since the publication of the RTK SNP study, however, more studies reported the identification of polymorphisms associated with decreased patient survival. Varga *et al.* reported a polymorphism of *PSMB1* associated with a lower PFS [147] whereas Poi *et al.* reported an *ANRIL* SNP also associated with a worse PFS [148]. Moreover, in the second conducted amplicon study rare RTK SNPs were associated with the adverse prognostic factor del17p furthermore indicating rare RTK SNPs as potential adverse prognostic markers. However, the rare SNPs detected in patients of the DSMM XII trial have to be further analyzed in regard to patient survival and response to therapy to strengthen this hypothesis.

8.2 Mutations detected in the DSMM XII study cohort accumulate in the extracellular domain

To further elucidate the role of rare RTK SNPs, the CDS of the six RTKs *EGFR*, *ERBB3*, *EPHA2*, *IGF1R*, *NTRK1* and *NTRK2* was resequenced in a new patient cohort of the DSMM XII containing 75 tumor and 184 normal samples. This second amplicon sequencing validation approach identified 23 different mutations affecting a total of 24 patients which could be furthermore classified into 20 rare SNPs and 3 SNVs. As seen in the previously conducted study, the detected rare SNPs were either not listed in common databases such as dbSNP, 1000 genomes and ExAC or had a MAF below 1%. Only two mutations (ERBB3 c.2595G>T, IGF1R c.3852G>T) were also detected in the first amplicon sequencing study which is in conclusion with several observations that recurrent mutations are only present in a small amount of patients [35, 37, 38]. The identified mutations were present in all investigated genes with *IGF1R* again being among the most frequently mutated genes (Figure 7, Figure 11) [124]. However, an enrichment of mutations in the tyrosine-kinase domain was not observed in the second amplicon sequencing study. Identified mutations were predominately located at the extracellular protein domains and regions with an accumulation of mutations in the signaling peptide of *EGFR* and *IGF1R* and the ligand-binding domain of *EGFR* and *EPHA2* (Figure 11). Especially, the identified mutations in the signaling peptides are of particular interest. The correct transport of proteins to their required subcellular location is crucial for the accurate protein function and requires N-terminal signaling peptides [149]. Mutations in the signal peptide of proteins have been reported to impact the correct subcellular protein localization and may even be responsible for a number of diseases. Datta and colleagues reported that a mutation in the signal peptide of human preproparathyroid hormone causes aberrant protein secretion and localization in autosomal dominant familial isolated hypoparathyroidism [150]. Moreover, a study by Dunning *et al.* showed that a SNP in the signal peptide of the transforming growth factor β1 (*TGFβ1*) is associated with increased protein secretion [151]. These studies indicate that single missense mutations in the signaling peptide can clearly influence the secretion and subcellular protein localization. Aberrant localization of mutated RTKs to the ER or cytoplasm can furthermore lead to abnormal activation of signaling pathways. Choudhary *et al.* demonstrated that the abnormal localization of the mutated RTK Flt3 to the ER alters the phosphorylation pattern as well as the activation of the downstream signaling. Mutated Flt3 activated the STAT5 pathway if localized in the ER, however, if localized

at the plasma membrane the MAPK and PI3/AKT pathways were switched on [152]. In a further study they additionally showed that the deregulated localization to the ER or Golgi apparatus can, to some extent, lead to the activation of downstream signaling effectors e.g. RAS in the absence of ligand [153]. Moreover, the intracellular localization of TrkA, the protein encoded by the *NTRK1* gene, results in the incapability to activate the MAPK pathway [154]. It would therefore be of particular interest to investigate whether the detected mutation localized in the signal peptide have an influence on the subcellular localization and activation of RTKs.

Additionally, mutations accumulated in the ligand-binding domain, especially of *EGFR*. As mentioned previously, mutations affecting the ligand-binding domain may alter the binding ability of ligands by changing the accessibility of the binding pocket and thereby leading to a change in downstream signaling. Mutations in the *EGFR* ligand-binding or rather in the extracellular domain in general are of particular interest due to their frequent incidence in glioblastomas [155]. The deletion of the coding sequence for the amino acids 6-273, affecting the ligand-binding domain, has been reported to lead to a constitutive ligand-independent EGFR-activation leading to the enhanced cell growth [155, 156]. Moreover, several missense mutations in the ligand-binding and extracellular domain of *EGFR* have been reported and were shown to be transforming events resulting in anchorage-independent growth and enhanced tumorigenicity in NIH-3T3 cells, even in the absence of a ligand [157]. It has been furthermore demonstrated that these EGFR-activating mutations of the extracellular domain result in an increased ligand-binding affinity by altering the interface between the first ligand-binding and the furin-like cysteine rich domain that follows [158]. Additionally, Gilmore and colleagues have demonstrated that a missense mutation in the second ligand-binding domain results in the increased binding-affinity for neuregulin-2β which only binds with a low affinity to WT *EGFR*. In the absence of a ligand the mutation even led to a constitutive active PI3K/AKT signaling pathway and thereby to the inhibition of apoptosis [159]. These studies show that even single mutations in the ligand-binding and extracellular domain of *EGFR* can result in the aberrant activation of downstream signaling pathways and may influence patient survival. It would therefore be interesting to see, how the mutations detected in the ligand-binding domains of the sequenced RTKs affect the binding affinity of their ligands e.g. IGF1 or EGF.

8.3 Rare SNPs as predisposing risk factors for MM development

SNPs have been previously implicated to influence cancer risk in different cancer entities e.g. breast and prostate cancer or Non-Hodgkin lymphoma [160-162]. In MM, however, only a small number of genetic susceptibility loci have been described so far including SNPs in *CBX7*(22q13.1), *CDCA7L/DNAH11*(7p15.3), *DNMT3A* (2p23.3), *PSORS1C1*(6p21.33), *TERC*(3q26.2), *TNFRSF13B*(17p11.2) *and ULK4*(3p22.1) which were identified by genome wide association (GWA) studies [163]. However, one of the drawbacks of these GWA studies is the problem that low frequency variants are not identified [163]. The rare RTK SNPs identified in both of our amplicon sequencing approaches would have therefore not been identified by current GWA studies due to their low minor allele frequency (MAF). The detected rare SNPs in both patient cohorts were, as mentioned previously, either not present in 1000 genomes or dbSNP database or had a MAF <1 % at time of analysis, predicting their role as MM specific risk factors. Additionally, the rare RTK SNPs detected in the DSMM XI study cohort, were also present in non-hematological normal samples (Supplementary Figure 1) suggesting that they occur during embryogenesis or are inherited variants that may lead to MM development in cooperation with other genetic aberrations. [124] Even though the detected SNPS were rare, they may still play a role in the predisposition for MM. The importance of rare variants has already been shown for other cancer entities e.g. prostate cancer. Rare variants with MAF <1 % were recently shown by Mancuso and colleagues to be responsible for the genetic risk of prostate cancer in African-American men [164]. Moreover, Grin *et al.* reported a rare SNP at the chromosomal position 8q24 which is associated with an increased prostate cancer risk in North American men. However, in contrast to Mancuso *et al.* this rare SNP was predominantly found in Caucasians [165]. It has furthermore been shown that multiple rare genetic variants in colorectal adenomas may contribute to the inherited susceptibility of the disease [166]. In another study consisting of 12 different cancer types, rare germline missense mutations were also detected and 101 of these rare germline mutations were listed as pathogenic [167]. These studies show that even variants with MAF <1 % which are thereby considered rare, can have an influence on the genetic susceptibility to different cancer entities. To further elucidate the role of rare RTK SNPs as predisposing risk factors in MM, more retrospective and prospective studies with larger uniformly treated patient cohorts together with independent healthy control cohorts have to be conducted.

8.4 The influence of IGF1R mutations on MM pathogenesis

IGF1R is known to be a key player in human development and disease and has been shown as an adverse prognostic factor in diverse cancer entities including MM [68, 80, 83, 108]. Furthermore, the overexpression of IGF1R leads to an increase in cell proliferation, tumor growth, cell migration and a decrease in apoptosis [87, 88]. While a large number of studies have shown that overexpressed IGF1R leads to malignant transformation and enhanced signaling in cancer cells, only a small number of studies have investigated the influence of *IGF1R* mutations on receptor activity, downstream signaling and cell proliferation of cancer cell lines [168]. Moreover, to our knowledge, no IGF1R activating mutations have been described so far [169]. However, a number of studies demonstrated that *IGF1R* mutations are associated with growth retardation and one mutation has been shown to lead to an aberrant localization of the mutated IGF1R to the ER [170, 171]. In a deep-sequencing approach of uniformly treated patients of the DSMM XI and DSMM XII, *IGF1R* was among the most frequently mutated gene in the MM patient cohorts (Figure 7, Figure 11) [124]. To elucidate the role of IGF1R mutations on receptor activity and signal pathway activation, stable IGF1R knockdowns were established in the IGF1R-mutant HMCL L363 and the IGF1R WT HMCL U266. Surprisingly the knockdown of IGF1R resulted in an increase in the phosphorylation of MEK and ERK in both knockdown cell lines indicating an increase in pathway activation. Moreover, the L363-C/C9 cell line exhibited an enhanced phosphorylation level of CRAF and enhanced protein levels of c-myc and integrin β1. The increase in phosphorylation of important molecules of the MAPK pathway would suggest an increase in cell proliferation as well. However, BrdU and cell proliferation assay of the L363 and L363-C/C9cells clearly showed that the cell proliferation of L363 is decreased upon IGF1R knockdown, an observation in conclusion with previously conducted IGF1R inhibitor studies in other HMCLs [104, 172]. Although a decreased proliferation was expected, it remains unclear how the increase in MAPK signaling activity that was observed in Western blot experiments, resulted in the decreased cell proliferation of the L363-C/C9 cells. It was previously shown that after inhibition of IGF1R the activity of other RTKs, e.g. EGFR, is increased and thereby compensating for the loss of IGF1R [76, 173]. This compensation mechanism may not be strong enough to fully restore cell proliferation which is consistent with the observed decrease. Knockdown of IGF1R in the L363 cells clearly reduces but doesn't completely abolish cell proliferation (Figure 22, Figure 23). Moreover, it has previously been shown that the MAPK

pathway not only plays a role in cell proliferation, but has, under certain conditions, also been implicated in apoptosis, senescence and autophagy [174]. The activation of the MAPK pathway results in active ERK1/2 which has been demonstrated to activate the extrinsic as well as the intrinsic apoptotic pathway [174]. The role of the activated MAPK pathway in apoptosis might therefore explain why the higher phosphorylation of CRAF, MEK and ERK1/2 lead to a decrease in cell proliferation. However, further experiments are needed to elucidate the mechanism between an increase in MAPK pathway activity and decreased cell proliferation in the L363-C/C9 IGF1R-KD cells. Furthermore, proliferation assay of the U266-C/C9 IGF1R-KD HMCL have to be conducted to see if the effect observed in the L363-C/C9 IGF1R-KD cells is cell line specific or applicable to a wider range of HMCL.

To further study the role of the previously detected IGF1R mutations IGF1R D1146N and IGF1R N1129S, the L363-C/C9 cells and the IGF1R WT cell line AMO1 were used for the stable overexpression of the two mutants as well as IGF1R WT. Both mutants affect the tyrosine-kinase domain and were located in conserved domains according to the bioinformatics predictors PhastCons and GERP (Figure 7, Table 57). Western blots of overexpression cells exhibited similar IGF1R protein levels of WT and mutants indicating that the stability of IGF1R is not affected by the mutations. Interestingly, L363-C/C9 cells overexpressing IGF1R N1129S had an increased phosphorylation of the IGF1R tyrosine residues Y1135 and Y980 and an increased phosphorylation of AKT, ERK and MEK (Figure 27). These increased phosphorylation levels are in conclusion with the observed increased cell proliferation of the IGF1R N1129S cells compared to the L363-C/C9 IGF1R WT and L363-C/C9 IGF1R D1146N cell lines (Figure 28). To specifically activate IGF1R, stimulation assays with IGF1 were performed. Stimulation of all L363-C/C9 overexpression cell lines resulted in an increase in the downstream phosphorylation levels. However, the L363-C/C9 cell with an IGF1R N1129S overexpression showed a higher ERK1/2 phosphorylation level even under starved conditions and the highest ERK1/2 level upon IGF1 stimulation (Figure 29). In contrast to Western blots of unstimulated cells, the IGF1R D1146N cell line showed, under starved and stimulated conditions, a higher phosphorylation level of MEK and ERK compared to the IGF1R WT cells. These results indicate that in an IGF1 containing environment, like the bone marrow microenvironment [136], both IGF1R mutations might lead to an increase in the MAPK signaling pathway and a potential increase in cell proliferation. In an environment with a low amount or bound IGF1 present, only cells with an IGF1R N1129S might have an increased downstream signaling. Moreover,

the patient harboring the IGF1R N1129S mutation had a very low OS of only 5 months and displayed no adverse cytogenetic abnormalities such as del17p or del13q [124]. The short OS with no adverse cytogenetic abnormalities might therefore be another indication for the adverse influence of this mutation.

It is, however, unknown how the detected mutations might result in an increased downstream signaling. Mutations in the tyrosine-kinase domain of EGFR have been reported to lead to a higher kinase activity. The reported missense mutation has been hypothesized to lead to a repositioning of aa residues at important sites in the ATP binding pocket and thereby stabilizing the ATP interaction with the receptor [58]. Such a residue repositioning might also be possible for the detected IGF1R mutations though crystal structural analysis are required to further investigate the effect of the mutations on the 3D structure of IGF1R.

IGF1R consist of two α and two β chains forming a disulfide-bound homodimer [72]. Beyond the formation of this homodimer, IGF1R can also form a heterodimer hybrid receptor (HR) consisting of one α and on β subunit of the IGF1R and one α and on β subunit of the InsR [131]. In contrast to the IGF1R, this HR has a broader ligand specificity binding not only IGF1 with a high affinity, but also IGF2 and insulin [175]. The detected mutations might have an influence on the formation of the hybrid receptor. A higher content of HR might result in cells sensitive to more ligands and thereby leading to enhanced downstream signaling.

Another effect of the detected IGF1R mutations might be an influence on the translocation of the receptor to the nucleus. IGF1R was shown to translocate to the nucleus by clathrin-dependent endocytosis. Nuclear IGF1R is phosphorylated upon ligand stimulation followed by subsequent interaction with chromatin. This chromatin interaction suggests a role of nuclear IGF1R in transcriptional regulation. Moreover, higher concentrations of nuclear IGF1R were associated with an adverse patient survival in renal cell cancer. [176] Sarfstein and colleagues have furthermore shown that IGF1R can translocate to the nucleus and bind to its own promotor DNA leading to an enhanced *IGF1R* expression [177]. It was also shown that nuclear IGF1R can form a complex with LEF-1/TCF at the promotor region of *cyclin D1* resulting in enhanced cyclin D1 levels and increased cell cycle progression [178]. These reports all indicate an important role of nuclear IGF1R in cancer development and progression and it would therefore be interesting to see, if the detected mutations have an influence on the nuclear translocalization of IGF1R.

8.5 The cooperation of IGF1R and adhesion molecules in MM

In addition to the accumulation of mutations in RTKs, the recently conducted WES approach found an accumulation of mutations in adhesion molecules [39]. Moreover, activated IGF1R has been previously been shown to transiently associate with the adhesion molecule integrin β1 leading to enhanced cell adhesion and migration via the PI3K/AKT signaling pathway. IGF1 stimulation of MM cells furthermore led to an enhanced phosphorylation of FAK and paxilin phosphorylation and enhanced the interaction of integrin β1 with focal adhesion molecules. [99] Interestingly, first Western blot analyses showed an enhanced integrin β1 level in stimulated cell overexpressing IGF1R N1129S whereas the other overexpression cell lines showed no integrin β1 increase (Figure 29) indicating that the IGF1R N1129S mutations might influence the previously described interaction of IGF1R and integrin β1 upon IGF1 stimulation. In contrast to the study by Tai *e al.,* no FAK phosphorylation could be detected (data not shown) which might be due to the specific molecular phenotype of L363 cells which probably differs from the phenotype of MM.1S and OPM6 cells used by Tai *et al.*. The influence of the IGF1R mutations on the cooperation with integrin β1 should, in addition to Western blot analysis, furthermore be tested using co-immunoprecipitation with subsequent mass spectrometry and cell-based adhesion and migration assays.

Another adhesion molecule studied in this work is PYK2. PYK2 is a non-receptor tyrosine kinase with a broad range of functions including actin cytoskeleton reorganization, cell migration, cell adhesion and cell spreading. Increased levels of PYK2 have been associated with enhanced metastasis and reduced survival in hepatocellular carcinoma and lung cancer. [179, 180]. Moreover, Zhang *et al.* showed that PYK2 is highly expressed in MM patients, promotes tumor progression and results in a decreased survival *in vivo*. Inhibition and knockdown of PYK2 thus resulted in a decline of cell proliferation and adhesion. [181] Western blot analyses of the established IGF1R overexpression cells showed that PYK2 phosphorylation seems to be dependent on IGF1R activity. The L363-C/C9 IGF1R N1129S cells displayed not only the highest IGF1R-Y980 phosphorylation but also the highest PYK2 phosphorylation. A decrease in the IGF1R-Y980 phosphorylation also resulted in a decreased PYK2 phosphorylation level as seen in the IGF1R D1146N and IGF1R WT overexpression cell lines (Figure 29). This effect was not only seen in the L363-C/C9 overexpression cells but also in JJN3 cells overexpression IGF1R which were investigated in the Master thesis of Marlene Schwarzfischer [130]. In the JJN3 overexpression cells, however, PYK2 phosphorylation was independent of the IGF1R mutation

status and only dependent on IGF1R-Y980 phosphorylation. Interestingly, preliminary siRNA knockdown experiments of IGF1R in JJN3 seem to confirm this finding (unpublished data). Stimulation experiments with increasing levels of IGF1 should be conducted to elucidate if this effect is associated with the IGF1R mutation status. Still, these results indicate a cooperation between IGF1R and PYK2 to promote MM tumorigenesis. As a matter of fact, IGF1R and PYK2 were previously shown to co-localize upon ligand stimulation in urothelial cancer cells and PYK2 was shown to be important for IGF1R induced cell motility and invasion [89]. Further studies have to be conducted though the single and/or dual inhibition of IGF1R and/or PYK2 might be a new strategy for MM treatment in a subset of patients with mutated IGF1R and/or high PYK2 levels.

9 Future perspective

Amplicon sequencing of the RTKs *EPHA2*, *EGFR*, *ERBB3*, *IGF1R*, *NTRK1* und *NTRK2* enabled the identification and clinical characterization of mutations in a uniformly treated patient cohort. For the first time, rare SNPs affecting these RTKs were shown to be adverse prognostic markers resulting in a decreased patient survival. Moreover, the rare RTK SNPs detected in the DSMM XII patient cohort are the first molecular events that are associated with a 17p deletion which is a strong adverse prognostic marker in MM. However, to further analyze the potential role of rare RTKs as adverse prognostic markers as well as predisposing risk factors further studies have to be conducted. Rare SNPs that were detected in the six RTKs in the patient cohort of the DSMM XII have to be further analyzed to study their influence on patient survival and response to therapy. Moreover, an amplicon sequencing approach of an even larger patient cohort together with an independent healthy control cohort is needed to strengthen the hypothesis that these rare RTK SNPs are actual MM risk factors and not only in patients treated with distinct therapeutics.

The IGF1R-KD as well as IGF1R overexpression cell lines established in this work can be used as a model system to study the influence of drugs on cells with specific mutations. Due to the stable overexpression, these cell lines can also be used to co-express RTKs with other mutations to study the role of RTK cooperation in MM. Moreover, the established CRSIPR/Cas9 and Sleeping Beauty methods can be adjusted to study the functional effect of other mutations in the hard-to-transfect MM cells. The MM cell models can be used in future drug screens to analyze if a specific drug has the desired effect on tumor cells with distinct mutations. This might be an additional step into the direction of personalized cancer care.

Moreover, the cooperation of PYK2 and IGF1R should be subjected to further investigations. The co-localization and cooperation of both molecules has been shown in urothelial cancer cells, however, not yet in MM. The obtained results which point to a cooperation between PYK2 and IGF1R in MM promote further investigation including dual inhibitor studies.

First functional analyses indicate an activating role of the IGF1R N1129S mutation, however, further studies of both mutants together with the IGF1R WT have to be conducted to confirm these results. Kinase activity assays of isolated IGF1R WT, IGF1R D1146N and IGF1R N1129S might help to further elucidate the influence of the mutations on IGF1R activity. Additionally, further cell proliferation assays of IGF1 stimulated cells have to be performed, to analyze the influence of the IGF1R mutations in IGF1-rich environments such as the bone marrow. For this

purpose 3D cell culture models as well as co-culture experiments with bone marrow stromal cells might be of particular interest, to study the influence of the detected mutations on cells in the bone marrow microenvironment.

The ultimate aim should be the identification of a subset of MM patient who might respond to IGF1R inhibition.

10 Bibliography

1. Swerdlow, S.H., et al., *WHO Classification of Tumours of Haematopoietic and Lymphoid Tissues* 4th ed. 2008, Lyon: International Agency for Research on Cancer (IARC).
2. Rollig, C., S. Knop, and M. Bornhauser, *Multiple myeloma.* Lancet, 2015. **385**(9983): p. 2197-208.
3. Kyle, R.A., et al., *Review of 1027 patients with newly diagnosed multiple myeloma.* Mayo Clin Proc, 2003. **78**(1): p. 21-33.
4. Collins, C.D., *Problems monitoring response in multiple myeloma.* Cancer Imaging, 2005. **5 Spec No A**: p. S119-26.
5. Fitzmaurice, C., et al., *Global, Regional, and National Cancer Incidence, Mortality, Years of Life Lost, Years Lived With Disability, and Disability-Adjusted Life-years for 32 Cancer Groups, 1990 to 2015: A Systematic Analysis for the Global Burden of Disease Study.* JAMA Oncol, 2017. **3**(4): p. 524-548.
6. Landgren, O., et al., *Risk of monoclonal gammopathy of undetermined significance (MGUS) and subsequent multiple myeloma among African American and white veterans in the United States.* Blood, 2006. **107**(3): p. 904-6.
7. Kumar, S.K., et al., *Continued improvement in survival in multiple myeloma: changes in early mortality and outcomes in older patients.* Leukemia, 2014. **28**(5): p. 1122-8.
8. Greipp, P.R., et al., *International staging system for multiple myeloma.* J Clin Oncol, 2005. **23**(15): p. 3412-20.
9. Gonzalez, D., et al., *Immunoglobulin gene rearrangements and the pathogenesis of multiple myeloma.* Blood, 2007. **110**(9): p. 3112-21.
10. Joao, C., et al., *Long-term survival in multiple myeloma.* Clin Case Rep, 2014. **2**(5): p. 173-9.
11. Rajkumar, S.V., *Multiple myeloma: 2016 update on diagnosis, risk-stratification, and management.* Am J Hematol, 2016. **91**(7): p. 719-34.
12. Russell, S.J. and S.V. Rajkumar, *Multiple myeloma and the road to personalised medicine.* Lancet Oncol, 2011. **12**(7): p. 617-9.
13. Murphy, K. and C. Weaver, *Janeway's immunobiology*. 9th edition. ed. 2016, New York, NY: Garland Science/Taylor & Francis Group, LLC. xx, 904 pages.
14. Pieper, K., B. Grimbacher, and H. Eibel, *B-cell biology and development.* J Allergy Clin Immunol, 2013. **131**(4): p. 959-71.
15. Eibel, H., et al., *B cell biology: an overview.* Curr Allergy Asthma Rep, 2014. **14**(5): p. 434.
16. Küppers, R., *Mechanisms of B-cell lymphoma pathogenesis.* Nat Rev Cancer, 2005. **5**(4): p. 251-62.
17. Morgan, G.J., B.A. Walker, and F.E. Davies, *The genetic architecture of multiple myeloma.* Nat Rev Cancer, 2012. **12**(5): p. 335-48.
18. Prideaux, S.M., E. Conway O'Brien, and T.J. Chevassut, *The genetic architecture of multiple myeloma.* Adv Hematol, 2014. **2014**: p. 864058.
19. Palumbo, A. and K. Anderson, *Multiple myeloma.* N Engl J Med, 2011. **364**(11): p. 1046-60.
20. Kyle, R.A., et al., *Clinical course and prognosis of smoldering (asymptomatic) multiple myeloma.* N Engl J Med, 2007. **356**(25): p. 2582-90.
21. Kyle, R.A., et al., *Monoclonal gammopathy of undetermined significance (MGUS) and smoldering (asymptomatic) multiple myeloma: IMWG consensus perspectives risk factors for progression and guidelines for monitoring and management.* Leukemia, 2010. **24**(6): p. 1121-7.
22. Manier, S., et al., *Genomic complexity of multiple myeloma and its clinical implications.* Nat Rev Clin Oncol, 2017. **14**(2): p. 100-113.
23. Smadja, N.V., et al., *Hypodiploidy is a major prognostic factor in multiple myeloma.* Blood, 2001. **98**(7): p. 2229-38.
24. Chng, W.J., et al., *Molecular dissection of hyperdiploid multiple myeloma by gene expression profiling.* Cancer Res, 2007. **67**(7): p. 2982-9.

25. Avet-Loiseau, H., et al., *Rearrangements of the c-myc oncogene are present in 15% of primary human multiple myeloma tumors.* Blood, 2001. **98**(10): p. 3082-6.
26. Affer, M., et al., *Promiscuous MYC locus rearrangements hijack enhancers but mostly super-enhancers to dysregulate MYC expression in multiple myeloma.* Leukemia, 2014. **28**(8): p. 1725-35.
27. Walker, B.A., et al., *Translocations at 8q24 juxtapose MYC with genes that harbor superenhancers resulting in overexpression and poor prognosis in myeloma patients.* Blood Cancer J, 2014. **4**: p. e191.
28. Walker, B.A., et al., *A compendium of myeloma-associated chromosomal copy number abnormalities and their prognostic value.* Blood, 2010. **116**(15): p. e56-65.
29. Shaughnessy, J., *Amplification and overexpression of CKS1B at chromosome band 1q21 is associated with reduced levels of p27Kip1 and an aggressive clinical course in multiple myeloma.* Hematology, 2005. **10 Suppl 1**: p. 117-26.
30. Boyd, K.D., et al., *Mapping of chromosome 1p deletions in myeloma identifies FAM46C at 1p12 and CDKN2C at 1p32.3 as being genes in regions associated with adverse survival.* Clin Cancer Res, 2011. **17**(24): p. 7776-84.
31. Fonseca, R., et al., *Deletions of chromosome 13 in multiple myeloma identified by interphase FISH usually denote large deletions of the q arm or monosomy.* Leukemia, 2001. **15**(6): p. 981-6.
32. Fonseca, R., et al., *Clinical and biologic implications of recurrent genomic aberrations in myeloma.* Blood, 2003. **101**(11): p. 4569-75.
33. Tiedemann, R.E., et al., *Genetic aberrations and survival in plasma cell leukemia.* Leukemia, 2008. **22**(5): p. 1044-52.
34. Lode, L., et al., *Mutations in TP53 are exclusively associated with del(17p) in multiple myeloma.* Haematologica, 2010. **95**(11): p. 1973-6.
35. Walker, B.A., et al., *Mutational Spectrum, Copy Number Changes, and Outcome: Results of a Sequencing Study of Patients With Newly Diagnosed Myeloma.* J Clin Oncol, 2015. **33**(33): p. 3911-20.
36. Chapman, M.A., et al., *Initial genome sequencing and analysis of multiple myeloma.* Nature, 2011. **471**(7339): p. 467-72.
37. Lohr, J.G., et al., *Widespread genetic heterogeneity in multiple myeloma: implications for targeted therapy.* Cancer Cell, 2014. **25**(1): p. 91-101.
38. Bolli, N., et al., *Heterogeneity of genomic evolution and mutational profiles in multiple myeloma.* Nat Commun, 2014. **5**: p. 2997.
39. Leich, E., et al., *Multiple myeloma is affected by multiple and heterogeneous somatic mutations in adhesion- and receptor tyrosine kinase signaling molecules.* Blood Cancer J, 2013. **3**: p. e102.
40. Weissbach, S., et al., *The molecular spectrum and clinical impact of DIS3 mutations in multiple myeloma.* Br J Haematol, 2015. **169**(1): p. 57-70.
41. Walker, B.A., et al., *Aberrant global methylation patterns affect the molecular pathogenesis and prognosis of multiple myeloma.* Blood, 2011. **117**(2): p. 553-62.
42. Robinson, D.R., Y.M. Wu, and S.F. Lin, *The protein tyrosine kinase family of the human genome.* Oncogene, 2000. **19**(49): p. 5548-57.
43. Schlessinger, J., *Receptor tyrosine kinases: legacy of the first two decades.* Cold Spring Harb Perspect Biol, 2014. **6**(3).
44. Blume-Jensen, P. and T. Hunter, *Oncogenic kinase signalling.* Nature, 2001. **411**(6835): p. 355-65.
45. Ullrich, A. and J. Schlessinger, *Signal transduction by receptors with tyrosine kinase activity.* Cell, 1990. **61**(2): p. 203-12.
46. Lemmon, M.A. and J. Schlessinger, *Cell signaling by receptor tyrosine kinases.* Cell, 2010. **141**(7): p. 1117-34.
47. Schlessinger, J. and A. Ullrich, *Growth factor signaling by receptor tyrosine kinases.* Neuron, 1992. **9**(3): p. 383-91.

48. Hubbard, S.R. and J.H. Till, *Protein tyrosine kinase structure and function.* Annu Rev Biochem, 2000. **69**: p. 373-98.
49. Ward, C.W., et al., *The insulin and EGF receptor structures: new insights into ligand-induced receptor activation.* Trends Biochem Sci, 2007. **32**(3): p. 129-37.
50. Griffith, J., et al., *The structural basis for autoinhibition of FLT3 by the juxtamembrane domain.* Mol Cell, 2004. **13**(2): p. 169-78.
51. Schlessinger, J. and M.A. Lemmon, *SH2 and PTB domains in tyrosine kinase signaling.* Sci STKE, 2003. **2003**(191): p. RE12.
52. Regad, T., *Targeting RTK Signaling Pathways in Cancer.* Cancers (Basel), 2015. **7**(3): p. 1758-84.
53. Krause, D.S. and R.A. Van Etten, *Tyrosine kinases as targets for cancer therapy.* N Engl J Med, 2005. **353**(2): p. 172-87.
54. Hanahan, D. and R.A. Weinberg, *Hallmarks of cancer: the next generation.* Cell, 2011. **144**(5): p. 646-74.
55. Haglund, K., T.E. Rusten, and H. Stenmark, *Aberrant receptor signaling and trafficking as mechanisms in oncogenesis.* Crit Rev Oncog, 2007. **13**(1): p. 39-74.
56. Abella, J.V. and M. Park, *Breakdown of endocytosis in the oncogenic activation of receptor tyrosine kinases.* Am J Physiol Endocrinol Metab, 2009. **296**(5): p. E973-84.
57. Tsai, C.J. and R. Nussinov, *The molecular basis of targeting protein kinases in cancer therapeutics.* Semin Cancer Biol, 2013. **23**(4): p. 235-42.
58. Lynch, T.J., et al., *Activating mutations in the epidermal growth factor receptor underlying responsiveness of non-small-cell lung cancer to gefitinib.* N Engl J Med, 2004. **350**(21): p. 2129-39.
59. Tang, C.K., et al., *Epidermal growth factor receptor vIII enhances tumorigenicity in human breast cancer.* Cancer Res, 2000. **60**(11): p. 3081-7.
60. Jhiang, S.M., *The RET proto-oncogene in human cancers.* Oncogene, 2000. **19**(49): p. 5590-7.
61. Smith, K.M., R. Yacobi, and R.A. Van Etten, *Autoinhibition of Bcr-Abl through its SH3 domain.* Mol Cell, 2003. **12**(1): p. 27-37.
62. Watanabe, D., et al., *Suppressor of cytokine signalling-1 gene silencing in acute myeloid leukaemia and human haematopoietic cell lines.* Br J Haematol, 2004. **126**(5): p. 726-35.
63. Chesi, M., et al., *The t(4;14) translocation in myeloma dysregulates both FGFR3 and a novel gene, MMSET, resulting in IgH/MMSET hybrid transcripts.* Blood, 1998. **92**(9): p. 3025-34.
64. Chesi, M., et al., *Frequent translocation t(4;14)(p16.3;q32.3) in multiple myeloma is associated with increased expression and activating mutations of fibroblast growth factor receptor 3.* Nat Genet, 1997. **16**(3): p. 260-4.
65. Chesi, M., et al., *Activated fibroblast growth factor receptor 3 is an oncogene that contributes to tumor progression in multiple myeloma.* Blood, 2001. **97**(3): p. 729-36.
66. Derksen, P.W., et al., *The hepatocyte growth factor/Met pathway controls proliferation and apoptosis in multiple myeloma.* Leukemia, 2003. **17**(4): p. 764-74.
67. Lin, B., et al., *The vascular endothelial growth factor receptor tyrosine kinase inhibitor PTK787/ZK222584 inhibits growth and migration of multiple myeloma cells in the bone marrow microenvironment.* Cancer Res, 2002. **62**(17): p. 5019-26.
68. Bataille, R., et al., *CD221 (IGF-1R) is aberrantly expressed in multiple myeloma, in relation to disease severity.* Haematologica, 2005. **90**(5): p. 706-7.
69. Powell-Braxton, L., et al., *IGF-I is required for normal embryonic growth in mice.* Genes Dev, 1993. **7**(12B): p. 2609-17.
70. Ullrich, A., et al., *Insulin-like growth factor I receptor primary structure: comparison with insulin receptor suggests structural determinants that define functional specificity.* EMBO J, 1986. **5**(10): p. 2503-12.
71. Abbott, A.M., et al., *Insulin-like growth factor I receptor gene structure.* J Biol Chem, 1992. **267**(15): p. 10759-63.

72. Massague, J. and M.P. Czech, *The subunit structures of two distinct receptors for insulin-like growth factors I and II and their relationship to the insulin receptor.* J Biol Chem, 1982. **257**(9): p. 5038-45.
73. Adams, T.E., et al., *Structure and function of the type 1 insulin-like growth factor receptor.* Cell Mol Life Sci, 2000. **57**(7): p. 1050-93.
74. Chitnis, M.M., et al., *The type 1 insulin-like growth factor receptor pathway.* Clin Cancer Res, 2008. **14**(20): p. 6364-70.
75. Baserga, R., F. Peruzzi, and K. Reiss, *The IGF-1 receptor in cancer biology.* Int J Cancer, 2003. **107**(6): p. 873-7.
76. Tognon, C.E. and P.H. Sorensen, *Targeting the insulin-like growth factor 1 receptor (IGF1R) signaling pathway for cancer therapy.* Expert Opin Ther Targets, 2012. **16**(1): p. 33-48.
77. McCubrey, J.A., et al., *Roles of the Raf/MEK/ERK pathway in cell growth, malignant transformation and drug resistance.* Biochim Biophys Acta, 2007. **1773**(8): p. 1263-84.
78. De Luca, A., et al., *The RAS/RAF/MEK/ERK and the PI3K/AKT signalling pathways: role in cancer pathogenesis and implications for therapeutic approaches.* Expert Opin Ther Targets, 2012. **16 Suppl 2**: p. S17-27.
79. Arcaro, A., *Targeting the insulin-like growth factor-1 receptor in human cancer.* Front Pharmacol, 2013. **4**: p. 30.
80. Kasprzak, A., et al., *Insulin-like growth factor (IGF) axis in cancerogenesis.* Mutat Res, 2017. **772**: p. 78-104.
81. Vilmar, A., et al., *Insulin-like growth factor receptor 1 mRNA expression as a prognostic marker in advanced non-small cell lung cancer.* Anticancer Res, 2014. **34**(6): p. 2991-6.
82. Yeo, C.D., et al., *Expression of insulin-like growth factor 1 receptor (IGF-1R) predicts poor responses to epidermal growth factor receptor (EGFR) tyrosine kinase inhibitors in non-small cell lung cancer patients harboring activating EGFR mutations.* Lung Cancer, 2015. **87**(3): p. 311-7.
83. Bahnassy, A., et al., *Molecular biomarkers for prediction of response to treatment and survival in triple negative breast cancer patients from Egypt.* Exp Mol Pathol, 2015. **99**(2): p. 303-11.
84. Shimizu, C., et al., *Expression of insulin-like growth factor 1 receptor in primary breast cancer: immunohistochemical analysis.* Hum Pathol, 2004. **35**(12): p. 1537-42.
85. Sun, W.Y., et al., *Insulin-like growth factor 1 receptor expression in breast cancer tissue and mammographic density.* Mol Clin Oncol, 2015. **3**(3): p. 572-580.
86. Jones, R.A., et al., *Transgenic overexpression of IGF-IR disrupts mammary ductal morphogenesis and induces tumor formation.* Oncogene, 2007. **26**(11): p. 1636-44.
87. Wang, Z., et al., *Increased insulin-like growth factor 1 receptor (IGF1R) expression in small cell lung cancer and the effect of inhibition of IGF1R expression by RNAi on growth of human small cell lung cancer NCI-H446 cell.* Growth Factors, 2015. **33**(5-6): p. 337-46.
88. Heidegger, I., et al., *Oncogenic functions of IGF1R and INSR in prostate cancer include enhanced tumor growth, cell migration and angiogenesis.* Oncotarget, 2014. **5**(9): p. 2723-35.
89. Genua, M., et al., *Proline-rich tyrosine kinase 2 (Pyk2) regulates IGF-I-induced cell motility and invasion of urothelial carcinoma cells.* PLoS One, 2012. **7**(6): p. e40148.
90. Lahm, H., et al., *Growth regulation and co-stimulation of human colorectal cancer cell lines by insulin-like growth factor I, II and transforming growth factor alpha.* Br J Cancer, 1992. **65**(3): p. 341-6.
91. Cao, Y., et al., *Prediagnostic plasma IGFBP-1, IGF-1 and risk of prostate cancer.* Int J Cancer, 2015. **136**(10): p. 2418-26.
92. Guo, Q., et al., *IGF-I CA19 repeat polymorphisms and cancer risk: a meta-analysis.* Int J Clin Exp Med, 2015. **8**(11): p. 20596-602.
93. Qian, B., et al., *Genotypes and phenotypes of IGF-I and IGFBP-3 in breast tumors among Chinese women.* Breast Cancer Res Treat, 2011. **130**(1): p. 217-26.

94. Winder, T., et al., *Insulin-like growth factor receptor polymorphism defines clinical outcome in estrogen receptor-positive breast cancer patients treated with tamoxifen.* Pharmacogenomics J, 2014. **14**(1): p. 28-34.
95. Huang, X.P., W.H. Zhou, and Y.F. Zhang, *Genetic variations in the IGF-IGFR-IGFBP axis confer susceptibility to lung and esophageal cancer.* Genet Mol Res, 2014. **13**(1): p. 2107-19.
96. Bieghs, L., et al., *The insulin-like growth factor system in multiple myeloma: diagnostic and therapeutic potential.* Oncotarget, 2016. **7**(30): p. 48732-48752.
97. Asosingh, K., et al., *In vivo induction of insulin-like growth factor-I receptor and CD44v6 confers homing and adhesion to murine multiple myeloma cells.* Cancer Res, 2000. **60**(11): p. 3096-104.
98. Qiang, Y.W., et al., *Insulin-like growth factor I induces migration and invasion of human multiple myeloma cells.* Blood, 2004. **103**(1): p. 301-8.
99. Tai, Y.T., et al., *Insulin-like growth factor-1 induces adhesion and migration in human multiple myeloma cells via activation of beta1-integrin and phosphatidylinositol 3'-kinase/AKT signaling.* Cancer Res, 2003. **63**(18): p. 5850-8.
100. Georgii-Hemming, P., et al., *Insulin-like growth factor I is a growth and survival factor in human multiple myeloma cell lines.* Blood, 1996. **88**(6): p. 2250-8.
101. Ferlin, M., et al., *Insulin-like growth factor induces the survival and proliferation of myeloma cells through an interleukin-6-independent transduction pathway.* Br J Haematol, 2000. **111**(2): p. 626-34.
102. Scarfo, L. and P. Ghia, *Reprogramming cell death: BCL2 family inhibition in hematological malignancies.* Immunol Lett, 2013. **155**(1-2): p. 36-9.
103. Huo, J., et al., *Fas apoptosis inhibitory molecule is upregulated by IGF-1 signaling and modulates Akt activation and IRF4 expression in multiple myeloma.* Leukemia, 2013. **27**(5): p. 1165-71.
104. Mitsiades, C.S., et al., *Inhibition of the insulin-like growth factor receptor-1 tyrosine kinase activity as a therapeutic strategy for multiple myeloma, other hematologic malignancies, and solid tumors.* Cancer Cell, 2004. **5**(3): p. 221-30.
105. Rajkumar, S.V., et al., *Prognostic value of bone marrow angiogenesis in multiple myeloma.* Clin Cancer Res, 2000. **6**(8): p. 3111-6.
106. Kuhn, D.J., et al., *Targeting the insulin-like growth factor-1 receptor to overcome bortezomib resistance in preclinical models of multiple myeloma.* Blood, 2012. **120**(16): p. 3260-70.
107. Xu, F., et al., *Multiple myeloma cells are protected against dexamethasone-induced apoptosis by insulin-like growth factors.* Br J Haematol, 1997. **97**(2): p. 429-40.
108. Chng, W.J., A. Gualberto, and R. Fonseca, *IGF-1R is overexpressed in poor-prognostic subtypes of multiple myeloma.* Leukemia, 2006. **20**(1): p. 174-6.
109. Cong, L., et al., *Multiplex genome engineering using CRISPR/Cas systems.* Science, 2013. **339**(6121): p. 819-23.
110. Barrangou, R., et al., *CRISPR provides acquired resistance against viruses in prokaryotes.* Science, 2007. **315**(5819): p. 1709-12.
111. Garneau, J.E., et al., *The CRISPR/Cas bacterial immune system cleaves bacteriophage and plasmid DNA.* Nature, 2010. **468**(7320): p. 67-71.
112. Deltcheva, E., et al., *CRISPR RNA maturation by trans-encoded small RNA and host factor RNase III.* Nature, 2011. **471**(7340): p. 602-7.
113. Jinek, M., et al., *A programmable dual-RNA-guided DNA endonuclease in adaptive bacterial immunity.* Science, 2012. **337**(6096): p. 816-21.
114. Gasiunas, G., et al., *Cas9-crRNA ribonucleoprotein complex mediates specific DNA cleavage for adaptive immunity in bacteria.* Proc Natl Acad Sci U S A, 2012. **109**(39): p. E2579-86.
115. Mojica, F.J., et al., *Short motif sequences determine the targets of the prokaryotic CRISPR defence system.* Microbiology, 2009. **155**(Pt 3): p. 733-40.
116. Doudna, J.A. and E. Charpentier, *Genome editing. The new frontier of genome engineering with CRISPR-Cas9.* Science, 2014. **346**(6213): p. 1258096.

117. Mali, P., et al., *RNA-guided human genome engineering via Cas9.* Science, 2013. **339**(6121): p. 823-6.
118. Wu, Y., et al., *Correction of a genetic disease in mouse via use of CRISPR-Cas9.* Cell Stem Cell, 2013. **13**(6): p. 659-62.
119. Schwank, G., et al., *Functional repair of CFTR by CRISPR/Cas9 in intestinal stem cell organoids of cystic fibrosis patients.* Cell Stem Cell, 2013. **13**(6): p. 653-8.
120. Shalem, O., N.E. Sanjana, and F. Zhang, *High-throughput functional genomics using CRISPR-Cas9.* Nat Rev Genet, 2015. **16**(5): p. 299-311.
121. Shalem, O., et al., *Genome-scale CRISPR-Cas9 knockout screening in human cells.* Science, 2014. **343**(6166): p. 84-87.
122. Charpentier, E. and J.A. Doudna, *Biotechnology: Rewriting a genome.* Nature, 2013. **495**(7439): p. 50-1.
123. Kropff, M., et al., *DSMM XI study: dose definition for intravenous cyclophosphamide in combination with bortezomib/dexamethasone for remission induction in patients with newly diagnosed myeloma.* Ann Hematol, 2009. **88**(11): p. 1125-30.
124. Keppler, S., et al., *Rare SNPs in receptor tyrosine kinases are negative outcome predictors in multiple myeloma.* Oncotarget, 2016. **7**(25): p. 38762-38774.
125. Knop, S., et al., *Lenalidomide, adriamycin, dexamethasone (RAD) for induction followed by stem-cell transplant in newly diagnosed myeloma.* Leukemia, 2017.
126. Kronke, J., et al., *IKZF1 expression is a prognostic marker in newly diagnosed standard-risk multiple myeloma treated with lenalidomide and intensive chemotherapy: a study of the German Myeloma Study Group (DSMM).* Leukemia, 2017.
127. Pischimarov, J., *Bioinformatische Methoden zur Identifizierung und Klassifizierung somatischer Mutationen in hämatologischen Erkrankungen*, in *Institute for Pathology*. 2016, University of Würzburg: Würzburg.
128. van der Burg, M., et al., *Standardization of DNA isolation from low cell numbers for chimerism analysis by PCR of short tandem repeats.* Leukemia, 2011. **25**(9): p. 1467-70.
129. Waterhouse, A.M., et al., *Jalview Version 2--a multiple sequence alignment editor and analysis workbench.* Bioinformatics, 2009. **25**(9): p. 1189-91.
130. Schwarzfischer, M., *Functional characterization of mutations affecting the recceptor tyrosine kinase domain of mIGF1R in multiple myeloma*, in *Institute for Pathology*. 2017, University of Würzburg: Würzburg. p. 49.
131. LeRoith, D. and C.T. Roberts, Jr., *The insulin-like growth factor system and cancer.* Cancer Lett, 2003. **195**(2): p. 127-37.
132. Kulik, G., A. Klippel, and M.J. Weber, *Antiapoptotic signalling by the insulin-like growth factor I receptor, phosphatidylinositol 3-kinase, and Akt.* Mol Cell Biol, 1997. **17**(3): p. 1595-606.
133. Parrizas, M., A.R. Saltiel, and D. LeRoith, *Insulin-like growth factor 1 inhibits apoptosis using the phosphatidylinositol 3'-kinase and mitogen-activated protein kinase pathways.* J Biol Chem, 1997. **272**(1): p. 154-61.
134. Steinbrunn, T., et al., *Efficient transient transfection of human multiple myeloma cells by electroporation--an appraisal.* PLoS One, 2014. **9**(6): p. e97443.
135. Brito, J.L., et al., *Streptolysin-O reversible permeabilisation is an effective method to transfect siRNAs into myeloma cells.* J Immunol Methods, 2008. **333**(1-2): p. 147-55.
136. Hideshima, T., et al., *Understanding multiple myeloma pathogenesis in the bone marrow to identify new therapeutic targets.* Nat Rev Cancer, 2007. **7**(8): p. 585-98.
137. Schlessinger, J., *Cell signaling by receptor tyrosine kinases.* Cell, 2000. **103**(2): p. 211-25.
138. Zöllinger, A., et al., *Combined functional and molecular analysis of tumor cell signaling defines 2 distinct myeloma subgroups: Akt-dependent and Akt-independent multiple myeloma.* Blood, 2008. **112**(8): p. 3403-11.
139. Bommert, K., R.C. Bargou, and T. Stühmer, *Signalling and survival pathways in multiple myeloma.* Eur J Cancer, 2006. **42**(11): p. 1574-80.

140. Xu, J., et al., *Molecular signaling in multiple myeloma: association of RAS/RAF mutations and MEK/ERK pathway activation.* Oncogenesis, 2017. **6**(5): p. e337.
141. Steinbrunn, T., et al., *Mutated RAS and constitutively activated Akt delineate distinct oncogenic pathways, which independently contribute to multiple myeloma cell survival.* Blood, 2011. **117**(6): p. 1998-2004.
142. Hofmann, C., et al., *PI3K-dependent multiple myeloma cell survival is mediated by the PIK3CA isoform.* Br J Haematol, 2014. **166**(4): p. 529-39.
143. Steinbrunn, T., et al., *Combined targeting of MEK/MAPK and PI3K/Akt signalling in multiple myeloma.* Br J Haematol, 2012. **159**(4): p. 430-40.
144. Siegelin, M.D. and A.C. Borczuk, *Epidermal growth factor receptor mutations in lung adenocarcinoma.* Lab Invest, 2014. **94**(2): p. 129-37.
145. Davies, F.E., et al., *High-producer haplotypes of tumor necrosis factor alpha and lymphotoxin alpha are associated with an increased risk of myeloma and have an improved progression-free survival after treatment.* J Clin Oncol, 2000. **18**(15): p. 2843-51.
146. Neben, K., et al., *Polymorphisms of the tumor necrosis factor-alpha gene promoter predict for outcome after thalidomide therapy in relapsed and refractory multiple myeloma.* Blood, 2002. **100**(6): p. 2263-5.
147. Varga, G., et al., *Proteasome Subunit Beta Type 1 P11A Polymorphism Is a New Prognostic Marker in Multiple Myeloma.* Clin Lymphoma Myeloma Leuk, 2017.
148. Poi, M.J., et al., *Polymorphism in ANRIL is associated with relapse in patients with multiple myeloma after autologous stem cell transplant.* Mol Carcinog, 2017. **56**(7): p. 1722-1732.
149. Lodish, H.F., *Molecular cell biology*. 4th ed. 2000, New York: W.H. Freeman. xxxvi, 1084, G-17, I-36 p.
150. Datta, R., et al., *Signal sequence mutation in autosomal dominant form of hypoparathyroidism induces apoptosis that is corrected by a chemical chaperone.* Proc Natl Acad Sci U S A, 2007. **104**(50): p. 19989-94.
151. Dunning, A.M., et al., *A transforming growth factorbeta1 signal peptide variant increases secretion in vitro and is associated with increased incidence of invasive breast cancer.* Cancer Res, 2003. **63**(10): p. 2610-5.
152. Choudhary, C., et al., *Mislocalized activation of oncogenic RTKs switches downstream signaling outcomes.* Mol Cell, 2009. **36**(2): p. 326-39.
153. Köthe, S., et al., *Features of Ras activation by a mislocalized oncogenic tyrosine kinase: FLT3 ITD signals through K-Ras at the plasma membrane of acute myeloid leukemia cells.* J Cell Sci, 2013. **126**(Pt 20): p. 4746-55.
154. Watson, F.L., et al., *TrkA glycosylation regulates receptor localization and activity.* J Neurobiol, 1999. **39**(2): p. 323-36.
155. Frederick, L., et al., *Diversity and frequency of epidermal growth factor receptor mutations in human glioblastomas.* Cancer Res, 2000. **60**(5): p. 1383-7.
156. Batra, S.K., et al., *Epidermal growth factor ligand-independent, unregulated, cell-transforming potential of a naturally occurring human mutant EGFRvIII gene.* Cell Growth Differ, 1995. **6**(10): p. 1251-9.
157. Lee, J.C., et al., *Epidermal growth factor receptor activation in glioblastoma through novel missense mutations in the extracellular domain.* PLoS Med, 2006. **3**(12): p. e485.
158. Bessman, N.J., et al., *Complex relationship between ligand binding and dimerization in the epidermal growth factor receptor.* Cell Rep, 2014. **9**(4): p. 1306-17.
159. Gilmore, J.L., R.M. Gallo, and D.J. Riese, 2nd, *The epidermal growth factor receptor (EGFR)-S442F mutant displays increased affinity for neuregulin-2beta and agonist-independent coupling with downstream signalling events.* Biochem J, 2006. **396**(1): p. 79-88.
160. Charbonneau, B., et al., *CXCR5 polymorphisms in non-Hodgkin lymphoma risk and prognosis.* Cancer Immunol Immunother, 2013. **62**(9): p. 1475-84.
161. Michailidou, K., et al., *Large-scale genotyping identifies 41 new loci associated with breast cancer risk.* Nat Genet, 2013. **45**(4): p. 353-61, 361e1-2.

162. Eeles, R.A., et al., *Identification of 23 new prostate cancer susceptibility loci using the iCOGS custom genotyping array.* Nat Genet, 2013. **45**(4): p. 385-91, 391e1-2.
163. Morgan, G.J., et al., *Inherited genetic susceptibility to multiple myeloma.* Leukemia, 2014. **28**(3): p. 518-24.
164. Mancuso, N., et al., *The contribution of rare variation to prostate cancer heritability.* Nat Genet, 2016. **48**(1): p. 30-5.
165. Grin, B., et al., *A rare 8q24 single nucleotide polymorphism (SNP) predisposes North American men to prostate cancer and possibly more aggressive disease.* BJU Int, 2015. **115**(1): p. 101-5.
166. Fearnhead, N.S., et al., *Multiple rare variants in different genes account for multifactorial inherited susceptibility to colorectal adenomas.* Proc Natl Acad Sci U S A, 2004. **101**(45): p. 15992-7.
167. Lu, C., et al., *Patterns and functional implications of rare germline variants across 12 cancer types.* Nat Commun, 2015. **6**: p. 10086.
168. Craddock, B.P. and W.T. Miller, *Effects of somatic mutations in the C-terminus of insulin-like growth factor 1 receptor on activity and signaling.* J Signal Transduct, 2012. **2012**: p. 804801.
169. Chen, H.X. and E. Sharon, *IGF-1R as an anti-cancer target--trials and tribulations.* Chin J Cancer, 2013. **32**(5): p. 242-52.
170. Wallborn, T., et al., *A heterozygous mutation of the insulin-like growth factor-I receptor causes retention of the nascent protein in the endoplasmic reticulum and results in intrauterine and postnatal growth retardation.* J Clin Endocrinol Metab, 2010. **95**(5): p. 2316-24.
171. Juanes, M., et al., *Three novel IGF1R mutations in microcephalic patients with prenatal and postnatal growth impairment.* Clin Endocrinol (Oxf), 2015. **82**(5): p. 704-11.
172. Strömberg, T., et al., *IGF-1 receptor tyrosine kinase inhibition by the cyclolignan PPP induces G2/M-phase accumulation and apoptosis in multiple myeloma cells.* Blood, 2006. **107**(2): p. 669-78.
173. Buck, E., et al., *Feedback mechanisms promote cooperativity for small molecule inhibitors of epidermal and insulin-like growth factor receptors.* Cancer Res, 2008. **68**(20): p. 8322-32.
174. Cagnol, S. and J.C. Chambard, *ERK and cell death: mechanisms of ERK-induced cell death--apoptosis, autophagy and senescence.* FEBS J, 2010. **277**(1): p. 2-21.
175. Belfiore, A., *The role of insulin receptor isoforms and hybrid insulin/IGF-I receptors in human cancer.* Curr Pharm Des, 2007. **13**(7): p. 671-86.
176. Aleksic, T., et al., *Type 1 insulin-like growth factor receptor translocates to the nucleus of human tumor cells.* Cancer Res, 2010. **70**(16): p. 6412-9.
177. Sarfstein, R., et al., *Insulin-like growth factor-I receptor (IGF-IR) translocates to nucleus and autoregulates IGF-IR gene expression in breast cancer cells.* J Biol Chem, 2012. **287**(4): p. 2766-76.
178. Warsito, D., et al., *Nuclear IGF1R is a transcriptional co-activator of LEF1/TCF.* EMBO Rep, 2012. **13**(3): p. 244-50.
179. Lipinski, C.A. and J.C. Loftus, *Targeting Pyk2 for therapeutic intervention.* Expert Opin Ther Targets, 2010. **14**(1): p. 95-108.
180. Kuang, B.H., et al., *Proline-rich tyrosine kinase 2 and its phosphorylated form pY881 are novel prognostic markers for non-small-cell lung cancer progression and patients' overall survival.* Br J Cancer, 2013. **109**(5): p. 1252-63.
181. Zhang, Y., et al., *Pyk2 promotes tumor progression in multiple myeloma.* Blood, 2014. **124**(17): p. 2675-86.

11 Appendix

11.1 Clinical features of the DSMM XII patient cohort

Supplementary table 1: Clinical data of MM patients of the DSMM XII trial

Patient	Sex	HC	LC	RTK	gain 1q	gain 9q	del 13q	del 17p	t(4;14)	t(11;14)	t(14;16)
P1	m		L	-	-	-	-	-	-	-	-
P2	m		-	-			-	-	-		-
P3	w		K	**rare SNP**	+	+	-	-	-	-	-
P4	m		K	-	-	+	-	-	-	-	-
P5	m		-	-			+	-	-		-
P6	m		-	-			-	-	-		-
P7	w		L	-	+	-	-	-	+	-	-
P8	w		-	-			-	-	-	-	-
P9	m		K	-	-	-	-	-	-	-	-
P10	m		K	-	-	+	-	-	-	-	-
P11	w		-	-	+	-	+	-	+	-	-
P12	m		L	-	-	+	-	-	-	-	-
P13	w		L	-		+					+
P14	m		-	-	+	-	+	-	+	-	-
P15	m		-	-	-	-	-	-	-	+	-
P16	w		L	-	+	-	+	-	+	-	-
P17	m		K	-	-	+	-	-	-	-	-
P18	m	IgG	L	**rare SNP**	-	+	-	-	-	-	-
P19	m		K	-	+	+	-	-	-	-	-
P20	m		K	-			-	-	-	-	-
P21	m		L	-	-	-	-	-	-	-	-
P22	m		L	-			-	-	-		
P23	m		K	-	-	+	+	-	-	-	-
P24	w		L	-	-	-	+	-	-	-	-
P25	m		K	-	+	+	-	-	+	-	-
P26	m		-	-	-	-	-	-	-	-	-
P27	m		-	-	-	+	+	-	-	-	-
P28	m		-	-	-	-	-	-	-	-	-
P29	m		L	-	-	-	-	-	+	-	-
P30	m		K	-	-	+	-	-	-	-	-
P31	m		K	-			-	-	-		-
P32	m		L	-	+	+	-	-	-	-	-
P33	w		K	-							
P34	w		L	-	+	-	+	-	-	-	+
P35	m		K	-	+	+	+	-	-	-	-
P36	m		K	**rare SNP**	-	-	-	-	-	-	-
P37	m		K	-	-	+	+	-	-	-	-
P38	w		-	-	-	-	-	-	-	-	-
P39	w		L	-	-	+	-	-	-	-	-
P40	m	IgG	K	-	-	+	+	-	-	-	-
P41	m		K	-	+	+	+	-	-	-	-
P42	m		L	-	-	-	+	-	-	+	-

P43	m		-	-	-	+	-	-	-	-	-
P44	w		K	-	-	+	-	-	-	-	-
P45	m		K	-	+	-	+	+	+	-	-
P46	m		K	-	+	+	+	-	-	-	-
P47	m		K	-	-	+	-	-	-	-	-
P48	m		K	-	-	+	-	+	-	-	-
P49	m		K	-	+	-	+	-	+	-	-
P50	w		K	-	+	+	-	-	-	-	-
P51	w		K	-	-	-	-	-	-	-	-
P52	w		-	-	+	-	+	+	+	-	-
P53	w		K	-	-	-	+	-	-	+	-
P54	w		K	-	+	+	-	-	-	-	-
P55	w		L	-	+	-	-	-	-	-	-
P56	m		L	-	+	+	+	-	-	-	-
P57	m		K	**rare SNP**	-	-	-	-	+	-	-
P58	w		L	-	-	+	-	-	-	-	-
P59	m		K	-	-	-	-	-	-	+	-
P60	w	IgG	K	-	-	+	-	-	-	-	-
P61	m		K	-	-	+	-	-	-	-	-
P62	w		-	-	-	-	-	-	-	-	-
P63	m		L	**SNV**	+	+	+	-	-	-	-
P64	w		L	-	+	-	+	-	-	-	-
P65	w		K	-	-	+	+	-	-	-	-
P66	m		K	**rare SNP**							
P67	m		L	-	+	-	+	-	+	-	-
P68	m		K	-	-	-	+	-	-	+	-
P69	m		L	**rare SNP**	+	+	+	-	-	-	-
P70	w		-	-	+	+	-	-	-	-	-
P71	w		L	-							
P72	w		K	-	-	+	+	-	-	-	-
P73	m		K	**rare SNP**	-	+	-	+	-	-	-
P74	w		L	-	-	-	+	-	-	+	-
P75	m		K	**rare SNP**	-	+	-	-	-	-	-
P76	w		K	**rare SNP**	-	+	+	+	-	-	-
P77	w		K	-	-	+	-	-	-	-	-
P78	m		-	**rare SNP**	+	-	+	-	+	-	-
P79	w		L	-	+	+	-	-	-	+	-
P80	m		L	-	-	-	+	-	-	+	-
P81	m		K	**rare SNP**			+	-	-	-	-
P82	m		L	-			+	-	-		-
P83	m		K	**rare SNP**	-	+	+	+	-	-	-
P84	m		-	-	+	+	+	-	-	-	-
P85	m		K	-			-	-	-	-	-
P86	m		-	-	-	+	+	-	-	-	-
P87	m		-	-		-	-	-	-	+	-
P88	m		K	-	-	+	-	-	-	-	-
P89	m		-	-			+	-	-		
P90	m		L	-	-		-	-	-	-	-
P91	w		K	-	+	-	+	-	-	-	-
P92	m		K	**SNV**	+	-	+	-	+	-	-
P93	m		K	-			-	-	-	-	-
P94	w		K	-	-	+	-	-	-	-	-

P95	w		K	**rare SNP**	-	+	-	+	-	-	-
P96	m		K	-	-	+	-	-	-	-	-
P97	m		K	-							
P98	w		L	-	+	+	+	-	-	-	-
P99	m		-	-	-	+	-	-	-	-	-
P100	m		K	-	-	+	-	-	-	-	-
P101	w		-	**rare SNP**	-	-	-	-	-	+	-
P102	m		K	-	-	+	-	-	-	+	-
P103	m		L	-	-	+	+	-	-	-	-
P104	m		-	-			+	+	-	+	-
P105	m	IgG	K	-	-	+	-	-	-	-	-
P106	m		-	-	+	+	-	-	-	-	-
P107	w		K	-	+	-	-	-	-	+	-
P108	w		L	-			-	-	-	+	-
P109	w	IgA	K	-	+	-	+	-	+	-	-
P110	m		L	-	-	-	+	-	-	+	-
P111	w		L	-	-	-	-	+	-	+	-
P112	m		K	**rare SNP**	-	-	+	+	-	+	-
P113	m		K	-	+	+	+	-	-	-	-
P114	m		K	-	-	+	-	-	-	-	-
P115	m		-	-	+	-	+	+	-	-	-
P116	w		K	-	-	+	-	-	-	-	-
P117	m		L	-	-	+	-	-	-	-	-
P118	m		K	-	-	+	-	-	-	-	-
P119	m		-	-	-	+	+	-	+	-	-
P120	m		K	-	-	+	-	-	-	-	-
P121	m		L	-	+	+	+	-	+	-	-
P122	m		K	-	-	+	-	-	+	-	-
P123	m		K	-							
P124	m		K	-	-	-	-	-	-	+	-
P125	m		L	-	-	-	+	+	+	-	-
P126	w		K	-	-	-	+	+	+	-	-
P127	w		L	**rare SNP**	-	+	-	+	-	+	-
P128	m		L	-	-	-	+	+	+	-	-
P129	m		K	-	-	+	-	-	-	-	-
P130	m		L	-	-	-	-	-	-	-	-
P131	m		L	-	+	+	-	-	-	-	-
P132	m		K	-					-		-
P133	m		K	-	-	-	+	-	-	-	-
P134	m		K	-	-	-	-	-	-	+	-
P135	m		L	-	-	+	-	-	-	-	-
P136	m		L	-	-	+	+	-	-	-	-
P137	w		K	-	+	+	+	-	-	-	-
P138	w		K	-							
P139	m		L	-	-	-	-	-	-	-	-
P140	m		K	-	-	+	-	-	-	-	-
P141	w		-	-							
P142	m		L	**rare SNP**	+	+	-	-	-	-	-
P143	w		K	**SNV**	-	+	+	-	-	-	-
P144	w		K	-	-	+	-	+	-	-	-
P145	w		K	-	-	+	-	-	-	-	-
P146	m		-	-	-	-	-	-	-	-	-

P147	m		K	-	-	-	+	-	-	-	-
P148	m		L	-							
P149	m		K	**rare SNP**	+	-	+	-	-	-	-
P150	w		K	-	-	+	-	-	-	-	-
P151	m		-	-	-	-	-	-	-	+	-
P152	m		K	-	-	-	+	-	+	-	-
P153	m		K	-	+	+	-	-	-	-	-
P154	m		K	-	+	+	+	-	-	-	-
P155	m		K	**SNV**	-	+	-	-	-	-	-
P156	m		L	-	+	-	-	-	-	+	-
P157	m		L	-	-	-	+	-	+	-	-
P158	m		-	-	-	+	-	-	-	-	-
P159	m		-	-	-		+	-	-	-	-
P160	m		L	-							
P161	m		-	**rare SNP**	+	-	+	-	-	-	-
P162	m		-	-	-	-	-	-	-	-	-
P163	m		K	-	-	-	-	-	-	+	-
P164	m		-	-			+	-	-	-	-
P165	m		K	-	-	+	+	-	-	-	-
P166	w		L	-	-	+	+	+	-	+	-
P167	m		K	-	-	+	-	-	-	-	-
P168	w		K	-	-	-	+	-	-	+	-
P169	m		K	-	-	-	+	-	-	+	-
P170	m		-	-	-	-	-	-	-	+	-
P171	w	IgG	K	**rare SNP**	-	+	+	-	-	-	-
P172	w		L	-	-	-	-	-	-	-	-
P173	m		L	-	-	+	-	-	-	-	-
P174	m		K	-	-	-	-	-	-	-	-
P175	m		K	-	-	-	-	-	-	-	-
P176	m		K	-	-	+	-	-	-	-	-
P177	m		K	-	-	-	+	+	-	+	-
P178	w		L	-	-	-	-	-	-	+	-
P179	m		K	-	-	-	-	-	-	-	-
P180	m		K	-	-	+	+	+	-	-	-
P181	m		K	-	-	-	+	-	+	-	-
P182	m		K	-	-	-	-	-	-	+	-
P183	w		-	**rare SNP**	-	+	-	-	-	-	-
P184	w		L	-	-	+	-	-	+	-	-
P185	w		-	-	-	-	+	-	-	+	-

11.2 Supplementary figures

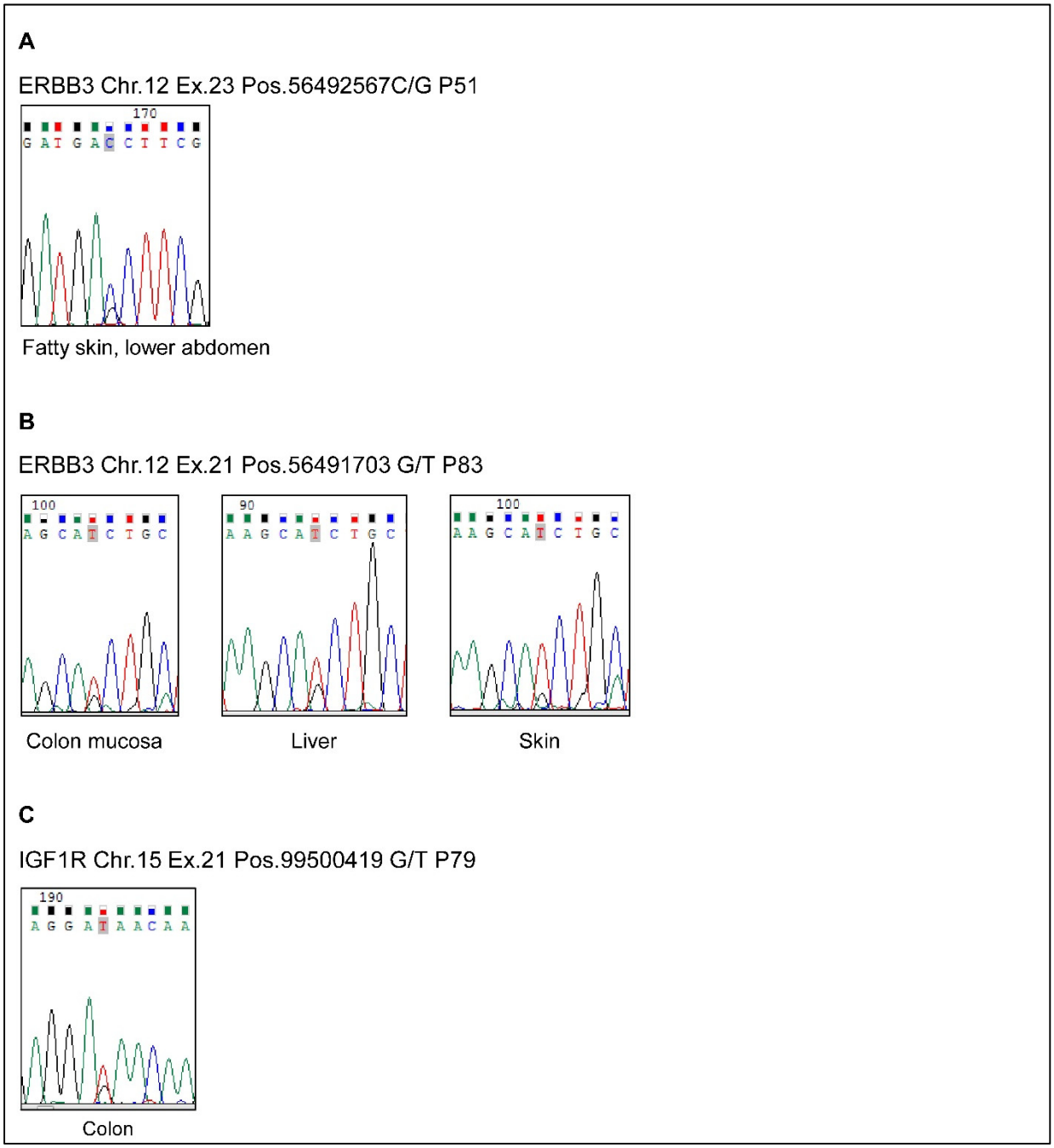

Supplementary Figure 1: Sanger sequencing of non-hematological normal samples [124]

11.3 Plasmid maps

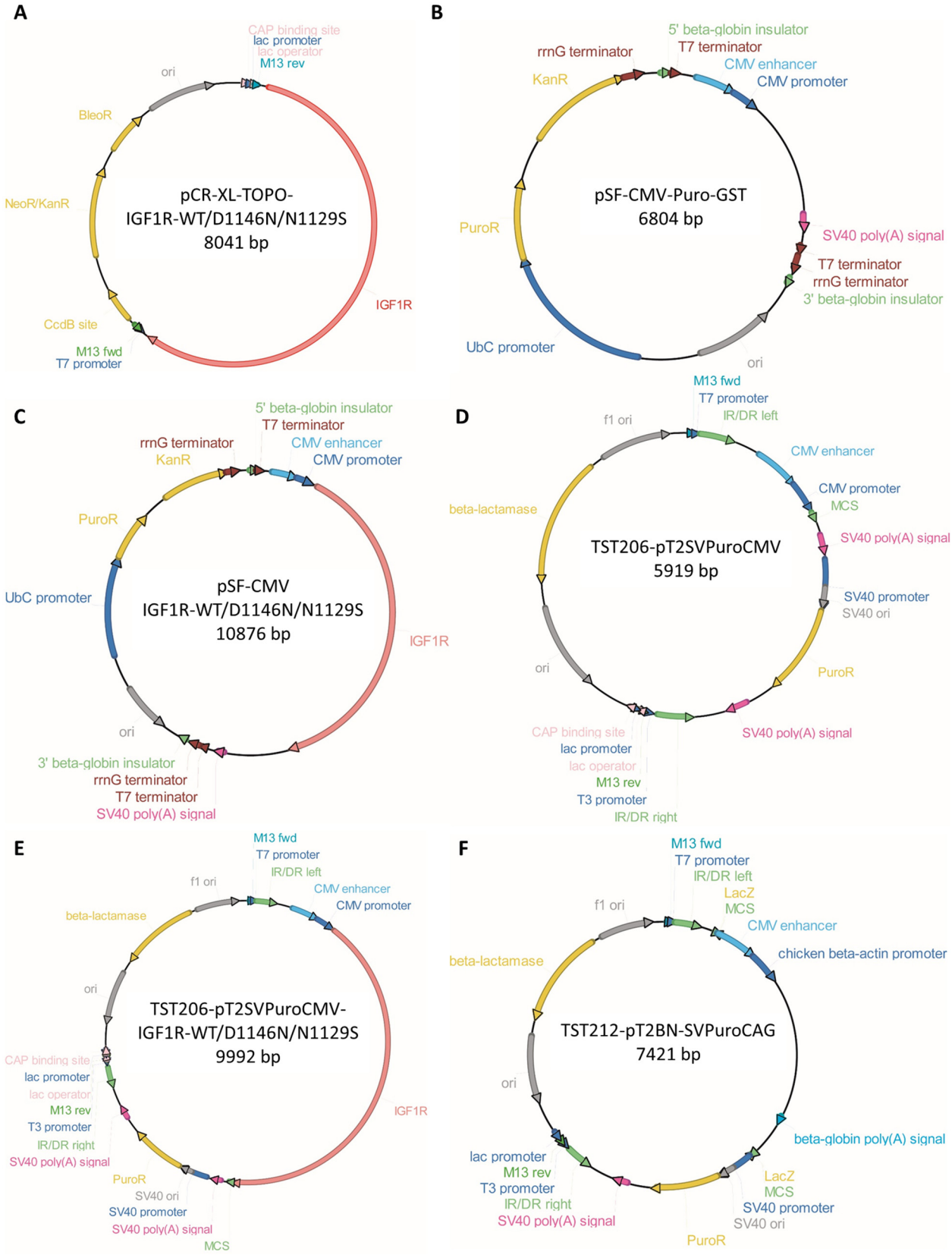

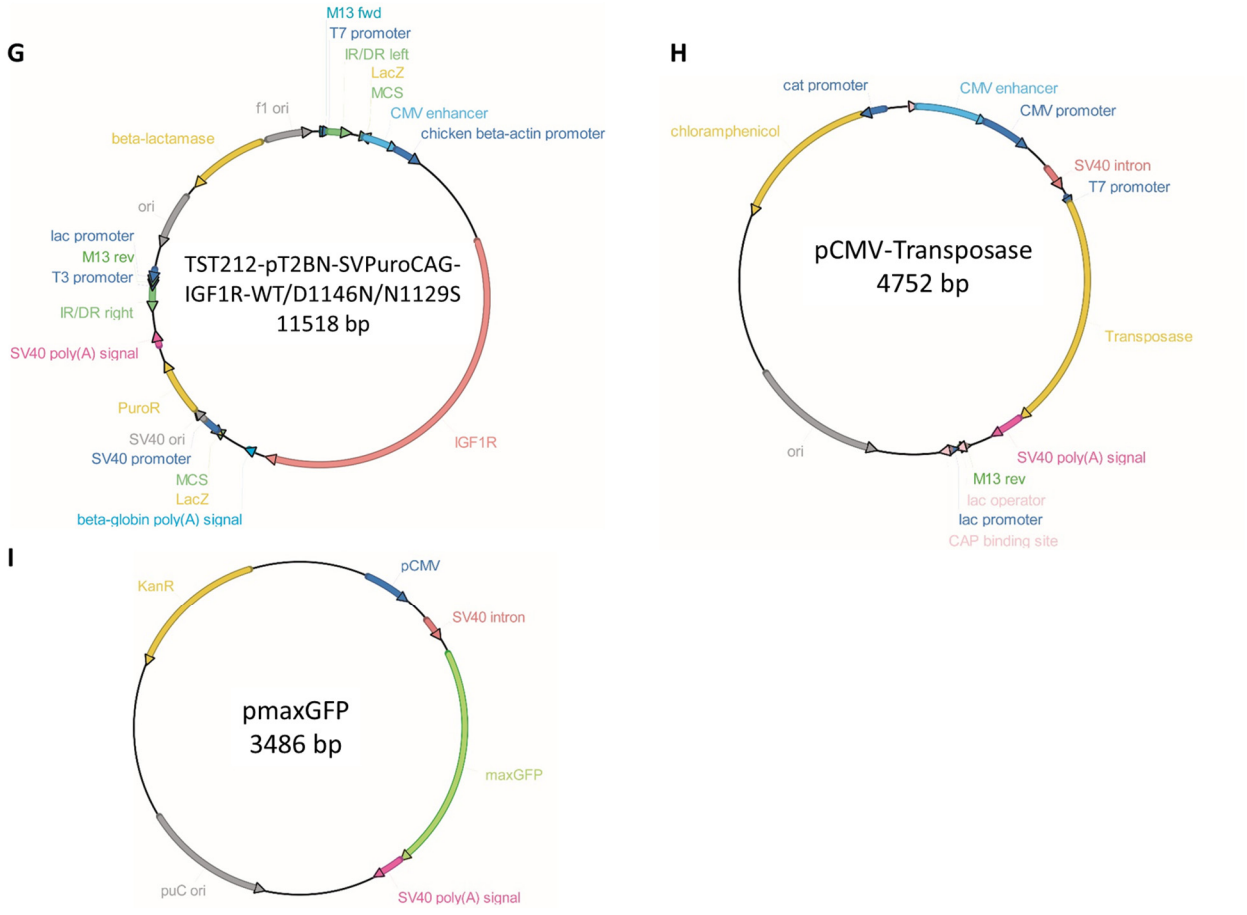

Supplementary Figure 2: Plasmid maps of vectors used in this work

11.4 Abbreviations

°C	degree Celsius
A	ampere
aa	amino acid
ACST	autologous stem cell transplantation
Amp	ampicillin
BCR	B-cell receptor
BM	bone marrow
bp	base pair
BSA	bovine serum albumin
BCR	B-cell receptor
Cas9	CRISPR associated protein 9
CCC MF	comprehensive cancer center Mainfranken
CD	cluster of differentiation
CDS	coding DNA sequence
Chl	chloramphenicol
Chr.	chromosome
CR	complete response
CRISPR	clustered regularly interspaced short palindromic repeats
crRNA	CRISPR RNA
CSR	class switch recombination
DMSO	dimethyl sulfoxide
DNA	deoxyribonucleic acid
dNTP	nucleoside triphosphate
DSB	double strand break
DSMM	German study group multiple myeloma (*Deutsche Studiengruppe Multiples Myelom*)
DTT	dithiothreitol
e.g.	for example
EDTA	ethylenediaminetetraacetic acid
EFS	event-free survival
EGFR	epidermal growth factor receptor
EGTA	ethylene glycol-bis(β-aminoethyl ether)-N,N,N',N'-tetraacetic acid
Eph	erythropoietin-producing human hepatocellular receptor
EPHA2	ephrin type-A receptor 2
ERBB3	erb-b2 receptor tyrosine kinase 3
ERK	extracellular signal-regulated kinase
F	forward
FAK	focal adhesion kinase
FBS	fetal bovine serum
FDC	focal dendritic cell
FGFR	fibroblast growth factor receptor
GAPDH	glyceraldehyde 3-phosphate dehydrogenase
GC	germinal center
HC	heavy chain

HCl	hydrogen chloride
HD	high dose
HDR	homology directed repair
HF	high fidelity
hg19	human genome version 19
HGF	hepatocyte growth factor
HMCL	human myeloma cell line
HRM	high resolution melting assay
HR	hybrid receptor
HRP	horseradish peroxidase
HSC	hematopoietic precursor cell
IGF1	insulin-like growth factor 1
IGF1R	insulin-like growth factor 1 receptor
Ig	immunoglobulin
Ig-H	immunoglobulin heavy chain
Ig-L	immunoglobulin light chain
IL-6	interleukin 6
InsR	Insulin receptor
IRS	Insulin receptor substrate
K_2HPO_4	dipotassium phosphate
Kan	kanamycin
KCl	potassium chloride
LB	lysogenic broth
LC	light chain
LD	loading dye
mA	milliampere
MAPK	mitogen-activated protein kinase
MEK	MAPK/ERK Kinase
$MgCl_2$	magnesium chloride
MGUS	monoclonal gammopathy of undetermined significance
min	minute/minutes
MM	multiple myeloma
MP	dry nonfat milk powder
M-proteins	monoclonal proteins
$Na_2HPO_4x2H_2O$	disodium hydrogen phosphate
NaCl	sodium chloride
NaOH	sodium hydroxide
NGS	next generation sequencing
NHEJ	non-homologous end joining
NLS	nuclear localization sequence
NP-40	nonidet P-40
NSCLC	non-small cell lung cancer
NTRK1	neurotrophic receptor tyrosine kinase 1
NTRK2	neurotrophic receptor tyrosine kinase 2
OS	overall survival

p	p-value
PAM	protospacer adjacent motif
PBS	phosphate buffered saline
PBS-T	phosphate buffered saline with Tween-20
PCL	plasma cell leukemia
PCR	polymerase chain reaction
PD	progressive disease
PFS	progression-free survival
PI3K	phosphatidylinositol 3-kinase
PIP_2	phosphatidylinositol 4,5-bisphosphate
PIP_3	phosphatidylinositol (3,4,5)-trisphosphate
PMSF	phenylmethylsulfonylfluoride
Pos.	position
PR	partial response
P/S	penicillin/streptomycin
PTB	phosphotyrosine binding domain
R	reverse
rcf	relative centrifugal force
Ref Base	Reference Base
RNA	ribonucleic acid
RNP	ribonucleoprotein
RT	room temperature
RTK	receptor-tyrosine kinase
s	seconds
SD	stable disease
SDS	sodium dodecyl sulfate
SDS-PAGE	sodium dodecyl sulfate polyacrylamide gel electrophoresis
sgRNA	single guide RNA
SH2	Src homology 2 domain
SHC	Src homology and collagen domain
SHM	somatic hypermutation
SMM	smouldering myeloma
SNP	single nucleotide polymorphism
SNV	single nucleotide variation
TBS	Tris buffered saline
TBS-T	Tris buffered saline with Tween-20
T_M	melting temperature
TNF-α	tumor necrosis factor alpha
tracrRNA	trans-activating crRNA
Tris	2-Amino-2-(hydroxymethyl)propane-1,3-diol
Trk	tropomyosin receptor kinase
UBC-9	ubiquitin carrier protein 9
V	volt or variable
VDJ	variable-diversity-joining
VAF	variant allele frequency

VEGF	vascular endothelial growth factor
VEGFR	vascular endothelial growth factor receptor
VGPR	very good partial response
WCL	whole cell lysate

11.5 List of figures

11.6 List of tables

11.7 List of equations

12 Publications, posters and presentations

Publications

Sarah Keppler*, Susann Weiβbach*, Christian Langer, Stefan Knop, Jordan Pischimarov, Miriam Kull, Thorsten Stühmer, Torsten Steinbrunn, Ralf Bargou, Hermann Einsele, Andreas Rosenwald, Ellen Leich **Rare SNPs in receptor tyrosine kinases are negative outcome predictors in multiple myeloma** Oncotarget. 2016; 7:38762-38774

*These authors have equally contributed to this work

Posters

Sarah Keppler, Susann Weiβbach, Christian Langer, Stefan Knop, Jordan Pischimarov, Miriam Kull, Thorsten Stühmer, Torsten Steinbrunn, Ralf Bargou, Hermann Einsele, Andreas Rosenwald, Ellen Leich ***(Germline) mutations in receptor tyrosine kinases: a negative outcome predictors in multiple myeloma?*** 78th Harden Conference: Protein Kinases in health and disease, Biochemical Society, Winchester UK, September 15th-18th 2015

Sarah Keppler, Susann Weiβbach, Christian Langer, Stefan Knop, Jordan Pischimarov, Miriam Kull, Thorsten Stühmer, Torsten Steinbrunn, Ralf Bargou, Hermann Einsele, Andreas Rosenwald, Ellen Leich ***(Germline) mutations in receptor tyrosine kinases: a prognostic marker in multiple myeloma?*** 15th International Myeloma Workshop, Rome, September 23rd – 26th 2015

Sarah Keppler, Marlene Schwarzfischer, Severin Fink, Susann Weißbach, Ralf Bargou, Hermann Einsele, Andreas Rosenwald, Thorsten Stühmer, Ellen Leich ***The role of IGF1R mutations in multiple myeloma*** 3rd International Symposium: Control of Cell Motility in Development and Cancer; SFB 850 Universität Freiburg, Freiburg, March 22nd -24th 2017

Presentations

Sarah Keppler, Marlene Schwarzfischer, Severin Fink, Ralf Bargou, Hermann Einsele, Andreas Rosenwald, Thorsten Stühmer, Ellen Leich ***Functional investigation of IGF1R mutations in multiple myeloma using genome editing tools*** Jahrestagung der Deutschen, Österreichischen und Schweizerischen Gesellschaften für Hämatologie und Medizinische Onkologie (DGHO, OeGHO, SGHO), Stuttgart, September 29th –October 3rd 2017, *accepted*